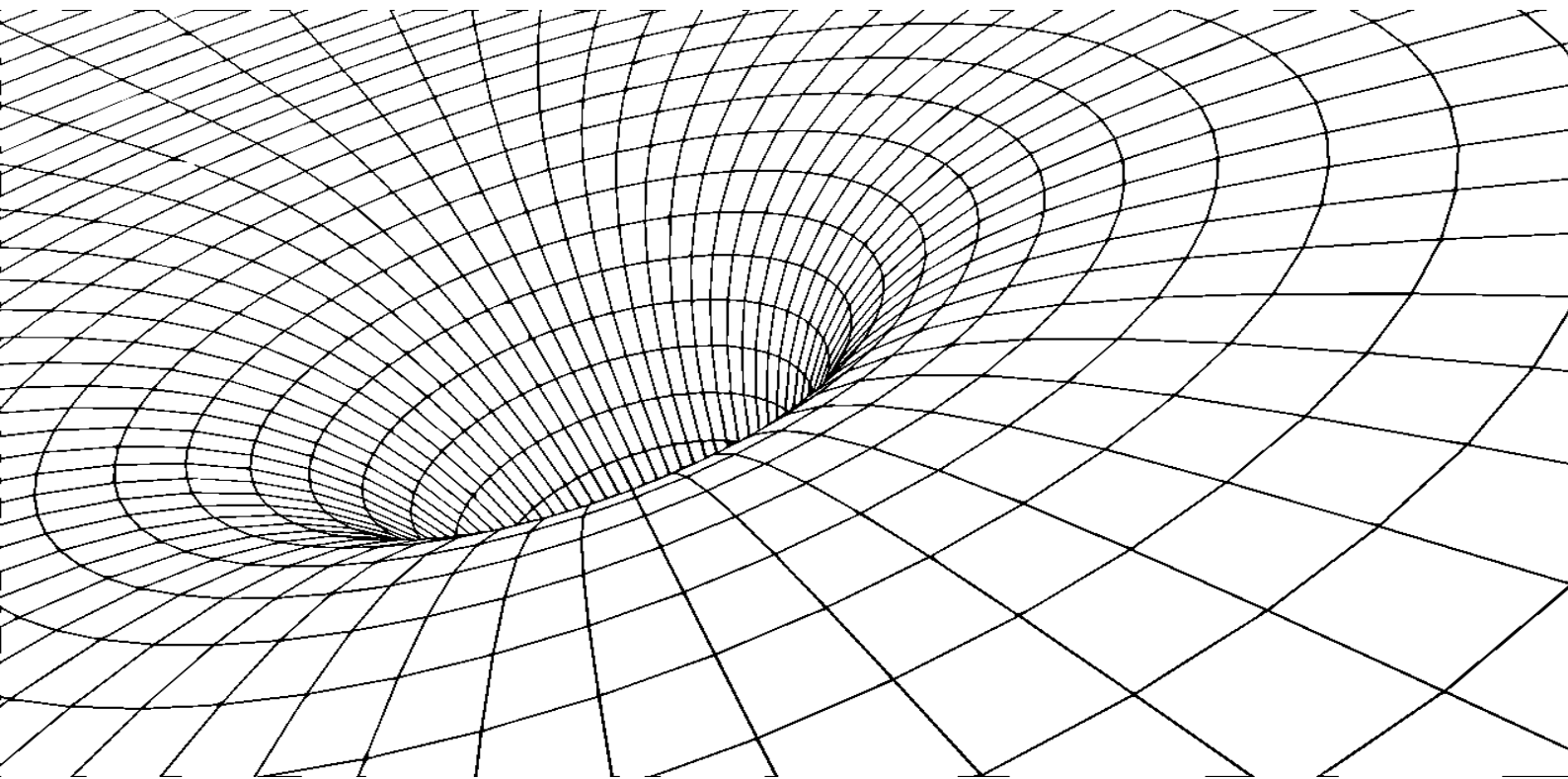


OPTIMAL PATH FOR ORBITAL DEBRIS

Anelí Bongers and José L. Torres

University of Málaga



SPACE ECONOMICS

Working Paper n. 06/2025

OPTIMAL PATH FOR ORBITAL DEBRIS

ANELÍ BONGERS

Department of Economics, University of Malaga, Spain

JOSÉ L. TORRES

Department of Economics, University of Malaga, Spain

This paper introduces the DISE-2024 (Dynamic Integrated Space Economy) model, an Integrated Assessment Model (IAM) designed to analyze the economics of efficient mitigation policies for orbital debris. The DISE-2024 model integrates an optimal neoclassical economic growth framework with a physical model of the Earth's orbital environment, capturing the dynamics of orbital debris and the likelihood of collisions. The economic component of the model determines the optimal consumption path and investments across two capital assets: Earth capital and space capital (i.e., satellites). The physical component models the endogenous generation of orbital debris, accounting for factors such as launch activity, in-orbit breakups, and collisions. The model is simulated over a 200-year horizon under various policy scenarios, including no intervention, de-orbiting policy, no breakups, reusable launch vehicles, debris-free launch systems, collision avoidance, and the European Space Agency's (ESA) zero debris policy. A key finding of the study is that mitigation policies targeting debris emissions alone have a limited impact on reducing the long-term accumulation of orbital debris. Only scenarios involving complete collision avoidance can prevent the catastrophic chain reaction predicted by Kessler syndrome. (JEL Classification: D62; E21; E22; Q53; Q58).

KEYWORDS. Outer space, Orbital debris, Satellites, Integrated assessment model, Debris mitigation guidelines, Optimal policy.

Anelí Bongers: abongers@uma.es

José L. Torres: jtorres@uma.es

We thank Michael Tamor, Sébastien Roullion, Benedetto Molinari, César Ortiz, and participants in the IX Workshop on International Economics Alicante 2024, XIV EDASS International Conference Rome 2025, XXIII Conference on International Economics 2025, and seminar at the University of Bordeaux, for very useful comments on a previous draft. The authors gratefully acknowledge financial support from the Spanish Ministry of Science, Innovation, and Universities through Grant PID2023-152748OB-I00. The authors have no conflicts of interest or financial interests to disclose. Full replication code in GAMS and in MATLAB is publicly available at <https://spaceeconomics.org/dise2024code>. This paper is accompanied with a GAMS MIRO app for a complete sensitivity analysis of the parameters of the model (https://miro.gams.com/gallery/app_direct/dise_2024/).

1. INTRODUCTION

The history of human activities in space is relatively brief compared to humanity's long presence on Earth, beginning in 1957 with the launch of *Sputnik-1*. This marked the first instance of a human-made object reaching outer space. Since then, humanity's presence in space has expanded significantly. Milestones include the first human in space in 1961, the first spacewalk in 1965, the Moon landing in 1969, the establishment of permanently inhabited space stations starting in 1986, and the deployment of thousands of satellites and other spacecraft orbiting Earth. Today, the space environment surrounding Earth plays a critical role in modern life and future aspirations for space exploration. The advent of space exploration and satellite technology has revolutionized communication, navigation, Earth observation, and scientific research. Defense, national security, and modern warfare now rely heavily on satellite systems, and the militarization and weaponization of outer space are expanding alongside commercial space activities. Every day, a variety of satellite services are used when we drive a car, watch TV, look for a location in a map, take a flight, look at weather forecast, use an ATM, etc., and satellites are key capital assets for transport and logistics, telecommunications, agriculture, financial and banking services, natural resource management, and urban planning.

However, this progress has come at a cost: the deterioration of the space environment, particularly through the proliferation of orbital debris, commonly referred to as space junk. This issue has become a new challenge, as environmental concerns are no longer limited to Earth. While threats like climate change, plastic and chemical waste, microplastics, and antibiotic-resistant superbugs dominate Earth's environmental discourse, human activity in space has introduced pollution and environmental degradation beyond our planet. Orbital debris represents a unique form of pollution distinct from terrestrial sources such as greenhouse gas emissions, due to the specific conditions of the space environment. Low Earth Orbit (LEO)¹, in particular, is now cluttered with millions of pieces of human-produced orbital debris traveling at hypervelocity (around 10 km per second). This debris includes a wide variety of objects, such as defunct satellites abandoned in orbit, fragments from intentional destruction of satellites, spent rocket upper stages, fragments from collisions or spacecraft breakups, paint flakes, propellant droplets, and even tools accidentally left behind by astronauts. All of these objects travel at extremely high speeds, posing risks to active satellites and other spacecraft, and the future sustainability of space operations.

The National Aeronautics and Space Administration (NASA) defines orbital debris as *"any human-made object in orbit that no longer serves a useful purpose, including spacecraft fragments and retired satellites."* Orbital debris is widely recognized as a form of space pollution that poses significant risks to commercial and other activities in outer space (Liou and Johnson, 2006). The impacts of orbital debris manifest in several ways. It can damage or destroy operational satellites, causing a sudden depreciation of high value space capital assets, increase operational and design costs, and disrupt satellite services to Earth's customers. Even small-size debris with low mass can cause catastrophic damage due to the high velocities at which they travel. Additional costs are incurred for tracking space

¹LEO ranges between 180 km and 2,000 km.

objects, performing collision avoidance procedures, and managing reduced satellite lifespans caused by fuel consumption during such maneuvers. A particularly concerning aspect of orbital debris is its self-propagating nature: collisions generate more debris fragments which contribute to further collisions resulting in an endogenous process of debris accumulation. This phenomenon, known as the "Kessler Syndrome", describes a cascade of collisions that can render certain orbital regions unusable over time (Kessler and Cour-Palais, 1978; Kessler, 1991).

Given the unique characteristics of space pollution, two distinct non-exclusive mitigation policies can be considered. The first type consists in orbital debris emissions mitigation policies. The second type is a post-emission policy and consist in cleaning space by removing debris from orbit. This is the so-called active debris removal (ADR) policy. To address the issue of orbital debris, it is crucial to focus on both mitigating the creation of new debris and reducing the population of existing debris. This paper focuses in the first. Given the consideration that outer space is a global common, international cooperation and the establishment of a legal framework are essential to coordinate any orbital debris mitigation policy. Emission mitigation strategies aim to reduce the generation of new debris and include the development of a number of guidelines to be adopted by spacefaring agents. Both the United Nations and national space agencies have developed a number of non-binding debris mitigation guidelines, and the ESA has introduced a "zero debris" emission strategy for 2030. These guidelines focus on enhancing design standards and operational procedures for satellite end-of-life disposal, such as safely de-orbiting defunct satellites or moving them to a graveyard orbit, minimizing the release of operational and mission-related debris, passivating satellites at the end of their life and rocket bodies to prevent breakups, and preventing on-orbit collisions.

The economic literature has dealt with the orbital debris problem using alternative modeling strategies to assess the economic costs of orbital debris and to investigate optimal environmental policies in space. Seminal papers studying the economic consequences of orbit debris are Adilov, Alexander and Cunningham (2015, 2018), Macauley (2015), and Rouillon (2020). The role of environmental policies (i.e., launch taxes or orbital-use fees) to mitigate orbital debris has been studied by Béal, Deschamps and Moulin (2020), Rao, Burgess and Kaffine (2020), Adilov et al. (2020), and Guyot and Rouillon (2022). The implications related to ADR policies have been studied by Klima et al. (2016), Grzelka and Wagener (2019), Adilov et al. (2020), Guyot and Rouillon (2022), and Bernhard et al. (2023). For a review of the literature, see Bongers et al. (2024).

In the literature, we can find some proposals of integrated models for simulating trajectories of the space environment. Rao et al. (2020) developed an integrated model that uses physical and economic data from 1957 to 2015 to predict open-access trajectories and optimal launches up to 2040. Rao and Letizia (2022) combined an econometric model of space activity with a debris environment model based on a Particle-in-a-Box (PIB) model. Another example is the OPUS (Orbital Unified with Economic Systems) model developed by Rao et al. (2023), which incorporates an astrodynamics propagator to assess the state of objects in orbit, combined with a simple economic model to determine launch activity. Rao and Rondina (2025) focus on study the conditions under which the Kessler syndrome,

defined as a situation in which the level of objects implies that the orbit will eventually become unusable in finite time, can be optimal in a centralized economy. Nevertheless, as it is pointed out by Traeger (2014) among others, to evaluate optimal environmental policy, it is necessary to integrate the endogenous evolution of the environment into economic growth models. Some recent studies have used neoclassical growth models in a further step to analyze space activity with full integrated assessment models (IAMs). Nozawa et al. (2023) develop an IAM with space activity where the economic module is based on the neoclassical growth model and estimate that orbital debris could cause damage equivalent to approximately 1.95% of global GDP in 200 years if no remediation efforts are taken. Corrado et al. (2023) study the connections between the space economy and economic growth, estimating the size of the spillover effects of space activity. Bongers et al. (2025) develop a dynamic integrated space-economy (DISE) model based on a partial-optimal growth model with a space module balancing parsimony with realism to study the long-run implications of different orbital debris emission mitigation policies.

This paper contributes to the literature by introducing an optimal IAM for policy analysis of the global economy and space environment, where economic growth theory is unified with space engineering science. The purpose in developing this space-economy IAM is to make available a tool for assessing the evolution of optimal trajectories for the relevant variables under different policy scenarios. We can argue that IAMs have become the primary analytical tool for evaluating potential policy responses to environmental changes. These models integrate information about human behavior and the environment to predict future environmental changes and their consequences. The exercise follows the tradition by Nordhaus (1992, 1993, 2008, 2018) and Barrage and Nordhaus (2024) with the Dynamic Integrated Climate Economy (DICE) model, arguably the most influential climate-change economic IAM. In the environmental economics literature, there is a long tradition of using different IAMs to evaluate the cost of carbon emissions and for the design of optimal climate-change policies.² It makes sense to extend this tradition by developing integrated economy-space models to understand the impact of orbital debris and to formulate optimal policies. Similarly to other IAMs, the model consists of two sub-models: an economic model, and a physical model. The economic part is designed to offer insights into the best economic decisions made by agents influencing human activity in space. The physical part aims to provide information about the impact of economic activity on the space environment. Both sub-models are linked such as economic activity influences space environment, which has an impact on the economy. Orbital debris is a by-product of human activity in space, and therefore space pollution is sensitive to changes in economic factors. We call this model DISE-2024 (Dynamic Integrated Space Economy).

Specifically, the DISE-2024 model looks at the economics of orbital debris through the lens of a world economy neoclassical optimal growth model grounded on Ramsey (1928), and later reformulated by Koopmans (1963) and Cass (1965), in which it is considered not only activities in the Earth but also in the space. The model considers a central

²Other examples of IAMs are the ETA-MACRO (Model of Energy-Economy Interactions) by Manne (1977), the GLOBAL-2100 model of Manne and Richels (1992), the CETA (Carbon Emissions Trajectory Assessment) model by Peck and Teisberg (1992), the MERGE (Model for Evaluating Regional and Global Effects) model by Manne et al., (1995), or the work of Golosov et al. (2000).

planner who maximizes social welfare by taking optimal decisions on investment under alternative debris mitigation scenarios. The final output is a function of labor (population) and two types of capital: Earth capital and space capital (i.e., satellites). The accumulation process of space capital produces orbital debris. Damages produced by orbital debris result in the destruction of space capital, affecting the growth rate of capital stock which evolves endogenously. Three exogenous sources of growth are considered: Aggregate neutral technological progress, investment-specific technological progress to satellites, and population dynamics.

The physical part of the model describes the dynamics of orbital debris as a function of economic activity and the in-orbit endogenous processes for the generation of debris. We distinguish three types of debris: derelict satellites, rocket bodies, and fragments. The distinction among the three objects is due to two factors: First, the population of specific types of debris can be affected by different emission mitigation policies. Second, fragments are dead objects, but derelict satellites and upper stages rocket bodies are objects subject to breakups resulting in a cloud of fragments. The debris evolutionary model has been calibrated to reproduce the tracked population of debris by the US Space Command (USSC), and estimates by the ESA (European Space Agency) and NASA.

A finite-horizon approximation of the calibrated infinity-horizon model is numerically solved as a nonlinear programming problem for a simulation horizon of 200 years, where a central planner maximizes social welfare. In the context of forward-looking expectations this requires imposing a terminal condition for the expected values of variables beyond the chosen simulation horizon (Mercenier and Michel, 1994). Several simulations are carried out under alternative policy scenarios based on the existing debris mitigation guidelines established by the United Nations Inter-Agency Space Debris Coordination Committee (IADC), and the different national space agencies. The model is simulated for a no-intervention scenario, reusable launch vehicles, a mandatory de-orbiting policy for end-life satellites and rocket bodies, no-breakup of big objects (derelict satellites and rocket bodies), debris-free launch systems, collision avoidance, and ESA's zero debris policy. The main scenario involves comparing the optimal debris mitigation policy with the no-intervention benchmark scenario, where the social planner does not use any specific debris mitigation policy instrument to drive the orbital debris accumulating process.

The model generates optimal trajectories for key economic variables, such as per capita consumption, output, Earth capital investment, and space capital investment, as well as for physical variables like the quantity of orbital debris, the number of launches, the number of satellites in orbit, and the number of satellites destroyed by collisions. Using these trajectories, the probability of collision is estimated as a measure of the likelihood of the Kessler syndrome. From the simulation exercises, we made four main findings. First, per capita output growth emerges as a major driver of future trends in launches, satellites, and orbital debris. As economic activity expands, human activity in space intensifies, increasing the number of satellites and the accumulation of orbital debris. However, a tipping point is identified in some scenarios: once orbital debris surpasses a critical threshold, the loss of space assets becomes significant, reducing the number of operational satellites. Second, compulsory debris mitigation policies, such as de-orbiting, prevention

of breakups, reusable launch vehicles, and debris-free launch systems, as well as combinations of these measures, significantly slow the growth of orbital debris in the short and medium terms. However, in the long term, these policies are less effective unless collisions are completely avoided or under the ESA's zero debris policy. Over extended time horizons, collisions between orbital debris and operational satellites become the dominant source of debris if they are not avoided. Third, the probability of a catastrophic event like the Kessler syndrome increases across all scenarios, but the extent varies significantly. Without intervention, the probability of collisions surpasses 60% over a 200-year horizon, while combining mitigation policies reduces this probability to around 25%. Finally, the economic impact of orbital debris is considerable. Compared to a scenario without debris, global output losses are projected to range between 0.4% and 0.6% of GDP over 200 years. These losses are particularly striking given the relatively small size of space capital compared to Earth capital.

The remainder of the rest of the paper is organized as follows. Section 2 offers a background on some key characteristics of the space environment, as a number of concepts used in the model are not economics but related to space sciences. In Section 3, a global economy-space model is developed to show the relationship between the final output of the World economy and the amount of satellites in a space environment affected by orbital debris. In Section 4, the model is parameterized and calibrated. Section 5 describes the different policy scenarios. Section 6 presents the main results from the simulation of the model. Section 7 carries out a sensitivity analysis. Finally, Section 8 presents some conclusions.

2. THE EARTH' ORBIT AND DEBRIS ENVIRONMENT

Before describing the space-economy theoretical framework and the simulation exercises carried out for assessing the economics and environmental implications of alternative debris mitigation policies, this section describes some important aspects related to the space environment that are not standard in economics but important for understanding of key aspects of the model. The space environment around Earth, known as near-Earth space, is a complex and dynamic region that plays a crucial role in various scientific, technological, and environmental aspects of our planet. This environment, extending from the upper atmosphere to the outer reaches of the Earth's magnetosphere, is influenced by both terrestrial and extraterrestrial factors.

Outer space is generally considered to start at the Kàrmàn line, which is located at an altitude of 100 kilometers (62 miles) above Earth's sea level. This boundary is widely recognized by international organizations as the point where the atmosphere becomes too thin to support conventional aircraft flight, and space conditions begin, although some authors set the limit at 80 km (McDowell, 2018). The magnetosphere is a region dominated by Earth's magnetic field, which protects the planet from the solar wind, a stream of charged particles emitted by the Sun. This region extends tens of thousands of kilometers into space, forming a protective bubble around Earth. These are two concentric belts of charged particles trapped by Earth's magnetic field (the so-called Van Allen Radiation Belts). The inner belt, located about 1,000 to 5,000 km above Earth's surface, contains

high-energy protons. The outer belt, extending from about 13,000 to 60,000 km, is dominated by high-energy electrons. Human activity in space is concentrated, depending on the purpose of the activity, in the range 180-36,000 km.

2.1 *Earth's orbit*

The near-Earth space (below the outer Van Allen Belt) is populated by thousands of satellites used for communications, navigation, weather forecasting, military applications, and scientific research. Satellites play a crucial role in modern life, providing services ranging from communications and navigation to weather forecasting and scientific research. The specific path a satellite follows around the Earth, known as its orbit, is fundamental to its function and utility. In practice, there are different types of satellite orbits each one with their particular characteristics, and their applications. In general, we can distinguish three types of orbits: Low Earth orbit (LEO), Medium Earth orbit (MEO), and Geostationary orbit (GEO).³

LEO ranges from an altitude of around 180 km (Kármán line is about 100 km), to 2,000 km above the Earth's surface. Satellites in LEO travel at high speeds, completing an orbit in approximately 90 to 120 minutes. Proximity to Earth offers a number of applications: Earth Observation that provide high-resolution images for environmental monitoring, urban planning, disaster management, and military reconnaissance; Communication: LEO satellites are used in satellite phone networks and internet services, such as those provided by the Starlink and OneWeb constellations; and Scientific Research: The International Space Station (ISS) and the Tiangong Space Station (TSS), which orbit in LEO, serve as a platform for scientific experiments in microgravity. LEO is the most populated orbit by both satellites and orbital debris.

Medium Earth Orbit (MEO) covers an altitude ranging from 2,000 km to 35,786 km. MEO satellites have longer orbital periods, typically between 2 to 12 hours. They offer a balance between the high-speed low orbits and the wide coverage of higher orbits. In this orbit are place navigation satellites constellations, such as the U.S. Global Positioning System (GPS), Russian's GLONASS, European's Galileo, and Chinese's BeiDou. These constellations of satellites provide precise positioning and timing services essential for navigation, mapping, and timing. MEO is also used by communication satellites, particularly in providing coverage for areas where ground infrastructure is lacking.

Finally, the Geostationary Orbit (GEO) is a particular orbit at an altitude of 35,786 km above the equator. A satellite in GEO orbits the Earth at the same rate that the Earth rotates, making it appear stationary relative to a fixed point on the ground. This allows for constant coverage of a specific area which is an ideal orbit for communications and

³In practice, there is more types of orbits. Apart from LEO, MEO and GEO, the ESA also consider the Polar Orbit (PO), Sun-synchronous orbit (SSO), Highly Eccentric Orbit (HEO), Transfer orbits and geostationary transfer orbit (GTO), Lagrange points (L-points), and Heliocentric orbit (HO), all of them with different characteristics. For example, HEO orbit is characterized by their elongated elliptical shape, with a low perigee (closest point to Earth) and a high apogee (farthest point from Earth). This orbit allows satellites to spend extended periods over specific regions, particularly at high latitudes.

Earth's observation satellites. GEO satellites provide stable and continuous communication links for television broadcasting, satellite radio, and internet services. Weather satellites in GEO, such as the GOES series, offer continuous monitoring of weather patterns, aiding in storm tracking and climate research. GEO satellites are also used for military and strategic surveillance, providing consistent monitoring of specific regions. In GEO, the limited number of orbital slots leads to competition and regulation to prevent interference between satellites.

2.2 *Orbital debris emissions*

Space debris emissions are generated from various sources, depending on the type of technology used in the design of launch vehicles and spacecraft, the operational procedures followed by spacefaring entities, and, in some cases, by intentional actions by governments for military purposes. The primary source of orbital debris originates from launch activities. These include the so-called mission-related objects (MRO), such as payload fairings, bolts, lens covers, paint flecks, connecting components from launch vehicle stages, and other materials released during normal operations like satellite deployment or spacecraft maintenance. This category also encompasses rocket bodies and engines from the final stages of launch vehicles. A secondary in-orbit endogenous source of debris arises from satellite post-mission management, breakups, and collisions. Examples include non-functional satellites abandoned in orbit, fragments resulting from the breakup of satellites and rocket bodies, and debris generated by collisions. The main cause of in-orbit explosions is often residual fuel left in the tanks of rocket upper stages or within derelict satellites and batteries. Over time, the extreme conditions of outer space cause mechanical degradation, leading to fuel leaks and accidental mixing of volatile components, which can result in explosions. These explosions frequently fragment rockets and other spacecraft, generating significant amounts of debris. In addition to accidental breakups, deliberate actions, such as self-destruction of satellites with explosive charges, and anti-satellite weapon tests, have become a substantial contributor to the orbital debris problem. These tests involve the intentional destruction of satellites, creating large quantities of high-velocity debris (Bongers and Torres, 2024). A notable example is the deliberate destruction of the Chinese *Feng-Yun 1C* satellite by a missile in January 2007, which alone increased the trackable space debris population by 30% (OECD, 2020). Most debris (around 85%) is at a Low Earth Orbit (LEO) altitude (below 2,000 kilometers), with peak concentration around an altitude of 700-900km (NASA, 2020). According to the European Space Agency (ESA) and NASA, by December 2023, there are approximately 36,500 pieces of debris larger than 10 cm, around 1,000,000 objects ranging from 1 cm to 10 cm, and more than 130,000,000 fragments between 1 mm and 1 cm. While debris smaller than 1 cm poses a low risk of causing fatal damage, it can still significantly impair critical systems and shorten the operational lifespan of satellites. In contrast, fragments larger than 1 cm can have catastrophic consequences due to the high velocities at which they collide (Krisko, 2007; and Mains et al., 2024).

2.3 *Altitude-dependent parameters*

Space environment heavily depends on the altitude. Various forces, such as gravitational pull from the Moon and Sun, atmospheric drag, and solar radiation pressure, can alter any object, including spacecraft, orbit trajectory. The primary force governing any object in orbit is Earth's gravity, which determines the satellite's trajectory and velocity. These physical properties have important consequence for the calibration of some key parameters of the model. First, natural decay rate of any space object depends on gravity attraction. Thus, survival rate of a space object is a parameter depending on the altitude. Natural orbital decay is caused by any mechanism that absorb energy from the orbital motion, and includes fluid friction, gravitational anomalies, or electromagnetic effects. For bodies in LEO, the most significant effect is atmospheric drag and solar conditions. As a consequence, the survival time of an object in orbit is very sensitive on its altitude. The higher the altitude, the longer the orbital debris will typically remain in Earth orbit. Debris left in orbits decay time is measured in hours for objects below 200 km, weeks for objects between 200 and 400 km, a time of around 20 years for objects around 600 km, 200 years for an altitude of 900 km, 1,000 years for an altitude of 1,000 km, to 50,000 years for an altitude of 2,000 km (Australian Space Weather Agency, 1999).

On the other hand, the number of satellites and orbital debris are not homogeneously distributed across altitude. Hence, the probability of collision also depends on the altitude, given the heterogenous distribution of objects in orbit. Some orbits are more densely populated than others which affect the likelihood of collision. LEO is the most congested region due to its accessibility and suitability for many applications. GEO, while less populated than LEO in absolute terms, faces its own unique challenges. Satellites in GEO occupy fixed orbital slots to maintain their position relative to the Earth's surface, which leads to clustering in certain areas. Moreover, debris at this altitude is particularly problematic because it remains in orbit indefinitely due to the lack of atmospheric drag to facilitate natural decay. Over time, this accumulation creates a significant long-term hazard for operational satellites in GEO.

2.4 *Damages*

Orbital debris is a global negative environmental externality that can affect social welfare in a number of ways. The main damage is that resulting from the loss of space capital by the destruction or by putting out of service operational satellites. The damage cost of collisions is not only instantaneous in the form of foregone space capital assets, but is long lasting as collisions produce additional debris that can provoke more collisions. There exist the possibility of collisions between a piece of debris and an operational satellites but also between two pieces of debris. In the last case, the cost is only related to the new fragments produced. Other costs, are launch costs to check for a launch window, tracking and prediction of collision probability costs, costs related to avoiding collision maneuvers, including and costs for reducing life-span of operational satellites, and costs related to interruption of services produced by satellites conducting avoiding collision maneuvers.

The cost of a collision between a satellite and a piece of debris can vary significantly based on several factors, including the size and function of the satellite, the nature of the

debris, and the specific circumstances of the collision. The cost to design, build, launch, and operate a satellite can range from a few million dollars for small, simpler satellites to over a billion dollars for large, complex systems like geostationary communication satellites or advanced scientific instruments. On the other hand, the nature of the collision can range from minor damage, such as to a solar panel or antenna, to catastrophic failure, where the satellite is completely destroyed or rendered inoperable. In some cases, even minor damage can result in significant costs if it leads to a loss of functionality. If a collision occurs, it could create additional debris, which not only complicates future space operations but also poses risks to other satellites. Damages from orbital debris do not only occur in space but there is the possibility of producing damages in the Earth. Although rare, some debris re-enters the atmosphere and can pose risks to populated areas. While most objects burn up upon re-entry, larger fragments can survive and fall back to Earth, raising concerns about potential harm to Earth's infrastructure and human life.

2.5 *Collision avoidance operations*

Collision avoidance operations involve a set of procedures and strategies used by satellite operators and space agencies to prevent collisions between spacecraft and space debris or other spacecraft. These operations are crucial for maintaining the safety and longevity of satellites, as well as for minimizing the creation of additional space debris. Every day, hundreds of collision avoidance maneuvers have to be conducted by satellite operators. As an example, only the SpaceX Starlink satellites had to make more than 275 collision avoidance maneuvers every day during 2024.

A key aspect of collision avoidance is the Monitoring and Tracking of space objects. Various organizations, including the U.S. Space Surveillance Network (SSN), NASA, ESA, and other national space agencies and private firms, track objects in space to predict potential collisions. Orbital debris are tracked using Earth-based radar and optical sensor facilities. The principal orbital tracking system is the United States SSN. These devices can track orbital objects larger than 10 centimeters in size in LEO (larger than 30 cm in GEO), although some tracked objects are smaller than 10 centimeters. These organizations maintain catalogs of all known (tracked) objects in orbit, including active satellites and large enough debris. These entities use models to predict the closest approach between two orbiting objects. When two objects are predicted to come within a certain distance, it is called a "conjunction event." Conjunction analysis helps determine the risk of collision; Once a potential conjunction is identified, the probability of collision is calculated. Factors such as the size, shape, and relative velocity of the objects are considered. The conjunction assessment helps to decide whether avoidance maneuvers are necessary. If the probability of collision exceeds a certain threshold, the satellite operator may decide to perform an avoidance maneuver. This involves changing the satellite's orbit slightly to avoid the predicted collision path. Collaboration and communication between different space agencies and satellite operators are crucial. They often share tracking data and collision alerts to coordinate avoidance maneuvers, especially in geostationary orbits and other crowded regions. Advanced algorithms and artificial intelligence are increasingly being used to predict and manage conjunction events. Automated systems can provide faster and more accurate collision risk assessments and maneuver planning.

As the number of satellites in orbit grows rapidly due to increased activities in space, collision avoidance has become a critical component of satellite operations. This process comes with significant costs that can be categorized into operational, technical, and opportunity costs. First, collision avoidance maneuvers involve monitoring potential threats, analyzing orbital data, and executing thruster burns to adjust a satellite's trajectory. These activities require highly skilled personnel, advanced tracking technologies, and software systems capable of analyzing large amounts of data to predict conjunctions. Maintaining such infrastructure and expertise entails ongoing expenses, especially as the volume of orbital objects increases. Second, there is a cost due to fuel expended. Satellites often rely on limited onboard fuel for propulsion. Each avoidance maneuver consumes some of this precious resource, reducing the satellite's operational lifespan. As a result, operators face long-term economic impacts, needing to plan for earlier satellite replacements or mission terminations. Finally, there is an opportunity cost. Collision avoidance maneuvers temporarily disrupt the primary mission of a satellite, such as communications, imaging, or data collection. For commercial satellites, this could translate to revenue losses due to interrupted service. Scientific missions may lose critical data if operations are paused during maneuvers.

2.6 Catastrophic event: *The Kessler syndrome*

The possibility of catastrophic events and disasters is a constant consideration in environmental analyses (see, for example, Barro, 2006; Weitzman, 2009; Barro and Jin, 2011; Barro and Ursúa, 2012). In space, natural disasters and catastrophic events also pose significant threats to humanity. These include solar activity, such as geomagnetic superstorms like the Carrington Event (Carrington, 1859) and the Miyake Event (Miyake et al., 2012), as well as the potential for asteroids on a collision course with Earth. Additionally, human activity in space has the potential to cause disasters through the emission and endogenous accumulation of orbital debris. In extreme cases, this process could render Earth's orbit unusable, posing severe consequences for humanity's access to and use of space.

The Kessler Syndrome (Kessler and Cour-Palais, 1978; Kessler, 1991; Kessler et al., 2010), named after NASA scientist Donald J. Kessler who proposed the theory in 1978, describes a scenario in which the density of objects in Earth orbit becomes so high that collisions between objects cause a cascade of further collisions, exponentially increasing the amount of space debris. This phenomenon presents a significant challenge for space exploration and satellite operations, posing both practical and theoretical concerns for the sustainability of space activities.

Kessler's hypothesis arose from the observation that space debris, comprising defunct satellites, spent rocket stages, and other fragments from previous collisions or satellites destruction, can remain in orbit for extended periods (forever for high altitudes). As the number of these objects increases, so does the likelihood of collisions. When two objects collide, they break apart into many smaller pieces, each of which can then collide with other objects, creating a chain reaction of fragmentation. This process exponentially increases the number of debris particles in orbit endogenously, significantly raising the probability of further collisions. The critical aspect of the Kessler Syndrome is that once

a certain threshold is crossed, the process becomes self-sustaining. Even if no new objects are launched into space, the debris already present could continue to collide and fragment, perpetuating the cycle. This runaway scenario could lead to an environment so littered with orbital debris that it becomes hazardous or even impossible to operate satellites, manned missions, and other space ventures safely.

In the literature, we find different definitions of the Kessler syndrome. For some authors the Kessler syndrome occurs when the space is unusable with a collision probability of one (Adilov et al., 2018), whereas for other authors is a process in which the number of fragments is increasing even if the population of intact objects remains constant (Kessler et al., 2010), and for others, the Kessler syndrome has already started (Bonnal et al., 2013). On the other hand, the engineering interpretation of the Kessler syndrome as a physical phenomenon is different from the economic interpretation of it. In the manuscript we adopt a more flexible interpretation, and we argue that the likelihood of the physical Kessler syndrome can be approximated by the probability of collision.

2.7 Debris mitigation guidelines

Kessler and Cour-Palais (1978) called for the implementation of different effective methods to reduce orbit debris. These methods include improved engineering designs to reduce the frequency of satellite breakups from structural failure and explosions in space. Macauley (2015) enumerates different technological strategies to mitigate debris generation and/or collision risk, including shielding, increased surveillance and tracking of debris, improved maneuverability capabilities to avoid collisions, and reserve fuel to de-orbiting end-life satellites.

Given the raising concerns about the threat posed by orbital debris and in an attempt to stop their proliferation, space national agencies have adopted particular space debris mitigation guidelines; NASA in 1995, the Japan Aerospace Exploration Agency (JAXA) in 1996, the French Space Agency (Centre National D'Etudes Spatiales, CNES) in 1999, Russian Federation Roscosmos in 2000, the China National Space Administration (CNSA) in 2005, and the ESA in 2006. At an international level, the United Nations Inter-Agency Space Debris Coordination Committee (IADC) proposed a number of voluntary debris mitigation measures, and the United Nations for Outer Space Affairs (UNOOSA) established a set of Space Debris Mitigation Guidelines in 2007. These guidelines are the following: Limit debris released during normal operations, minimize the potential for breakups during operational phases, limit the probability of accidental collision in orbit, avoid intentional destruction and other harmful activities, minimize potential for post-mission breakups resulting from storing energy, limit the long-term presence of spacecraft and launch vehicle orbital stages in the low-Earth orbit (LEO) region after the end of their mission, and limit the long-term interference of spacecraft and launch vehicles orbital stages with the geosynchronous Earth orbit (GEO) region after the end of their mission. International mitigation guidelines are applicable to all spacecraft and launch vehicles, but on a voluntary basis.

The first debris emission guideline refers to post-mission disposal (PMD) or de-orbiting. After a satellite, rocket, or spacecraft completes its mission, it is ideal for it to

either burn up upon reentry or be placed in a “graveyard” orbit, far from active orbital paths. For satellites in LEO, this typically involves lowering their orbit to re-enter Earth’s atmosphere within 25 years, where they will burn up and disintegrate. For satellites in GEO, operators often move them to a graveyard orbit where they are unlikely to interfere with active satellites. A second guideline focuses on minimizing the release of materials during a spacecraft’s operation. For example, spacecraft should be designed to minimize the release of small parts, such as bolts and insulation panels, during separation or maneuvering. In general, this type of debris is formed by small particles that are difficult to track but pose significant risks. A third guideline focuses on reducing the likelihood of breakups of big debris. Satellites and rocket stages should be equipped with end-of-life passivation measures to prevent explosions after their operational life. Passivation involves releasing any remaining energy—such as fuel, batteries, or pressurized fluids, once the mission is completed. This significantly reduces the likelihood of accidental explosions, which are a source of endogenous creation of space debris. A fourth guideline puts the emphasis on preventing collisions. Operators are encouraged to use collision avoidance maneuvers for active satellites. Such measures include tracking debris and adjusting a satellite’s orbit to reduce the risk of collisions. Finally, more recently, it has been incorporated recommendations encouraging active debris removal (ADR) interventions. ADR is a developing field that involves capturing or deorbiting space debris. Although no fully operational ADR missions exist yet, technological demonstrations have shown potential solutions, such as robotic arms, nets, and lasers to deorbit debris.

However, there are important challenges in implementing mitigation guidelines. While the guidelines are theoretically sound, implementing them poses practical, financial, and legal issues. The costs of designing spacecraft with mitigation measures can be large. Additionally, the lack of enforceable international space law means compliance is often voluntary, leading to inconsistent adherence. There are also geopolitical issues; some countries may hesitate to adopt certain practices due to national security concerns or competition. In this context, international cooperation is critical for the implementation of debris mitigation guidelines. Space is a shared domain, meaning international cooperation is essential for space debris mitigation to succeed. Organizations like the IADC, UNOOSA, and the International Telecommunication Union (ITU) can be valid instruments to facilitate dialogue among spacefaring countries to create and adopt unified standards.

Recent updates in space debris mitigation guidelines reflect a global push toward sustainable space practices to address the increasing amount of debris in orbit. Among the notable developments are the ESA’s new “Zero Debris” guidelines introduced in 2023 to be accomplished by 2030. These guidelines implement stricter measures for ESA missions, aiming for zero debris impact in Earth orbits by 2030 and introduce requirements for effective disposal, collision avoidance, and mission passivation (neutralizing remaining energy sources to prevent explosions). The guidelines also reduce the time permitted in low-Earth orbit (LEO) post-mission from 25 years to less than 5 years, requires that the cumulative probability of collision with any debris larger than 1 cm in size is below 1 in 1000 for the entire period of a mission’s life, until it reenters Earth’s atmosphere, and mandate a 90% probability for safe satellite disposal by the incorporation of critical disposal functions such as enough fuel for manoeuvres and functional thrusters. ESA also requires

new satellites, particularly in large constellations, to include interfaces allowing for active debris removal operations if self-disposal fails. Furthermore, ESA's updated policy emphasizes reducing orbital collisions with increased use of automated collision avoidance systems, refined space traffic management, and the prohibition of intentional debris release, such as fairings or protective covers, which previously contributed to orbital congestion. The guidelines also extend to lunar and geostationary orbits and incorporate specific standards to protect astronomy by limiting interference with dark and quiet skies. This policy shift reflects an emphasis on cooperation with global initiatives like the "Zero Debris Charter", which encourages space actors worldwide to adhere to these principles.

3. THE OPTIMAL DYNAMIC INTEGRATED SPACE ECONOMY (DISE-2024) MODEL

This section describes the structure of the DISE-2024 model. The model is a global space-economy model that covers not only the planet Earth but also the outer space. The theoretical framework used is a type of integrated assessment model (IAM) similar to the ones commonly used in climate-change environmental economics. A remarkable climate-change IAM example is the DICE (Dynamic Integrated Climate-Economy) model by Nordhaus (1992, 1993, 2008). The DISE-2024 model has a similar general structure to climate-change IAMs but adapted to the particular characteristics of the outer space environment and specifically designed to study the economic and welfare implications of orbital debris. As standard climate-change IAMs, the DISE-2024 model is a combination of two sub-models: an economy model and an environmental model of pollution in the space. Emissions of debris, in-orbit endogenous generation of debris, and damage functions link the two sub-models. Figure 1 shows a schematic flow chart of the model.

The main components of the DISE-2024 model are the following:

1. A social welfare functions in terms of the discounted sum over time of per capita utility from consumption for the World population.
2. The final world output is split among consumption, investment in Earth capital, and investment in space capital.
3. A damage function resulting in the destruction of operational satellites as a result of collision with orbital debris.
4. Two types of debris emissions: Related to economic activity and endogenous dynamics in orbit from collisions and breakups of intact objects.
5. A system of dynamic equations for the motion of three types of orbital debris: derelict satellites, rocket bodies, and fragments.

The economic part is represented by an optimal growth model for the world economy comprising two capital inputs, where "satellites" are an additional type of capital in the aggregate production function. It is based on the neoclassical general equilibrium

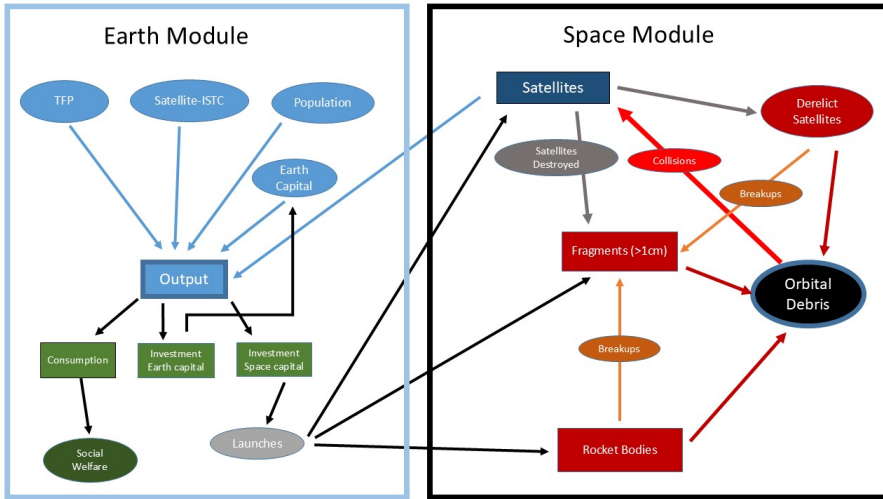


FIGURE 1. Schematic flow chart for DISE-2024

growth model initially developed by Ramsey (1928). The model includes a negative externality that emerges from the pollution of outer space with orbital junk.⁴ Unlike standard environmental economic models, pollution does not directly reduce output by reducing aggregate productivity. The cost of pollution on Earth's orbit comes from the fact that orbital debris increases the risk of collision and destruction of operational satellites. This, in turn, reduces the stock of in-orbit equipment and thus indirectly reduces production if the destroyed equipment is not replaced or reduces available resources for alternative uses in the case of replacement. In addition, the externality can impact economic growth, by affecting capital investment, both in the space and in the Earth, and the stock of capital in future periods.

The physical part of the model is represented by a tractable aggregate orbital debris evolutionary model that accounts for all types of debris emissions, with the exception of intentional debris emissions. As with the economy, the space model is also a global model for all orbits, from LEO to GEO. Together with the population of operational satellites (and other spacecraft, including two space-stations) we consider the dynamics of the population of orbital debris. The population of debris considered are objects greater than 1 cm. Debris are divided into three types: Derelict non-deorbited dead satellites, rocket bodies, and fragments. A key characteristic of the model is that dead satellites and rocket bodies can breakup either by internal factors or by collision with other objects, generating additional fragments.

One particular characteristic of DISE-2024 is that the model includes variables that are defined in two dimensions: physical variables and output-measured variables. We consider a mapping between physical variables of the space sector (i.e., number of satellites, number of satellites destroyed by collision) and the corresponding variables of the

⁴Orbital debris is not the only existing externality in Earth's orbit. Other externalities are congestion at particular altitudes, electromagnetic pollution, and radio-spectrum interference of nearby satellites. This paper focuses on pollution by orbital debris.

economic model (i.e., the value of satellite assets). Physical variables are represented in capital letters, while economic output-measured variables are represented in lowercase letters.

3.1 The economy model

The economy part of the model is based on the Ramsey (1928) optimal neoclassical growth model tailored to consider human activity in space. Time is discrete running to an infinity horizon. The economy is inhabited by a large number of infinity-lived identical households. There is a representative household with instantaneous utility $U(\hat{c}_t, N_t)$, defined over per capita consumption \hat{c}_t , and where N_t is population. The aggregate consumption, c_t , is defined as $c_t = \hat{c}_t N_t$. The function $U(\hat{c}_t, N_t)$ is the flow of utility which it is assumed to represent social well-being. The function $U(\cdot)$ is assumed to be concave and twice continuously differentiable.

The problem to be solved by the stand-in household consists in choosing the optimal consumption path that maximizes the sum of discounted utility,

$$\max_{\{\hat{c}_t\}_{t=0}^{\infty}} \sum_{t=0}^{\infty} \left(\frac{1}{1+\rho} \right)^t U(\hat{c}_t, N_t) \quad (1)$$

where $\rho > 0$ is the subjective intertemporal preference parameter or the pure rate of social time preference. The social discount factor, $0 < \beta < 1$, is defined as $\beta = 1/(1+\rho)$.

This household satisfies the following budget constraint which coincides with the feasibility constraint of the economy:

$$c_t + i_t^k + i_t^s = y_t \quad (2)$$

where i_t^k is investment in physical capital other than satellites (Earth capital), i_t^s is investment in satellites (space capital), which also include all costs to insert satellites into orbit, and y_t is final output. All prices are defined in output units and normalized to one.

Inserting a satellite into orbit requires the use of a launch vehicle, which is costly. As a result, not all space investment spending is converted into productive space capital. Launch vehicles, typically multi-stage rockets, represent a significant share of the total cost of satellite deployment. To account for this, investment in space capital is divided into two components:

$$i_t^s = h_t + l_t \quad (3)$$

where h_t is the cost of satellites, and l_t is the cost of launch. The launch cost is interpreted as an installation cost necessary to build up the stock of satellites. To deploy a satellite capable of providing services, a launch vehicle must be used. This launch cost is modeled as a fixed adjustment cost per unit of investment, reflecting the fact that launch prices are typically fixed per kilogram of satellite mass, though they may vary depending on the target orbit. Alternatively, the launch cost can be viewed as a wedge or premium over the purchase price of space capital.

We assume that all firms have access to the same technology, so we use a representative firm and a representative aggregate production function. Output is assumed to be a

function of aggregate productivity, the stock of physical capital in the Earth, k_t , the stock of satellites, s_t , and labor, N_t ,

$$y_t = a_t f(k_t, s_t, N_t) \quad (4)$$

where a_t is the total factor productivity (TFP), representing Hicks-neutral technological change. Labor is assumed to be equal (or proportional) to population, and hence the labor growth rate is equal to the population growth rate.

The capital other than satellites accumulation process is the standard inventory equation:

$$k_{t+1} = (1 - \delta_k)k_t + i_t^k \quad (5)$$

where $0 < \delta_k < 1$ is the Earth capital depreciation rate.

The stock of satellites, measured in final output units as an equipment asset, is denoted by s_t , and is given by the following process,

$$s_{t+1} = (1 - \delta_s)s_t + q_t(i_t^s - l_t) - x_t \quad (6)$$

where $0 < \delta_s < 1$ is the depreciation rate for satellites, and x_t is the loss of satellites assets by collisions (damage from space pollution) to be defined later. This accumulation process establishes the link between the space environment and economic activity. Damage results in the destruction of satellites, the reduction of space capital stock used in production, and the reduction of the final output if the loss asset is not replaced. The stock of satellites law of motion incorporates an investment-specific technological change component (ISTC), denoted by q_t , (see Greenwood et al., 1997). For simplicity, it is assumed that ISTC only occurs in the space sector.

The installation cost function is defined as:

$$l_t = b_t i_t^s \quad (7)$$

where b_t is the fraction of launch costs over the total investment cost in space capital. The installation cost is assumed to represent only a fraction of the total investment cost. In the macroeconomic literature, investment adjustment costs are commonly used to smooth capital accumulation and to replicate observed investment dynamics. These costs reflect the idea that adjusting the capital stock is not frictionless, that is, firms cannot install or reallocate capital instantly or without cost. For space capital, this consideration is particularly important, as installation costs reduce the effective amount of new capital that can be accumulated from each unit of investment expenditure. Adjustment costs are typically modeled as convex functions, implying that the marginal cost of investment increases with the scale of adjustment. However, non-convex or fixed adjustment cost structures have also been proposed in the literature (see, for example, Lucas, 1967; Caballero and Engel, 1999; Christiano et al., 2005). In the case of space investment, though, launch costs do not exhibit these properties as they are effectively fixed costs, determined primarily by the satellite's mass and target orbit altitude, and are charged as a constant amount per kilogram. Therefore, the fraction of investment in space capital that accumulates into operational satellites is defined as,

$$h_t = (1 - b_t)i_t^s \quad (8)$$

It is assumed that b_t is a decreasing function of time, representing decreasing launch costs based on a learning curve. The launch cost at each period is given by,

$$b_{t+1} = \exp(g_{b,t})b_t \quad (9)$$

$$g_{b,t} = g_{b,0}(\exp(-\delta_b t)) \quad (10)$$

where $g_{b,0} < 0$ is the initial change in the launch cost.

3.2 Exogenous growth sources

The model incorporates three exogenous sources of growth: aggregate neutral technological change, investment-specific technological change for satellites, and aggregate labor growth. The growth rates of technical change and population are not constant, but similarly to climate change AIMs it is assumed that the growth rate declines over time. Aggregate productivity technological progress is characterized as,

$$a_{t+1} = \exp(g_{a,t})a_t \quad (11)$$

where $g_{a,t}$ is the growth rate of TFP defined as,

$$g_{a,t} = g_{a,0}\exp(-\delta_a t) \quad (12)$$

where δ_a is the decay rate in the TFP growth rate, and $g_{a,0}$ is the TFP growth rate at the initial period ($t = 0$). We assume a similar specification for the satellite investment-specific technological progress,

$$q_{t+1} = \exp(g_{q,t})q_t \quad (13)$$

where $g_{q,t}$ is the growth rate of ISTC defined as,

$$g_{q,t} = g_{q,0}\exp(-\delta_q t) \quad (14)$$

where δ_q is the decay rate in ISTC for satellites, and $g_{q,0}$ is ISTC growth rate at the initial period.

Finally, we define the dynamics of the population, N_t . Population is another source of growth as it is assumed that labor equals population. Following the specification by Hassell (1975), population dynamics is defined as,

$$N_{t+1} = N_t \left(\frac{N^*}{N_t} \right)^\zeta \quad (15)$$

where N^* is the asymptotic population at the end of the simulation period and ζ is a parameter driving the population growth rate.

3.3 Economic to physical variables mapping

Space environment is defined by physical variables. However some variables have an economic counterpart. In order to ensure that economic and physical variables are integrated correctly, a mapping between the economy and the space must be established. We use satellites as the numerary for this mapping. The first step in creating this mapping involves connecting the stock of satellites as a capital asset to output units, s_t , with the number of satellites, S_t , is given by,

$$S_t = \mu s_t \quad (16)$$

where the parameter μ represent a conversion parameter that transforms "economic" values into "physical" values. Notice that satellite's ISTC affects the productivity value of the asset but not the quantity of assets. ISTC is considered as an embodied technological progress in new vintages of satellites. The higher the value of q_t , the larger the output-value of new satellites per unit of investment. In practice, a positive trend in q_t would reflect the decreasing launch costs and manufacturing costs of satellites.

Similarly the number of satellites destroyed by collisions, X_t , is

$$X_t = \mu x_t \quad (17)$$

A second mapping is assumed between investment in satellites and the number of new satellites inserted into orbit, H_t ,

$$H_t = \mu q_t h_t \quad (18)$$

where the number of new satellites is proportional to investment in space capital and the level of ISTC.⁵

By substituting the above mappings into the restriction (6), we can derive the equivalent accumulation process for the number of satellites. Therefore, the stock of satellites, represented by the number of representative satellites, can be expressed as,

$$S_{t+1} = (1 - \delta_s)S_t + H_t - X_t \quad (19)$$

where $0 < \delta_s < 1$ is the depreciation rate of satellites, and X_t is the number of destroyed satellites by collision with debris. Satellites is an equipment asset in orbit. Therefore, each period, the amount $\delta_s S_t$ of satellites becomes non-operational and hence, automatically considered dead intact objects. Satellites that are no longer useful but remain in orbit are classified as orbital debris if not removed.⁶

⁵Alternatively, we can define the number of satellites inserted into orbit as $H_t = \mu h_t$, where the number of new satellites depends on the ISTC, and hence, $S_t = \mu s_t / q_t$, and $X_t = \mu x_t / q_t$. Results do not change.

⁶Defunct satellites can be removed from orbit by raising their altitude to a graveyard orbit for geostationary satellites, or by decreasing their altitude to increase atmospheric drag for low and medium Earth orbit satellites, causing them to burn up in the Earth's atmosphere. Any large piece of debris that survives re-entry is disposed of in the spacecraft cemetery located in the Pacific Ocean, in an uninhabited area east of New Zealand.

3.4 Launches

The value of launches is just a fraction of investment in space capital in the economic part of the model but the number of launches plays a key role in the physical part. First, it is important to define the number of launches as an additional variable, given that the primary source of debris emission is the launching activity. Standard launch systems imply the use of rockets with several (two to four) stages. Some of these stages (parts of the launch vehicle, including fuel deposits and engines) remain in orbit once the payload has been inserted in orbit. Moreover, during the insertion phase, additional debris are generated as protection parts (i.e., fairings). Second, the number of launches is not equal to the number of satellites inserted into orbit. Indeed, the number of satellites per launch has been dramatically increased during the last decade. The availability of more powerful launch vehicles with higher payloads, together with the reduction in the size and weight of satellites has increased the number of satellites per launch. Therefore, the number of satellites inserted into orbit, H_t , is assumed to be a proportion η of the number of launches, L_t :

$$H_t = \eta L_t \quad (20)$$

and therefore, the parameter η can be interpreted as the the number of satellites per launch. Combining expressions (8), (18) and (20), we obtain the relationship between investment in space capital and the number of launches, given by,

$$L_t = \frac{\mu(1 - b_t)}{\eta} q_t i_t^s \quad (21)$$

3.5 Orbital debris evolutionary models

The space engineering literature, along with national space agencies, has developed various models of different scales to simulate the population dynamics of orbital debris. Notable examples include models proposed by researchers such as Farinella and Cordelli (1991), Talent (1992), Cordelli et al. (1993), Rossi et al. (1994), Rossi (1997), Lewis et al. (2009), Lafleur (2011), and Percy (2015). Additionally, significant contributions have been made by governmental space agencies, including NASA (EVOLVE and LEGEND models), ESA (DELTA and MASTER models), JAXA (NEODEEM model), CNSA (SOLEM model), CNES (MEDEE model), and the UK Space Agency (DAMAGE model).

Farinella and Cordelli (1991) developed a simple yet effective model using two differential equations to describe the dynamics of satellites and orbital debris. Simulations from this model predicted that collisions between orbital debris and artificial satellites would become the dominant source of debris within a few decades. Talent (1992) introduced a "Particles-in-a-Box" (PIB) model, based on collision theory, which divides the low Earth orbit (LEO) into 50-km spherical shells and categorizes debris into four classes. Talent's model is similar to Farinella and Cordelli's but simplifies the dynamics with a single differential equation. Lewis et al. (2009) extended Talent's approach with the FADE (Fast Debris Evolution) model, a first-order differential equation estimating the addition and removal of objects larger than 10 cm in size. Lafleur (2011) further advanced the model by incorporating collisions between intact satellites (both operational and non-operational),

fragments, and natural decay rates. Percy (2015) added a third differential equation to Lafleur's model to distinguish between operational and non-operational intact objects.

National space agencies have developed orbital debris evolutionary models as a tool for collision risk assessment and the evaluation of debris mitigation policies. The first model is EVOLVE, a model developed by the NASA in 1986 to predict long-term dynamics for LEO debris environment between 200 and 2000 km altitude (Krisiko et al., 2001). The EVOLVE model is a simplified breakup and orbital propagator models based in Monte Carlo simulations for historical debris generation events. The EVOLVE debris model has been replaced by the LEGEND (LEO-to-GEO Environmental Debris) model in the early 2000s (Liou et al., 2004). The LEGEND model extends the environment to GEO based on a 3-dimensional algorithm propagators, which reproduces historical debris environment from LEO to GEO. Similarly, the ESA has developed their own debris evolutionary models. Initially, the ESA developed the DELTA (Debris Environment Long Term Analysis) model, based on the NASA' EVOLVE model. The DELTA model has been substituted by the MASTER (Meteoroid and Space Debris Terrestrial Environment Reference) model. The core of the MASTER model is the Program for Orbital Debris Environment Modeling (POEM) for simulating fragmentation and impact events. The UKSA has developed the DAMAGE (Debris Analysis and Monitoring Architecture for the Geosynchronous Environment) model, specific for the GEO orbit (Lewis, 2020), whereas the JAXA developed the NEODEEM (Near Earth Orbital Debris Environment Evolutionary Model), and the CNSA introduced the SOLEM (Space Objects Long-term Evolution Model; Wang and Liu, 2019).

The economic literature has used different debris evolutionary modules to be integrated with economic models. These debris evolutionary models have been designed to keep a balance between explanatory power of the model for the space environment and simplicity of the debris dynamics to be integrated with an economic model. For example, Rouillon (2020) and Guyot and Rouillon (2023) develop a simplified model with two types of debris: big objects (non-operational intact objects), and small fragments. Rao and Letizia (2022) use a multi-shell and multi-species PIB model of the debris environment. Rao et al. (2023) use a PIB model, called MOCAT-4S by Lifson et al. (2022). Guyot (2024) extends the two-population debris model of Rouillon (2020) and Guyot and Rouillon (2023) to different altitude layers, where atmospheric drag move debris from upper layers to down layers. In this paper, we use a version of the debris environment module of Bongers et al. (2024b), where the population of debris comes from three accumulation processes for derelict satellites, rocket bodies, and fragments.

3.6 *The space model*

The space environment is vastly different from that of Earth. Space pollution can be either natural or man-made and can take the form of objects moving at high speeds that have the potential to collide with and destroy other objects. Any human-made object that is not functional and is orbiting around Earth is considered space junk. We will only consider man-made space debris since natural space pollution is rare and poses little threat to humans except in cases where a relatively large object is headed toward Earth. The Earth's atmosphere works as a protective shield against smaller objects that collide with our planet.

Therefore, any damage resulting from such collisions remains confined to space. Here, we describe the physical space model incorporated into DISE-2024. This space-environmental module includes four main functions: the damage function, and three laws of motion for three types of orbital debris.

3.6.1 Damage Space pollution can cause a range of damages. Orbital debris poses a significant risk of collision with operational satellites and other spacecraft, leading to the loss of valuable equipment and the generation of even more debris. Although it is possible for uncontrolled large debris in low Earth orbit to re-enter the atmosphere and cause harm to life or property on the ground, the likelihood of such events is very low. However, orbital debris significantly increases operational costs for spacefaring entities.

The literature offers several alternative methods for calculating the probability of collision in space. Most approaches are based on the work of Farinella and Cordelli (1991), where the probability of collision is modeled as a function of the population of operational satellites and orbital debris. According to their framework, the number of satellites destroyed each period due to collisions with debris is assumed to depend on the amount of debris, the number of operational satellites, and the effectiveness of collision avoidance technologies,

$$X_t = (1 - v_t)\theta D_{2,t}S_t \quad (22)$$

where $\theta > 0$ is a parameter representing the probability of collision, $0 \leq v_t \leq 1$ is a variable representing successful avoidance collision maneuvers, and $D_{2,t}$ is the population of orbital debris larger than 1 cm. If u_t takes the value of one, all possible collisions are avoided and no damage results from orbital debris. Notice that, given the above expression, the value of satellite assets destroyed by collision, x_t , is defined as,

$$x_t = (1 - v_t)\theta D_{2,t}S_t \quad (23)$$

given that $X_t = \mu x_t$ and $S_t = \mu s_t$. When $(1 - v_t)\theta D_{2,t} = 1$, any space assets are destroyed rendering the space unusable. This point is reached when the pollution stock is $D_{2,t} = 1/((1 - v_t)\theta)$.

3.6.2 The stock of pollution The stock of orbital debris consists of all non-operational, human-made objects in orbit, excluding functional satellites and other active spacecraft. However, not all orbital debris are incorporated into the damage function. Prior to the first launch in 1957, the stock of orbital debris was zero, as humans had not yet ventured into space. Debris are highly heterogenous in size, mass, and composition. Following the standard classification by ESA, we distinguish three categories for fragments: Fragments larger than 10 cm ($F_{1,t}$), fragments between 1 cm and 10 cm ($F_{2,t}$), and fragments between 1 mm and 1 cm ($F_{3,t}$). Orbital debris is measured as the number of non-functional objects in orbit with a size greater than 1 cm.⁷ The stock of debris as a function of their size, $D_{i,t}$,

⁷The destruction power of debris smaller than 1 cm is estimated to be low and non-fatal in the case of a collision with a representative satellite, although they can cause serious damage in critical systems, reducing functionality and lifespan, and even disable small satellites. However, debris larger than 1 cm is potentially deadly due to the high velocity of the impact. Therefore, for computing the risk of collision and the damages, we consider the estimated number of pieces of debris larger than 1 cm.

can be defined as,

$$D_{i,t} = W_t + Z_t + F_{i,t} \quad \text{for} \quad i = 1, 2, 3 \quad (24)$$

where we distinguish three types of debris: W_t is the stock of derelict satellites abandoned in orbit, Z_t is the number of last stages rocket bodies, and $F_{i,t}$ are fragments of size i . The key distinction is that fragments are dead debris, but both derelict satellites and rocket bodies are intact objects that can breakup, generating a large number of fragments, and can fragment in case of collision with each other or with other objects.

3.6.3 Debris generation Debris originates from various sources, including launch activities which generate derelict rocket upper stages and fuel tank remnants, and other mission related objects; derelict satellites that are not removed from orbit; accidental explosions and breakups; and the intentional creation of debris during military drills, such as destroying a satellite with an anti-satellite missile. The integrated model categorizes these into six main sources of orbital debris.

The first source of debris consists of mission-related objects (MRO), which are associated with the number of launches. This debris generation process is modeled as ωL_t , where ω represents the amount of debris created per launch during the launch period. This type of debris is classified as "fragments" and includes items such as protective fairings, covers, adapters, bolts, and cables. In addition to fragments, launches also generate another type of debris: the upper stages of launch vehicles, which often remain in orbit after deploying the payload. These rocket bodies constitute large intact debris with a significant risk of breaking apart over time. The number of rocket bodies generated per launch is given by φL_t , where $0 \leq \varphi < 1$ represents the fraction of launches producing this type of debris. We assume that φ is strictly less than one, reflecting the existence of reusable launch vehicles and/or de-orbiting practices of upper stages once the payload has been inserted into orbit. Over time, these upper stages rocket bodies accumulate into a stock of debris, which will be formally defined later. The third source of debris consists of derelict satellites (W_t). These are satellites that have reached the end of their operational lives—typically due to fuel depletion—and are abandoned in orbit rather than being de-orbited. Each period, the number of end-of-life satellites is represented by $\delta_s S_t$, where S_t is the total number of active satellites. Of these, a fraction $0 \leq \chi \leq 1$ is abandoned in orbit each period, contributing to the stock of derelict satellites.

The fourth source of debris generation is fragmentation events, which occur due to explosions and breakups of both derelict satellites and rocket bodies. These events can be either unintentional or deliberate. Unintentional fragmentation debris arises from the breakup of operational satellites, rocket bodies, or engines. The primary cause of in-orbit explosions is the residual fuel left in the tanks of upper-stage rockets and satellites. In the harsh conditions of outer space, mechanical components and devices degrade quickly, leading to leaks that mix fuel components. This can trigger self-ignition, resulting in accidental explosions that destroy the source object and scatter its mass into countless fragments of varying sizes and velocities. Batteries can also explode.

The fifth source of debris is also in-orbit endogenously driving, and is the result of collision among both operational and non-operational objects. The model distinguishes

two types of collisions: The collision between a piece of debris and an operational satellite, and the collision of intact debris (i.e., derelict satellites and upper stages rocket bodies) with each other and with fragments.

Finally, intentional fragmentation events, on the other hand, involve deliberate actions such as spacecraft interceptions using surface-launched missiles. These have been significant contributors to debris in recent years. Four countries, the United States, Russia, China, and India, have conducted direct-ascent anti-satellite (ASAT) tests, significantly increasing the population of orbital debris.

From these sources of emissions, we identify three equations describing the accumulation process for three types of orbital debris: Derelict satellites, rocket bodies and fragments. The two first types of debris are intact objects which are subject to fragmentation events. The stock of derelict satellites in orbit decreases due to natural decay, breakups, and collision with debris, and increases with end-life satellites abandoned in orbit. Formally, the law of motion of derelict satellites is given by,

$$W_{t+1} = (1 - \delta_w)W_t - \varepsilon_w W_t - \theta(D_{2,t} + (1 - v_t)S_t)W_t + \chi\delta_s S_t \quad (25)$$

where δ_w is the natural decay rate of derelict satellites due to atmospheric drag and solar conditions, and ε_w is the fraction of derelict satellites that breakup each period. The term $\theta(D_{2,t} + S_t)W_t$ reflects the number of derelict satellites that are destroyed by collision with fragments, other derelict satellites, rocket bodies and operational satellites. The dynamics of the stock of abandoned end-life satellites into orbit would depend on the regulatory policies about end-mission disposal. Mandatory de-orbiting of any dead spacecraft implies that $\chi = 0$, and therefore, the stock W_t would tend to zero in the long-run due to natural decay, breakups, and collisions. In case of explosion, it is assumed that the number of debris generates is $\phi_z \varepsilon_w W_t$, where ϕ_z is the number of fragments resulting from the breakup. The number of debris produced by collisions of a derelict satellite with any other object is $\gamma_w \theta(D_{2,t} + (1 - v_t)S_t)W_t$.

The accumulation process for rocket bodies is similar. The law of motion for the stock of upper stage body rockets is defined as,

$$Z_{t+1} = (1 - \delta_z)Z_t - \varepsilon_z Z_t - \theta(D_{2,t} + (1 - v_t)S_t)Z_t + \varphi L_t \quad (26)$$

where δ_z is the natural decay rate of rocket bodies, and ε_z is the fraction of body rockets that breakup each period. The number of debris produced by rocket bodies breakups is $\phi_z \varepsilon_z Z_t$, where ϕ_z is the amount of debris produced by the breakup of a body rocket. Mandatory de-orbiting of rocket bodies implies that $\varphi = 0$, and therefore, the stock Z_t would tend to zero in the long-run due to natural decay, breakups, and collisions. The number of debris produced by collisions of a rocket bodies with any other type of object is $\gamma_z \theta(D_{2,t} + (1 - v_t)S_t)Z_t$.

Finally, the third type of debris considered are fragments. The stock of fragments increases depending on the number of launches, fragments from breakups of derelict satellites and body rockets, and collisions between debris and operational satellites. We assume that the law of motion of fragments larger than 10 cm is given by,⁸

$$F_{1,t+1} = (1 - \delta_f)F_{1,t} + \omega L_t + \gamma_s X_t + \phi_w \varepsilon_w W_t + \phi_z \varepsilon_z Z_t + \gamma_w \theta D_{2,t} W_t + \gamma_z \theta D_{2,t} Z_t \quad (27)$$

where δ_f is the natural decay of debris fragments, ω is the amount of debris produces per launch (MRO), and γ_s is the amount of debris creates by a collision and destruction of operational satellites. The parameter γ_w is the number of fragments from the collision of derelict satellites, and γ_z is the number of fragments from collision of rocket bodies. The model excludes the possibility that operational satellites can breakup due to design failures, and fragments resulting from military anti-satellite (ASAT) tests with direct-ascend missiles.

It is worth noting that the model considers two distinct processes for orbital debris generation. The first is tied to economic activity, specifically launches and the operational procedures of launch vehicles. The second is an endogenous process involving in-orbit emissions from breakups and collisions. The calibration of debris generation per launch recognizes that debris is not only created at the time of the launch but also in subsequent periods. This includes debris from rocket bodies, engines, and abandoned derelict satellites, which can generate additional fragments through breakups and explosions caused by residual fuel, and collisions.

3.7 Finite-horizon conditions

The growth model considers that the economy is populated by forward-looking rational expectations agents who take their economic decisions in an infinite-horizon but numerical solutions can only be obtained for a finite number of periods. In practice, we numerically solve a non-linear infinite-horizon economic growth model in a finite-horizon. This means what we need some kind of transformation of the original infinite-horizon optimal control problem into an equivalent finite-horizon optimal control problem. The key issue involved in approximating an infinite-horizon equilibrium for a neoclassical growth model is what is the size of the capital stock in the terminal period of the finite-horizon solution.

As pointed out by Mercenier and Michel (1994) numerical solution using mathematical programming techniques of nonlinear infinite-horizon continuous-time optimization problems requires reformulating the problem into a discrete finite horizon approximation. The central issue is that the solution of the model over the period of interest does not be affected by the selection of the horizon or the selection of the terminal condition. This reformulation requires three decisions. The first consists in the choose of the length

⁸The model computes the population of fragments ($F_{1,t}$) and debris larger than 10 cm ($D_{1,t}$) for two reasons. First, there is a computational reason for limiting the scale of this variable. Second, most parameters are calibrated using data about cataloged objects in orbit, which usually include only objects larger than 10 cm. From that we obtain the population of debris larger than 1 cm ($D_{2,t}$) using a scale parameter based on the estimation of debris between 1 cm and 10 cm from the ESA.

of the finite planning horizon. The second is the treatment of post-terminal behavior from the finite horizon to the infinity. The third is related to the choice of the specific sequence of time intervals in the discretization process. Problems with the optimal trajectory can be solved by increasing the length of the decision horizon at the cost of increasing the computational cost, or by reducing the frequency of the time intervals.

The general infinity-horizon problem can be defined as an utility maximization problem which is divided in two parts,

$$\max_{c_t} W = \sum_{t=0}^T \left(\frac{1}{1+\rho} \right)^t U(c_t) + \sum_{t=T+1}^{\infty} \left(\frac{1}{1+\rho} \right)^t U(c_t) \quad (28)$$

where the first part is the finite-horizon already solved from $t = 0$ to T , and the second part represents the economy behavior from period $T + 1$ to infinity, and where the two sub-problems are linked through the capital stock at period $T + 1$.

The literature has dealt with this issue proposing alternative terminal conditions to be incorporated into the model to determine investment in the last computational period (T) but using some adjustment to approximate choices over the period $T + 1$ to infinity. The simplest approach is to assume that the world ends at period T . This can be a valid method when the value of T is large and the discount rate is high just to minimize the effects of the terminal values on the optimal path. Because $\beta^t \rightarrow 0$ as $t \rightarrow \infty$, we can truncate the infinite horizon at a large finite period T . Other approaches assume that the economy reaches its steady state at time T . Blake and Westaway (1995) argue that any distortionary effects of a terminal condition can be minimized by setting a terminal condition consistent with the steady state of the model and sufficiently distant so that it does not affect model properties over the horizon of interest, so that a change either in the horizon period or in the terminal condition does not alter the solution over the period of interest.⁹

An alternative frequently used in climate-change economics is to use a fixed saving rate for the last periods of the simulation together with the use of large time intervals. This is the strategy followed by, for instance, Nordhaus (1992, 1993) in solving the DICE model. For instance, in DICE-2016 (Nordhaus, 2017) it is used a constant saving rate equal to the long-run saving rate for the last 10 periods (50 years). In DICE-2023 (Nordhaus, 2024) it is used a saving rate of 0.28 for periods larger than 37 (last 185 years). using an alternative approach, Nordhaus (2008) assumes that investment at the terminal time must be at least 2% of the capital stock at the terminal time. Cai et al. (2012) also solve the DICE model and assume that at the terminal time, the world reaches a partial equilibrium. They solve the model for a horizon of 600 years and estimate utility for a further 800 years using complete Chebyshev polynomial over the states.

⁹During the 1960s, this issue has been extensively studied by the literature of economic planning, where alternative strategies for dealing with the terminal condition have been proposed. Frisch (1955) proposes the use of geometric growth terminal conditions for numerical planning problems. Chakravarty (1962) considers that terminal capital stock is given by a proportion relative to the initial capital stock which implies that capital stock grows at some exogenous rate. Stoleru (1965) introduces the terminal condition that capital stock growth rate after T equals the exogenous rate of labor force (i.e., population). Manne (1970) formulates sufficient conditions for any planning problem to provide a solution which is not only optimal for a horizon T , but is also optimal for all finite horizon greater than T .

Barr and Manne (1967) assume that at the terminal period T , the economy is at the steady state where the growth rate is g_y . Under these assumption, expression (28) can be written as,

$$\max_{c_t} W = \sum_{t=0}^{T-1} \left(\frac{1}{1+\rho} \right)^t U(c_t) + \sum_{t=T}^{\infty} \left(\frac{1}{1+\rho} \right)^t U(c_t(1+g_y^{t-T})) \quad (29)$$

where the second term is a constant. Abstracting from the constant term, the maximization problem can be written as,

$$\max_{c_t} W = \sum_{t=0}^{T-1} \left(\frac{1}{1+\rho} \right)^t U(c_t) + \frac{1+\rho}{\rho(1+\rho)^T} U(c_T) \quad (30)$$

$$\max_{c_t} W = \sum_{t=0}^T \hat{\beta}^t U(c_t) \quad (31)$$

where the discount factor would be,

$$\hat{\beta}^t = \begin{cases} \left(\frac{1}{1+\rho} \right)^t & \text{for } t < T \\ \frac{(1+\rho)^{1-T}}{\rho} & \text{for } t = T \end{cases} \quad (32)$$

At the terminal period, gross investment is determined by the size of capital stock in the terminal period, the exogenous growth rate (all quantities growth at the same rate in the steady state), and the capital depreciation rate. The constraint of investment would be,

$$i_T = (g_y + \delta)k_T \quad (33)$$

Rutherford (1995) and Lau, Pahlke and Rutherford (2002) propose the use of a terminal condition for investment to assure steady-state growth in the post-terminal period that does not require the specification of an ex-ante growth rate at the final period T , and instead assumes that investment growth rate is equal to the output (or consumption) growth rate. Formally,

$$\frac{i_T}{i_{T-1}} = \frac{y_T}{y_{T-1}} \quad (34)$$

where i_t is investment and y_t is output.

This is the strategy we follow for the baseline solution of the model, by combining the discount factor given by expression (32), with the following two investment constraints for Earth and space capital, respectively,

$$i_T \geq (g_y + \delta_k)k_T \quad (35)$$

and

$$h_T \geq \frac{(g_y + \delta_s)s_T}{q_T} \quad (36)$$

4. MODEL PARAMETERIZATION, DATA, AND CALIBRATION

This section describes the parameterization of the model, the data used for setting the initial values for the relevant variables in the base period and for the calibration of the parameters of the models. A full description of the procedure can be found in the appendix.

4.1 Model parameterization

We solve a deterministic version of the model by assuming perfect-foresight. There is a continuum of identical households, each of whom has preference that are characterized by the following instantaneous constant relative risk-aversion (CRRA-type) utility function,

$$U(c_t, N_t) = \left(\frac{\hat{c}_t^{1-\sigma} - 1}{1-\sigma} \right) \quad (37)$$

where the parameter $\sigma > 0$ represents the intertemporal marginal consumption elasticity also equal to the relative risk aversion. The parameter σ can also be interpreted as a measure of social aversion to changes in consumption (Nordhaus, 1993).

It is assumed that the production function is of Cobb-Douglas type with constant returns to scale, where labor equals population,

$$y_t = a_t k_t^{\alpha_1} s_t^{\alpha_2} N_t^{1-\alpha_1-\alpha_2} \quad (38)$$

where $0 < \alpha_1, \alpha_2 < 1$, are the elasticities of output with respect to Earth capital and space capital, respectively.

4.2 Data and initial values

For the numerical simulation of the model we consider the year 2023 as the initial period. Initial values for the base year are taken from variety of data sources (see appendices A and B), comprising economic databases from the World Bank, International Monetary Fund (IMF), Penn World Table (PWT), Bureau of Economic Analysis (BEA), and United Nations, and space activity databases from NASA, ESA, Union of Concerned Scientists, (UCS), Space-Track (US Space Forces), Satellite Industry Association (SIA), Space Foundation, and Jonathan C. McDowell databases.

Population (labor) for the year 2023 is taken from the United National Population Unit, with a value of 8,056 million and an asymptotic population value of 10,200 million. Initial value for World GDP is taken from the World Bank Economic Indicators, and takes a value of 184.65 trillions in 2023 international US\$. World capital stock is taken from the IMF Investment and Capital Stock Dataset, 1960-2019, as the sum of private and public capital for the year 2019, with a value of 316.25 in trillions 2017 international US\$. The corresponding figure from the PWT is higher, 535,12 trillions 2017 international US\$. Comparing both databases, we find a large difference in the estimates for the capital stock. Using data from the IMF, the World capital/GDP ratio is 2.55, whereas using the PWT, the ratio is 4.26. Given that difference, we choose a middle value for the capital stock to output ratio of 3. Therefore, initial value for the capital stock is 553.95 trillions international US\$

for the capital stock. We split this figure between Earth capital and space capital using the shares and depreciation rates for each type of capital asset in steady state. Hence, initial Earth capital stock is estimated to be 552.23 trillions and initial space capital is 1.72 trillions international US\$. These values means that the ratio of space capital to Earth capital is 0.0031. Launch cost varies depending on the type of satellite and the orbit, ranging from a 10% to 60% of total cost. Initial launch cost as a fraction of space capital investment is fixed to be a 30% of total investment ($b_{2023} = 0.30$).

Initial values for space variables are the following. The number of launches in 2023 was 217. The number of operational satellites in Earth orbit in 2023 resulting from the simulation of the equation of the model for the period 1957 to 2023 is of 8,391. This figure is similar to the one estimated by ESA for December 2023 of around 8,500 operational satellites. Initial value of derelict satellites in orbit and rocket bodies have been estimated by using the accumulation equations of the model for the period 1957 to 2023. The estimated number of derelict satellites in orbit for the year 2023 is 3,524, whereas the estimated number of rocket bodies is 2,050 (see Appendix A). The total number of pieces of debris tracked by the United States Space Surveillance Network (SSN) is 31,150. Most of the activity takes place at Low-Earth-Orbit (LEO, between 200 and 2,000 km), and at Geostationary Orbit (GEO, at 35,786 km). The standard classification of orbital debris is a function of its size and on the technical possibility of tracking it. Projections obtained using different models for debris (for example, the ESA's MASTER (Meteoroid and Space Debris Terrestrial Environment Reference) model, or the NASA's LEGEND (LEO-to-GEO Environment Debris Model) have estimated amounts of around 36,500 pieces of debris larger than 10 cm diameter, 1,000,000 objects between 1 cm and 10 cm, and over 130 millions fragments between 1 mm and 1 cm.

4.3 Calibration of economic parameters

The calibration of economic parameters corresponds to the World economy. It is true that the US is the absolute leading spacefaring country. Private spacefaring firms are also dominated by US companies such as SpaceX. However, an increasing number of countries are also developing space industries and gaining spacecraft launch capabilities, and consumers of satellite services are worldwide. Therefore, the model is calibrated to an artificial world economy, where outer space is an international common (Hardin, 1968).

Only a few economic parameters must be calibrated, namely the social intertemporal preference parameter, the relative risk aversion parameter, the technological parameters of the production function, and the depreciation rates for physical capital and satellites. For that set of parameters, we use standard values from the literature. Additionally, the model includes two technological growth processes: total factor productivity, and investment-specific technological change in satellites (see appendices C and E for additional details).

Preference parameters are calibrated as follows. In the literature, the intertemporal marginal consumption rate σ takes values between 1 (a logarithmic instantaneous utility function) and 3. For example, Stern (2006) uses a value of 1, Nordhaus (2008) uses a value of 1.5, whereas Nordhaus (2017) uses a value of 2. Here, we fixed the value of σ to 1.5 in the baseline calibration. For calibrating the pure intertemporal preference parameter, that

is, the social discount rate, we rely on the values used in the climate-change literature. The values move between the 2% per year used by Weitzman (2007) and the 0.1% used by Stern (2006). With a CRRA instantaneous utility function, we have that $r_t = \rho + \sigma g_{c,t}$, where r_t is the discount rate and $g_{c,t}$ is the growth rate of consumption. With a steady-state consumption growth of 2% and a relative risk aversion parameter of 2, the discount rate ranges between 6% (Nordhaus, 2017) and 4.1% (Stern, 2006), values that are consistent with those used in standard dynamic stochastic general equilibrium macroeconomic models. For the baseline calibration, we fix the value of ρ to be 1.5% per year, as in Nordhaus (2008).

Second, for the calibration of technological parameters, we proceed as follows. First, we fixed the labor share to be 0.65. This means that, given the assumption of constant returns to scale, the sum of the technological parameters for Earth capital and space capital is 0.35 (i.e., $\alpha_1 + \alpha_2 = 0.35$). Corrado et al. (2023) calibrate the space sector share on the whole economy on 0.0056. The Bureau of Economic Analysis (BEA, 2023) estimates that space industry contributed to 129,9 billion dollars to the US economy in 2021 (0.6% of GDP), with a total of 360,00 full- and part-time jobs in the private space industry. Space Foundation (2023) estimates that the global space economy has an impact of \$546 billion for the year 2022. Satellite Industry Association (SIA, 2023) estimates that the global space economy accounts for \$384 billions for the year 2022. Using this information we split the capital share between Earth capital and space capital. The elasticity of output with respect to satellites equipment is calculated as $\alpha_2 = 0.35 \times 0.006 = 0.0021$. Hence, the elasticity of output with respect to Earth capital is $\alpha_1 = 0.35 - 0.0021 = 0.3479$. Nozawa et al. (2023) calibrated a Cobb-Douglas production function with labor, capital and satellites, and they use a value of 0.002 for the elasticity of output to the stock of satellites. The depreciation rate of capital other than satellites, δ_k , is fixed to a standard value of 0.07. For calibrating the depreciation rate of satellites we use data from NASA. The life-span depends on the type of satellite, and varies from 6 months for CubSats (miniaturized satellites) to 15 years of GEO satellites. For LEO satellites the life-span varies from 3 to 8 years. Bongers and Torres (2023) assume an average lifetime of 8 years, so the annual depreciation rate for satellites is fixed to 0.1733, whereas Nozawa et al. (2023) fixed a value of 0.216. Here, we calibrated this parameter by simulating the satellites accumulation equation for the period 1957-2023, to match the estimated number of operational satellites in 2023 by the ESA of around 3,500. The resulting value for δ_s is of 0.15.

Next, we calibrate the parameters driving the evolution of exogenous sources of growth. Initial TFP growth rate in the year 2023 is assumed to be 1.5% per year. We assume that TFP growth rate decays at a rate of 0.1% per year. Initial value for TFP is calculated as the ratio of initial output, over the combination of initial values for the three inputs. For the ISTC to satellites we proceed in a similar way. Initial ISTC growth rate is fixed to be 3% with a decay rate of 0.5% per year. Regarding launch cost, we assume that initial cost growth rate is -0.5%, with a decay rate of 0.1%. Finally, the conversion parameter is calculated as the ratio of initial number of active satellites in orbit over the value of the stock of active satellites (in trillion US\$), resulting in a value of $\mu = 4,941.9$.

	Parameter	Definition	Value	Source
Economy	ρ	Pure preferences parameter	0.015	Nordhaus (2008)
	σ	Risk aversion parameter	1.500	Nordhaus (2008)
	α_1	Capital share	0.3479	BEA
	α_2	Satellite share	0.0021	BEA
	δ_k	Capital depreciation rate	0.07	Standard
	δ_s	Satellite depreciation rate	0.15	NASA
	$g_{a,0}$	Initial TFP growth rate	0.015	Assumption
	$g_{q,0}$	Initial satellite ISTC growth rate	0.030	Assumption
	δ_a	TFP growth decay rate	0.001	Assumption
	δ_q	ISTC growth decay rate	0.005	Assumption
	$g_{b,0}$	Launch cost change	-0.05	Assumption
	δ_b	Launch cost change decay rate	0.01	Assumption
	ζ	Population growth parameter	0.05	United Nations
	μ	Conversion parameter	4,941	Internal
Space	η	Satellites per launch	13.6	NASA
	θ	Collision risk parameter	1.25×10^{-10}	ESA
	χ	Fraction of abandoned satellites	0.40	ESA
	δ_f	Fragment natural decay rate	0.01	NASA
	δ_w	Derelict satellites natural decay rate	0.00015	Lafleur (2011)
	δ_z	Rocket bodies natural decay rate	0.00015	Lafleur (2011)
	ε_w	Fraction of dead satellites breakups	0.0010	NASA
	ε_z	Fraction of body rocket breakups	0.0012	ESA
	φ	Body rockets per launch	0.60	ESA
	ω	Fragments > 10 cm per launch	4	ESA
	ϕ_w	Fragments > 10 cm per derelict satellite breakup	44.6	ESA
	ϕ_z	Fragments > 10 cm per rocket body breakup	100.2	NASA/ESA
	γ_s	Fragments > 10 cm per operational satellite collision	70	NASA/ESA
	γ_w	Fragments > 10 cm per derelict satellite collision	70	NASA/ESA
γ_z	Fragments > 10 cm per rocket body collision	70	NASA/ESA	

TABLE 1. Baseline calibration of the parameters of DISE-2024

4.4 Calibration of physical parameters

The calibration of the physical parameters is as follows (see appendix D for additional details). First, the number of satellites per launch is calibrated by dividing the number of new satellites launched on the number of launches for the base year. Number of launches in 2023 was 217, inserting into orbit a total of 2,950 satellites. The relationship between launches and new satellites in orbit is changing dramatically nowadays due to the use of small and micro satellites, and to the higher power and payload capacity of launch systems. We simply assume that this proportion remains fixed for the future, resulting in $\eta = 13.6$. The debris fragments decay rate (δ_f) is a function of altitude. The decay rate of debris depends on several factors, including the altitude, mass, area, solar radio flux, circularity of the orbit, and geomagnetic index. The Australian Space Weather Agency (1999) estimated that the lifetime of space objects varies from 1 day at 200 km, 1 month at 300 km, 1 year at 400 km, 10 years at 500 km, 100 years at 700 km, and 1000 years at 900 km (King-Hele, 1987). On the other hand, the distribution of debris as a function of altitude is

not homogeneous. The spatial density of debris shows that it is concentrated in the range 700-900 km (NASA, 2020).

For calibrating this parameter we take into account the current distribution of objects in orbit, where most activity is concentrated at an altitude of 550 due to the Starlink satellite constellation, and that Starlink sub-constellations are planned for 340 km and 1,200 km. Also, it is important to take into account that the OneWeb satellite constellation (currently there are 658 satellites in this constellation) orbit at an altitude of 1,200 km, where the lifetime of debris is of thousands of years. In the literature, we find alternative calibrated values for the debris decay rate. For instance, Nozawa et al. (2023) use a value of 0.0067, taken from Bongers and Torres (2023) who assume an average lifetime of around 150 years, a value similar to the one estimated by Lewis et al. (2009) of 0.0062 in the Fast Debris Evolution (FADE) model, whereas Rao and Rondina (2025) consider a value of 0.074. Lafleur (2011) calculates an average debris decay rate for objects in LEO (up to 2,000 km) using the ballistic coefficient for a value of 1.8 kg/m^2 as an approximate value for fragments, from which he calculates the drag coefficient for the solar-maximum and the solar-minimum conditions. Values are weighted by the distribution of objects at different orbit altitudes. At the solar-maximum conditions, the average lifetime of debris fragment is of 46.9 years (a decay rate of 0.021), whereas at the solar-minimum conditions, the average lifetime of debris fragments is of 332.8 years (a decay rate of 0.003), resulting in a mean value for the decay rate of 0.012 for LEO. Based on that information, in the baseline model we use a value of $\delta_f = 0.01$, that is, a debris decay rate of 1% per year, which approximately corresponds to an average orbit of about 750 km.

The natural decay rate of derelict satellites (δ_w) and rocket bodies (δ_z) is usually lower than that of fragments, due to the surface and mass of intact objects. Natural decay rate is heavily affected by the mass-to-surface ratio of the objects. Lafleur (2011) estimates that fragments have a mass-to-surface ratio of 1.8 kg/m^2 , whereas satellites have a ratio of 110 kg/m^2 . Using the weighted distribution of satellites at different orbit altitudes, Lafleur (2011) estimates that the average lifetime of derelict satellites ranges from 3,990 years (a decay rate of 0.00025 for solar-maximum conditions) to 24,850 years (a decay rate of around 0.00004 at solar-minimum conditions), resulting in a mean value for the natural decay rate of satellites at LEO of 0.000145. We assume that mass-to-surface ratio for rocket bodies is similar, and hence, $\delta_w = \delta_z = 0.00015$.

To calibrate the risk of collision (θ), we consider the population of pieces of debris larger than 1 cm, as they can cause deadly damage to a satellite. In the history of activity in outer space, a number of collisions, confirmed or suspected, between operational satellites and orbital debris have been reported. A risk of collision between operating satellites also exists, but in some cases they can be avoided by maneuvering, although there is a large number of satellites with slow or not maneuver capability. Farinella and Cordelli (1991) estimated a value of $\theta = 3 \times 10^{-10}$, for an estimated quantity of debris of 50,000. This means a number of satellite destroyed per year of 0.2, given a probability of collision ($\theta \times 50,000$) of 1.5×10^{-5} . Kawamoto et al. (2019) estimated that the current probability of collision is much higher. The total probability of collision of objects larger than 10 cm is around 0.1 for 800-900 km orbits, 0.05 for 900-1,000 km orbits, and 0.025 for 600-700 km orbits. Following Farinella and Cordelli (1991) we take the estimation of a total probability

of collision of 0.2 (i.e., one fatal collision every 5 years) as the reference, given the number of incidents observed during the last years (four collisions occurred in the period 1991 to 2009), resulting in a the probability of collision is $\theta \times D = 6.6 \times 10^{-5}$. Lafleur (2011) estimates a value of $\theta = 6.895 \times 10^{-10}$. Percy (2015) estimates a value of $\theta = 6.37 \times 10^{-10}$. Bongers and Torres (2023) estimate a value of $\theta = 6.37 \times 10^{-11}$, and Guyot and Rouillon (2024) use a value of $\theta = 4 \times 10^{-10}$. Here we use a value of 1.25×10^{-10} , which implies a probability of collision of $\theta \times D_{1,t} = 1.25 \times 10^{-4}$ (a fatal collision every five years).

Operational life of satellites is relatively short (a few years). Defunct satellites abandoned in orbit are another source of orbital debris. This occurs when satellites run out of fuel and cannot be moved to graveyard orbits. Once they are not-operational any more, they automatically represent a debris if remain in orbit. This was quite a common occurrence during the first stages of space conquest. Abandoned satellites pose considerable risk, given their mass. Indeed, one of the most harmful incident was the collision of the derelict *Kosmos-2251* with the operational *Iridium-33* in February 2009. The number of abandoned satellites is small relative to that of other forms of debris. Given the current tracked number of derelict satellites in orbit by NASA (3,524 in the year 2023), we estimate the fraction of abandoned satellites (χ) to be 0.40. However, with the pass of the years, increasing concerns about this practice has reduced the number of fraction derelict satellites in orbit. Additionally, new international standards for spacefaring countries and firms consider the necessity of including reserve fuel for de-orbiting maneuvers. Therefore, it is expected that the number of derelict satellites that are abandoned in orbit will tend to zero over time. The fraction of rocket bodies per launch (φ) left in orbit is estimated to be 0.6, to match the number of rocket bodies abandoned in orbit in the year 2023 (See McDowell, 2024). The fraction of dead satellites breakups (δ_w) and the fraction of rocket bodies breakups (δ_z) are calibrated to match the number of derelict satellites and rocket bodies estimated by NASA and ESA for the year 2023. Values are 0.001 and 0.0012, respectively. The number of pieces of debris per launch (ω) is the primary source of debris generation. This parameter includes only parts discarded in the process of inserting a satellite into the target orbit excluding rocket bodies. To match the number of tracked objects in orbit by NASA, we calibrate this parameter to represents debris larger than 10 cm (tracked debris), resulting in a value of 4. Indeed, all the parameters in the law of motion of fragments are calibrated considering fragments larger than 10 cm. Then, we multiply the number of fragments larger than 10 cm for the proportion of fragments larger than 1 cm.

Finally, the number of fragments per collision of operational satellites, derelict satellites and rocket bodies (γ_s , γ_w , and γ_z , respectively) and the number of fragment per breakup of derelict satellites and rocket bodies (ϕ_w and ϕ_z , respectively) are calibrated using estimations about the number of fragments from explosions and collisions. To calibrate these five parameters, we primarily used the NASA Breakups Database compiled by Anz-Meador et al. (2022). This report documents on-orbit breakups, collisions, and other anomalous events involving satellites, rocket bodies, and ullage motors through 15 April 2022. It includes information on the causes of fragmentation and the number of cataloged debris objects. In total, the report records 268 fragmentation events and 87 anomalous events. The fragmentation events are categorized as follows: 6 debris-causing collisions,

83 rocket body breakups, 7 anti-satellite tests, 53 ullage motor breakups, 51 satellite self-destructions, and 68 fragmentation events involving satellites or other spacecraft with unknown causes.

According to the NASA's breakups database (Anz-Meador et al., 2022), the number of collisions registered has been of 6, producing a total of 2,430 cataloged debris (an average of 347 pieces of debris per collision), although there is a total of 67 unknown breakup events producing a total of 3,436 cataloged debris (an average of 51 pieces per event). In the DISCOS database, the number of collisions between operational satellites and pieces of debris is 5, and the average number of cataloged fragments is of 483.6. Farinella and Cordelli (1991) assume an average of two unintentional explosions per year, each creating a few thousand fragments of mass greater than 1 gram, producing 70 new pieces of debris larger than 10 cm, resulting in a total number of new pieces of debris of 2,059 larger than 1 cm.¹⁰ Johnson et al. (2001) used the NASA Breakup model EVOLVE 4.0 to estimate the number of new fragments from an explosion: 238 larger than 10 cm and 9,509 larger than 1 cm. Lewis et al. (2009) estimated that the number of fragments larger than 10 cm generated by an explosion is 50 and that an average of 2.75 intact objects are added to the environment per launch. Lewis et al. (2009) found that the number of pieces of debris per catastrophic collision is 625 (collision with debris larger than 10 cm) and 25 for a damaging collision (collision with debris between 1 and 10 cm). Given that the probability of collision is calibrated for debris larger than 1 cm, and that the estimated number of pieces of debris between 1 cm and 10 cm is 1,000,000 to an estimated number of pieces of debris larger than 10 cm of 36,500, using the amount of debris per collision estimated by Lewis et al. (2009), this implies that the number of pieces of debris larger than 1 cm resulting from a catastrophic collision is 17,748, and 710 in the case of a non-catastrophic collision. The NASA Standard Breakup model calculates the number of fragments created from the collision between two objects depending on the size and the mass, based on laboratory hypervelocity impact experiments. Johnson et al. (2001) show that results are similar from both models for a mass of the two objects of 1,260kg for a catastrophic collision. This mass is not so different from the average mass of a medium satellite (Bryce, 2020). Assuming that the probability of collision is independent of the size of the debris, the final estimation is 1,309 pieces of debris per collision. This figure is not so different from the number of pieces of debris resulting from accidental explosions. From this information we assume $\gamma_s = 70$.

For calibrating the parameters γ_w and γ_z , due to lack of data, we assume that the number of debris produced by collision of derelict satellites and rocket rocket bodies is the same as for operational satellites. Derelict satellites have the same characteristics as operational satellites. Therefore, in case of collision, they will be fragmented in a way similar to that of the rest of the operational satellites. For the number of fragments per rocket body collision, we follow Kessler et al. (2010) and assume that they are equal to a payload collision, that is, $\gamma_z = 70$. Given the differences in mass and size between rocket bodies and satellites, we could expect a different fragmentation behavior in the event of

¹⁰Only 3.54% of the estimated pieces of debris are larger than 10 cm. The remaining 96.36% are between 1 cm and 10 cm. If an explosion produces 70 pieces of debris larger than 10 cm, the total number of pieces larger than 1 cm is estimated to be $70/0.034 = 2,059$.

a collision.¹¹ The source for the calibration of this parameter is Anz-Meador et al. (2022). However, there is only one collision between a rocket body (DMSP-5B-F5 Thor-Burner 2A rocket) and other debris on January 2005, producing 5 cataloged debris. Another collision was deliberate (the collision of USA-19 with the upper stage of USA-19), with the fragmentation of USA-19 in 13 cataloged debris and the fragmentation of the rocket body in 5 cataloged debris. However, we consider that this evidence is not representative given the size and mass of rocket bodies. As no additional information is available, we assume that the number of debris produced by the collision of a rocket body with other piece of debris is equal to the one produced by the collision of a satellite.

Finally, for the calibration of the amount of debris produced by derelict satellites breakups ϕ_w , in the NASA's breakups database (Anz-Meador et al., 2022) there is a total of 47 satellite breakups until 2022 (although one was an operational satellite), excluding deliberate destruction events by anti-satellite tests or by self-destruction with an explosive charges. These breakups are mainly due to unknown causes (36 out of 47). In other cases, the detected cause is battery explosion (9 confirmed cases), and due to propulsion (2 confirmed cases). The number of cataloged debris produced by these satellite breakups is of 2,289, an average of 49.3 cataloged fragments per event. Excluding the breakup of an operational satellite, the average cataloged fragments per derelict satellite breakup event is 44.6 ($\phi_w = 44.6$). For the calibration of the number of fragments per rocket body breakup (ϕ_z), as for the previous parameter, we use the information in Anz-Meador et al. (2022) about breakup events of rocket bodies and the number of debris produced. This database contains a total of 83 rocket body breakups, producing a total of 8,315 pieces of cataloged debris, an average of 100.2 pieces of debris per rocket body breakup. Therefore, we fix $\phi_z = 100.2$.

5. POLICY EXPERIMENTS

This section outlines the various policy experiments conducted using the calibrated DISE-2024 model. The model is specifically designed to capture the interactions between the economy and the space environment, where economic growth and the accumulation of orbital debris are interdependent. Across all scenarios, we assume the presence of a central planner who seeks to maximize social welfare by internalizing the negative externalities associated with orbital debris. The scenarios explored are based on the non-binding debris mitigation guidelines established by the United Nations and various national space agencies. These experiments focus exclusively on policies aimed at reducing debris emissions

¹¹Kessler et al. (2010) indicate that whereas a number of tests have been conducted to understand the size distribution from the collision of a payload, none have been conducted on rocket bodies, and the standard assumption in breakups models is that payloads and rocket bodies fragment under identical conditions and produce identical fragment distribution. However, as these authors note, the large tanks on rocket bodies may not absorb all the energy from a collision. Alternatively, they may dissipate the energy across the opposite tank wall, functioning similarly to a Whipple shield. Consequently, it remains uncertain whether a rocket body collision would generate more or fewer fragments than a satellite collision. We conducted a sensitivity analysis using a range of values from 50 to 200 for the number of fragments resulting from rocket body collisions. The trajectories of the variables exhibit similar patterns, and the conclusions remain consistent, although the rate of debris accumulation increases as the parameter value rises.

by imposing some limitations on orbit operational activities. To achieve this, the central planner utilizes a range of policy instruments, including the enforcement of standards for satellite design, launch vehicles, and operational procedures.

For the design of the different scenarios we take into account last movements in international organizations and space agencies regarding the issue of orbital debris. Different national space agencies and the United Nations have proposed a number of debris mitigation guidelines, although they are not binding. These guidelines encourage government space agencies and private spacefaring firms to adopt best practices when designing spacecraft and launch systems to minimize or eliminate debris generation. The United Nations Inter-Agency Space Debris Coordination Committee (IADC) established in 2007 the Space Debris Mitigation Guidelines, collecting previous debris mitigation guidelines elaborated by the different national space agencies. A list of seven guidelines are recommended to be considered for the mission planning, design, manufacture, and operational phases of spacecraft and launch vehicle orbital stages. These guidelines are the following: i) limit debris released during normal operations; ii) minimize the potential of breakups during operational phases; iii) limit the probability of accidental collision in orbit; iv) avoid intentional destruction and other harmful activities; v) minimize the potential for post-mission breakups resulting from stored energy; vi) limit the long-term presence of spacecraft and launch vehicle orbital stages in the low Earth orbit (LEO) region after the end of their mission; and vii) limit the long-term interference of spacecraft and launch vehicle orbital stages with the geosynchronous Earth orbit (GEO) region after the end of their mission. In a more ambitious further step, the ESA has recently adopted a "Zero Debris approach", first outlined in their Agenda 2025, which aims to significantly limit the production of debris in Earth and lunar orbits by 2030 for all of the ESA's future missions. See Spencer et al. (2025) for an evaluation of the degree of compliance to the debris mitigation guidelines.

The detailed physical sub-model incorporated in this study allows for a thorough examination of the implications of the strategies outlined in the orbital debris mitigation guidelines. Each scenario assumes that the central planner enforces these guidelines as mandatory. It is assumed that the mandatory debris mitigation guidelines are implemented at no cost. This assumption is similar to the standard "technological breakthrough" scenario used in climate-change economics, where it is assumed a geoengineering option that can offset global warming at no cost. We decided to adopt this assumption as the studied debris mitigation guidelines are already implemented by a private spacefaring operator: SpaceX. SpaceX's derelict satellites are deorbited, and the second stage of its Falcon 9 rocket is also deorbited once the payload has been inserted into orbit. Additionally, they operate a fully reusable launch system (*Starship*), and the satellites of the Starlink constellation perform collision avoiding maneuvers. For simplicity, all scenarios are simulated starting in 2024; however, the simulation framework allows the initiation of each scenario at any point in the future. The policy scenarios investigated are the following:

5.1 *Baseline scenario: No intervention*

This is the baseline scenario for alternative policies comparison. In this scenario there is a central planner that maximize social welfare, but no direct instrument to mitigate orbital

debris is available. This means that no debris mitigation policy is used and no mandatory debris mitigation guideline is enforced. Nevertheless, in this scenario the social planner fully internalize the orbital debris externality by choosing the optimal investment in Earth and space capital. This means that trajectories of the variables are optimal given the effect of the economy on the space environment. Climate-change literature usually identifies this scenario with the BAU (business-as-usual) case. Nordhaus (2008) interprets this scenario as a situation in which households and firms adapt to the environment but governments take no action to mitigate emissions or to internalize the environmental negative externality. However, as shown by Shiell and Lyssenko (2008) this is a social optimum solution in which the externality is fully internalized, even without policy instruments.

5.2 Reusable launch systems

Traditional launch vehicles are formed by two-to-four stages. Rocket bodies and engines of the last stages usually are not reusable and remain in orbit, being a big piece of orbital debris with a large risk of breakup due to internal explosions or collision with other objects. However, the entry in the orbital market of private firms has accelerated cost-reduction research investment, focusing on the development of partial or full-reusable launch systems. Rockets are expensive and hence there are incentives for the industry to develop fully reusable launch vehicles. An example of this new technology is the SpaceX reusable launch system program with the *Starship*. The first partially-reusable but almost debris-free launch system was the Space Shuttle (first flight April, 1981).¹² Nowadays, all space operators are developing or already using some type of reusable launch system. Therefore, it is expected that in the near future leading space operators will use totally reusable launch systems which would have a significant impact on the production of debris directly related to launches.¹³

This scenario represents a situation in which no upper stages of launch vehicles remain in orbit after releasing the payload. For simulating this scenario, the parameter φ , the ratio of rocket bodies in orbit per launch, is fixed equal to zero. Hence, no additional rocket body is left in orbit. This means that in the long-run, the stock of rocket bodies tends to zero through the natural process of decay or due to internal explosions and collision breakups.

¹²The NASA Space Shuttle was attached to a liquid oxygen and hydrogen tank and two solid rocket boosters. In a first stage, once solid combustible is exhausted, the two solid rocket boosters parachute into the ocean to be reused again. In a second state, once exhausted, the oxygen and hydrogen tank is jettisoned and breakup in the atmosphere ending in the ocean. Payloads (satellite or other spacecraft) are inserted in orbit using a robotic arm. Once the mission is finished, the orbiter vehicle returns to the Earth. The Space Shuttle program was designed to reduce costs of launch systems by reusing the orbiter vehicle. However, after two dramatic life-costly accidents (1986 and 2003), and due to high costs, the Space Shuttles were retired from service in 2011.

¹³A debris-free launch system does not necessarily mean a reusable launch system. Falcon-9 is an almost debris-free launch systems, but the second stage of the rocket is not reusable. Indeed, the initial plan of SpaceX was to reuse also the second stage of Falcon-9. The motor of the second stage of the Falcon-9 rocket was designed to be reusable but the additional mass of the required heat shield, and the need of low-powered landing engines and other landing mechanisms, forced SpaceX to abandon the project of making Falcon-9 fully reusable, not because of the financial costs, but due to the great performance penalty it implies. Other spacefaring companies have plans for the development of fully reusable launch vehicles, such as Stoke Space.

5.3 *De-orbiting policy*

In this scenario, we examine the mandatory de-orbiting of end-of-life satellites and rocket bodies once their payloads have been delivered into orbit. A major sources of orbital debris are derelict satellites that have reached the end of their operational lifespan and upper-stage rocket bodies. Many satellites become uncontrollable after depleting their fuel, rendering them unable to maneuver and effectively abandoning them in orbit. Similarly, in most cases, the final stage of a launch vehicle remains in orbit after releasing its payload. These pieces of debris are large and can be tracked by surveillance systems, but they still pose significant risks. Some have caused collisions in the past, and they present an additional threat as they can break up into thousands of fragments. Extreme conditions in space degrade components such as mechanisms, batteries, and tanks of chemicals, often leading to explosions. Debris mitigation guidelines recommend the de-orbiting of both non-operational satellites and rocket bodies, a process known as post-mission disposal (PMD). PMD involves the planned management and mitigation of mission-related remnants after the completion of their operational lifespan. It can include either guiding the spacecraft to re-enter Earth's atmosphere, controlled or uncontrolled, or, at higher altitudes, relocating the spacecraft to a stable "graveyard orbit" to prevent interference with active systems.

Debris mitigation guidelines have introduced a time limit for removing derelict satellites and rocket bodies from orbit, commonly referred to as the 25-year rule, proposed by the Inter-Agency Space Debris Coordination Committee (IADC) in 2002. This rule stipulates that satellites, rocket stages, and other spacecraft components in Low Earth Orbit (LEO) should be removed from their operational orbits within 25 years after the end of their mission. However, this 25-year timeframe has been widely criticized as too long to effectively mitigate the accumulation of orbital debris. Some countries and organizations have advocated for stricter requirements, proposing a mandatory disposal deadline and a significant reduction in the deorbit timeframe to 5 years. These calls for more stringent measures are driven by growing concerns over the anticipated launch of thousands of short-lived satellites in tightly packed mega-constellations over the coming years. Spencer et al. (2025) shows that the post-mission disposal success rate is well below the recommended practices, and that the current PMD success rate is below 50% in LEO and around 90% in GEO, leaving in space a large number of defunct and uncontrolled satellites or launcher bodies. Rao et al. (2023) study the implications of a disposal time of 5 years and compare the results with the 25-year de-orbit guideline.

Implementing a compulsory deorbiting rule would require new spacecraft to incorporate robust and reliable deorbit systems. Passive disposal strategies, which rely on atmospheric drag to naturally deorbit satellites, are particularly appealing because they do not depend on spacecraft propulsion systems—a significant advantage for many small satellites in LEO that lack onboard propulsion. Recent advancements in miniaturized propulsion technologies, however, are making it increasingly feasible to equip small satellites with active deorbiting capabilities. The inclusion of propulsion systems is becoming a standard feature for small satellites in commercial constellations, such as SpaceX's Starlink, where collision avoidance and orbital management are critical for their operations.

In this scenario, we run the model by considering a mandatory 1-year post-mission disposal rule for both satellites and upper stage rocket bodies. This means that satellites and upper stage rocket bodies must have all necessary devices, including a reserve fuel, for successful PMD. Simulation of this scenario implies that $\chi = 0$, for the de-orbiting of end-life satellites, and $\varphi = 0$ for the de-orbiting of upper stage rocket bodies, as in previous scenario.

5.4 *No breakups*

A significant secondary source of debris generation arises from the breakup of large objects such as derelict satellites, rocket bodies, and engines from the final stages of launch vehicles. This is an on-orbit endogenous driver of orbital debris accumulation. On-orbit breakups of large objects are critical events that exacerbate the growing issue of space debris. With thousands of inactive satellites and spent rocket stages orbiting Earth, the risk of fragmentation is considerable. Over time, these objects degrade under the harsh conditions of space, including exposure to radiation and extreme temperature fluctuations. Many rocket stages and satellites contain unspent fuel, pressurized tanks with chemical components (e.g., hydrogen, helium, oxidizers), and batteries. Prolonged exposure to the space environment can cause material degradation, leading to ruptures in tanks or explosions in batteries, resulting in the fragmentation of these objects. For example, the first recorded breakup event occurred in 1961, when a U.S. upper-stage rocket exploded, creating nearly 300 large debris fragments (NASA, 2011). As of September 20, 2024, the ESA's Space Debris Office estimates that over 650 breakups, explosions, collisions, or other anomalous fragmentation events have occurred.

The probability of on-orbit breakups of satellites and rocket bodies is closely tied to their design. In this scenario, it is assumed that standards are introduced for the design of satellites, rocket engines, and pressurized tanks to enhance their structural integrity and reduce the risk of breakups. While no compulsory deorbiting policy is implemented, these design improvements make satellites and spent rocket engines more resistant to the space environment, thereby minimizing failures caused by fuel residues or battery malfunctions. Additional preventative measures, such as passivation techniques, play a crucial role. Passivation involves eliminating leftover energy sources, such as residual propellants in tanks, depressurizing pressurized systems, and discharging batteries to prevent accidental explosions. In this scenario, these measures are assumed to significantly reduce fragmentation risks. To model this scenario, the parameters for satellite and rocket body breakups are set to zero ($\varepsilon_w = 0$ and $\varepsilon_z = 0$), effectively simulating a situation where such events do not occur.

5.5 *Debris-free launch systems*

This scenario combines the use of reusable launch vehicles with adherence to debris mitigation guidelines related to mission-related debris (MRO). We assume a situation where technological advancements enable the development of debris-free launch systems, or regulatory authorities mandate the exclusive use of such launch vehicles. In this scenario, all stages of the launch vehicles are recovered, as in the reusable launch vehicle

scenario. Additionally, payload deployment occurs without generating mission-related debris. Debris-free launch systems are not entirely new. A notable example is NASA's Space Shuttle program, where the orbiter vehicle returned to Earth, landing like an airplane after completing its mission. Payloads were deployed into orbit using a robotic arm, eliminating the release of debris during the process.

To simulate this scenario, the parameter ω , representing the number of mission-related debris generated per launch, and the parameter φ , representing the ratio of rocket bodies left in orbit per launch, are both set to zero. As a consequence, in this scenario debris emissions are not directly related to the number of launches.

5.6 No collision

Collision of orbital debris with satellites is another source of debris emission. On the other hand, collision avoidance operations are a critical aspect of satellite mission management. With the growing number of satellites and increasing space debris, these operations are becoming more complex and essential. The success of these operations depends on accurate tracking, effective communication, and timely decision-making, supported by both international collaboration and advanced technologies. In this scenario, it is assumed that all satellites and other spacecraft have maneuver capabilities, tracking system can alert of possible collisions and are conducted collision avoiding maneuvers. Monitoring and tracking orbital debris and collision avoiding maneuvers is costly.¹⁴ However, we assume that new satellites can have automatic collision detection devices that reduce such costs.

This scenario assumes that all satellites and other types of spacecraft have maneuvering capabilities, tracking systems can alert satellite operators for possible collisions (they can track fragments larger than 1 cm), and satellite operators can perform collision-avoiding maneuvers.¹⁵ To simulate this scenario, we consider a situation in which the number of operational satellites destroyed by collision is zero ($X_t = 0$), and the only collisions are between derelict satellites and rocket bodies with each other and other fragments. In the model, collision avoidance manoeuvres capability is represented by v_t . This scenario implies that v_t is fixed to one. This eliminates any damage to operational satellites from debris.

5.7 ESA zero debris

In the year 2023, the ESA introduced a new "Zero Debris" guidelines to be in place in 2030. These new guidelines have the objective to eliminate any orbital debris emission from ESA missions and with the aim that all spacefaring agents adhere to these guidelines. Hence, this scenario assumes that no debris emission is produced, limiting debris creation to the

¹⁴The literature identifies three main costs associated with collision avoidance: tracking, fuel consumption, and service interruptions. Locke et al. (2024) provide estimates for these costs.

¹⁵However, there are limitations to conducting collision avoidance maneuvers, particularly due to the difficulty of tracking small debris pieces that are still large enough to cause severe consequences in the event of a collision (Lewis and Skelton, 2024). Nevertheless, technological advancements are expected to improve the tracking of smaller debris and enable spacecraft to develop onboard conjunction detection and automatic orbit correction systems.

breakup of existing derelict satellites and rocket bodies. To simulate this scenario, the value of the parameters χ , φ , and ω are set to be zero. Additionally, also is assumed that $v_t = 1$. That is, this scenario encompasses all previous scenarios with the exception of the no-breakups scenario.

5.8 No debris (Clean space environment)

Finally, as a baseline to quantify the overall economic impact of orbital debris, we consider a "sci-fi" scenario in which there is no orbital debris, that is, a clean space environment. In this scenario we obtain the central planner solution with no environmental negative externality. This could be the case of an alternative launch system technology from the beginning of the space conquest, similar to the Space Shuttle vehicles developed by NASA, the implementation of a de-orbit policy to remove from orbit derelict satellites, and a better spacecraft design to avoid breakups. An alternative interpretation would be that orbital debris has no negative impact on the space environment and on the economy. This would be equivalent to the "ESA zero debris" scenario, but extended to the beginning of the space conquest.

6. SIMULATION RESULTS

This section presents the main results from the simulation of a centralized economy, where the objective is to maximize social welfare. To perform the numerical simulations, the model is reformulated as a non-linear programming (NLP) problem. Specifically, the simulations cover the period from 2023 to 2222, providing a planning horizon of 200 years, with results generated at an annual frequency. The model is implemented and solved using GAMS with the CONOPT4 algorithm. As highlighted by Cai (2019), GAMS offers greater flexibility compared to MATLAB, and CONOPT4 is recognized as a more reliable and efficient solver for non-linear programming problems than MATLAB's *fmincon* algorithm. To ensure robustness, the model is also solved in MATLAB using the CasADi solver framework (Andersson et al., 2019), following the implementation approach developed by Kellett et al. (2016). For context, the DICE (Dynamic Integrated Climate-Economy) model, originally developed by Nordhaus (1992, 1993), remains the most influential integrated assessment model (IAM) in the literature. Nordhaus's DICE model was initially designed and implemented in GAMS, but alternative implementations in other computing languages have emerged over time. For instance, Kellett et al. (2018) developed MATLAB code to solve DICE2013R and DICE2016R using CasADi, while Lemoine (2020) introduced a solution method for DICE2016R using the KNITRO solver.

The model is simulated departing from the initial values of the variables for the year 2023. The results can be compared with those obtained by Adilov et al. (2020), Nozawa et al. (2023), Rao et al. (2023), Rao and Rondina (2025), and Bongers et al. (2025). The papers by Adilov et al. (2020), Rao et al. (2023), and Rao and Rondina (2025) use different economic and space modules. By contrast, Nozawa et al. (2023) use a neoclassical growth model similar to the one used here but with a different space module. Bongers et al. (2025) also use the neoclassical growth model in the economic module, but with exogenous saving rates.

The main results from the model simulations are presented through figures that depict the optimal trajectories of key variables under each policy scenario over the simulation horizon. Figure 2 shows the evolution of orbital debris larger than 1 cm across various debris mitigation strategies. During the first 100 years of the simulation, the trajectories across scenarios appear nearly identical due to the initially slow pace of debris accumulation. However, starting around 2150, significant differences begin to emerge, especially between the ESA's zero debris and de-orbiting scenarios and the other policy alternatives. The simulation begins with an initial estimate of 1 million pieces of orbital debris larger than 1 cm, based on the ESA's MASTER model for the year 2023. Under the non-intervention scenario, in which no mitigation measures are implemented, the amount of debris grows exponentially by a factor of approximately 4,500 over the 200-year simulation period. A similar trajectory is observed in the no breakups scenario, indicating that passivation measures alone (e.g., for rocket bodies and satellites) offer limited long-term benefits. The trajectories for the reusable launch vehicles, debris-free launches, and no collisions scenarios show nearly identical patterns, with only marginal differences between them and little deviation from the non-intervention and no breakups cases. Even in the debris-free launch scenario, where newly launched spacecraft generate no additional debris, the improvements are modest. In all these scenarios, although the total debris remains slightly lower than in the non-intervention case, it still increases by roughly a factor of 4,000, highlighting the limitations of these mitigation strategies in preventing long-term environmental degradation in orbit. A more substantial improvement is observed under the de-orbiting scenario, where debris growth is notably reduced, increasing by only a factor of about 1,000 over the 200-year period. While still significant, this outcome demonstrates the potential effectiveness of actively removing derelict satellites and rocket bodies. This reduction is not due to fewer breakups, but rather to the elimination of high-risk collisions involving intact objects and debris fragments. The most effective mitigation is achieved through a combined strategy that includes de-orbiting, no breakups, and debris-free launches. In this scenario, the accumulation of orbital debris occurs at a much slower pace, with total debris increasing by only a factor of 200 over the simulation period. Finally, as expected, the ESA's zero debris strategy results in no net growth in orbital debris, demonstrating the ideal outcome in long-term debris mitigation.

Figure 3 offers a closer view of orbital debris accumulation over the next 100 years, allowing for a more detailed analysis of short- and medium-term trends. Among the scenarios, the lowest accumulation of debris—excluding the ESA's zero debris strategy, which results in a gradual reduction due to natural orbital decay, is achieved through the combined implementation of de-orbiting, no-breakups, and debris-free launch vehicles. This result underscores the effectiveness of addressing multiple sources of debris generation simultaneously, even in the near term. Interestingly, the no-collision scenario results in a higher level of debris accumulation, comparable to that of the reusable launch vehicles scenario, within this 100-year horizon. This counterintuitive outcome arises because, in the early stages of the simulation, collisions contribute relatively little to the total debris stock due to the low initial density of orbital objects. During this phase, the primary sources of debris are launch emissions and satellite breakups. However, comparing Figures 2 and 3 reveals a critical dynamic: as time progresses, collisions increasingly become

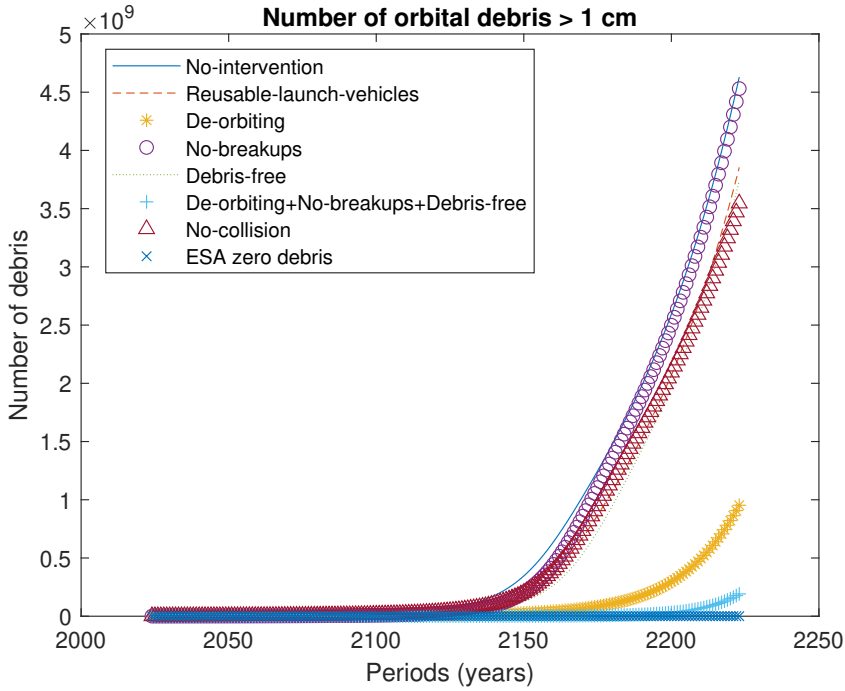


FIGURE 2. Orbital debris (larger than 1 cm)

the dominant driver of debris accumulation. This shift explains why, over the full 200-year horizon, the de-orbiting scenario outperforms all other mitigation strategies except the ESA zero debris scenario. In the long run, preventing collisions not only among active satellites but also involving defunct satellites and rocket bodies, becomes essential for curbing the self-reinforcing cycle of debris generation.

These results underscore the fact that the dynamics of orbital debris accumulation evolve significantly over time. This evolution is a direct consequence of the shifting relative importance of different sources of debris emissions and on damages on active satellites. In the short run, emissions from launches and breakups are the primary contributors to debris accumulation, making the combination of policies targeting these sources the most effective strategy. However, as debris accumulates over time and the orbital environment becomes increasingly crowded, the probability of collisions rises sharply. This endogenous process transforms collisions into the principal source of debris generation in the long run. Thus, while a comprehensive mitigation strategy combining de-orbiting, no-breakups, and debris-free vehicles is the best approach for managing debris accumulation over the next century, the no-collision scenario emerges as a counterproductive strategy for mitigating debris growth over time. This is explained by the fact the reducing the risk of collision of active satellites increases the optimal number of satellites in orbit. If no other mitigation measure is implemented, this also increases the number of non-active satellites and rocket bodies, and their collisions, resulting in a very polluted space environment. These findings highlight the need for dynamic, adaptive policies that account

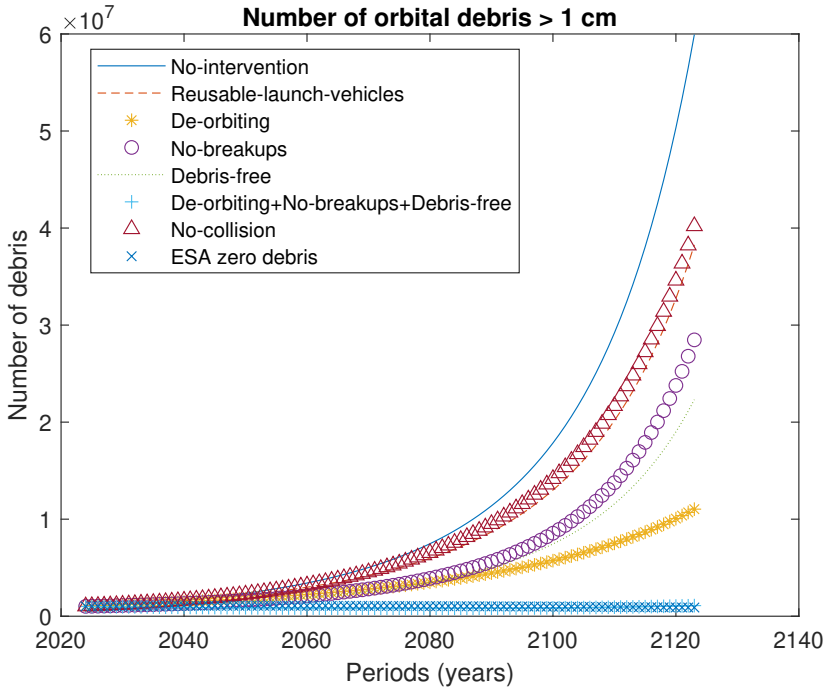


FIGURE 3. Orbital debris (larger than 1 cm). First 100 years

for the evolving nature of the orbital debris problem. In particular, prioritizing collision avoidance measures becomes increasingly critical as the debris population grows, reinforcing the accumulation of debris if not accompanied by other mitigation measures.

Figure 4 illustrates the optimal trajectory for the number of operational satellites in orbit under the baseline calibration. The increasing number of satellites over time is primarily driven by economic output growth. However, this trajectory is significantly influenced by the accumulation of orbital debris and the associated risk of satellite collisions, which act as constraints on further growth. In the initial periods of the simulation, the stock of satellites relative to Earth capital increases due to the positive impact of ISTC. However, as the probability of collisions begins to rise alongside growing space pollution, this ratio eventually declines, reflecting the increasing costs and risks associated with orbital congestion. A key observation is that, as the number of satellites increases and the orbital environment becomes more polluted, the optimal trajectories for satellite deployment begin to diverge across the different policy scenarios. At the bottom of these trajectories is the no-intervention scenario, where no mitigation policies are implemented. In this scenario, the number of satellites continues to grow initially, but reaches a peak around the year 2150, after which it begins to decline. This outcome is driven by the accumulation of orbital debris, which leads to significant damages and heightened collision risks, discouraging further investment in satellite infrastructure. The implementation of mitigation policies such as reusable-launch vehicles, no-breakups, and debris-free technologies, leads to only slightly higher values for the number of satellites. The implementation of

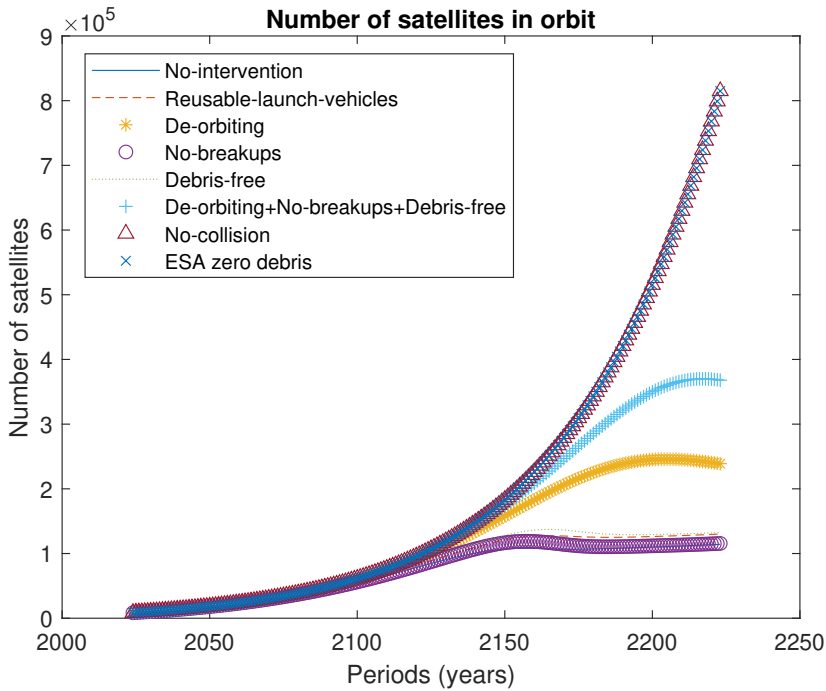


FIGURE 4. Optimal number of operational satellites in orbit

deorbiting policies has a more positive effect on the accumulation of space assets, but also a tipping point emerges at the end of the simulation period. This policy slows the rate of debris accumulation but does not fully eliminate the risk of collisions. Consequently, while they provide a short-term reprieve, their long-term impact remains limited, and the tipping point is merely postponed rather than averted. In contrast, the combined mitigation scenario, which integrates de-orbiting, no-breakups, and debris-free policies, achieves a more substantial delay in the tipping point. By addressing multiple sources of debris simultaneously, this approach slows the growth of orbital debris more effectively, allowing for a longer period of satellite expansion before the risk of collisions begins to dominate.

The most striking outcome, however, is observed in the no-collision and ESA zero debris scenarios. Here, the risk of orbital debris-induced damage is entirely eliminated, resulting in a consistently positive trajectory for satellite deployment. Without the constraint of debris-related risks, the stock of satellites continues to accumulate indefinitely, driven solely by economic growth and the technological benefits of space capital. These results underscore the critical role of orbital debris mitigation policies in sustaining long-term satellite deployment. While isolated policies provide limited short-term relief by slowing debris accumulation, a comprehensive and coordinated approach can substantially extend the period of sustainable growth. Nevertheless, the no-collision scenarios highlight an important benchmark: eliminating collisions altogether would unlock the full potential of space-based infrastructure, enabling indefinite growth in satellite deployment, even at the cost of more space pollution. This finding emphasizes the value of collision avoidance

measures as a long-term priority for both policymakers and the space industry, but alone does not ensure preservation of the space environment, which is only achieved in the case of the ESA zero debris scenario.

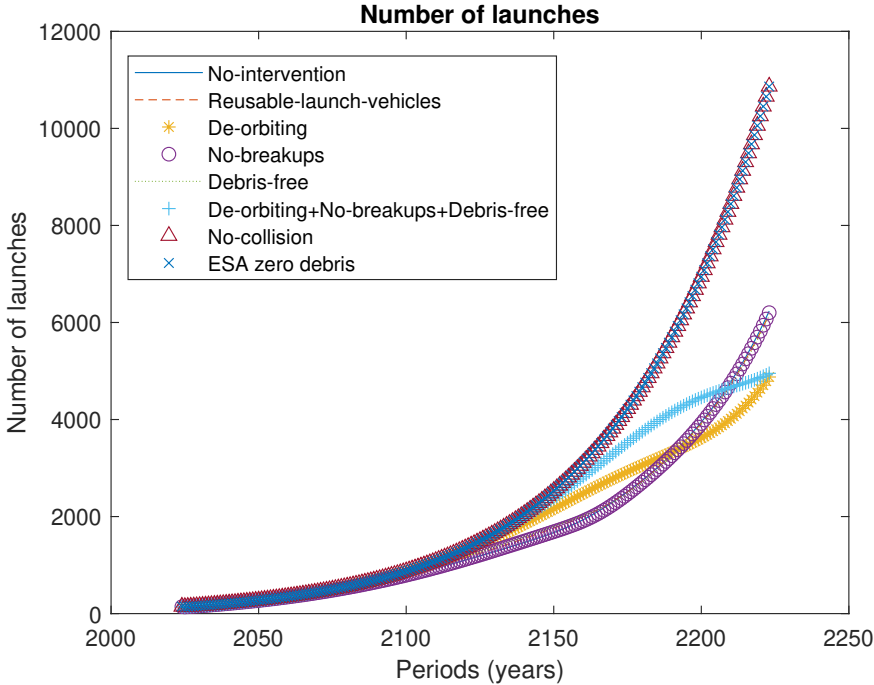


FIGURE 5. Number of launches

Figure 5 presents the number of launches required to achieve and maintain the optimal number of operational satellites in orbit over the simulation horizon. A key assumption is that the number of satellites per launch remains constant throughout the 200-year period, with an average of 13.6 satellites deployed per rocket launch (the average of the year 2023). The trajectory of launches is influenced not only by the target stock of satellites but also by the need to replace satellites that are destroyed due to collisions with orbital debris. Over the 200-year simulation, the number of launches required annually is projected to range between 5,000 and 11,000 per year, depending on the scenario. In scenarios where no-collision is considered, the number of launches increases steadily, given that no damages are produced and hence, no restriction exists for space capital accumulation. However, other scenarios with a high rate of satellite destruction caused by collisions creates a significant replacement burden, driving the need for an elevated number of launches. Despite this, non-intervention, de-orbiting, no-breakups, and reusable launch vehicles scenarios display remarkably similar long-run trajectories for the number of launches. This similarity arises because, while these policies slow the accumulation of orbital debris, they do not fully prevent satellite destruction from collisions, resulting in a continued demand for replacement launches. In the combined mitigation

scenario, which integrates de-orbiting, no-breakups, and reusable launch vehicles policies, a more noticeable reduction in the number of launches is observed in the long-run. This difference is explained by the lower number of satellites destroyed by collisions compared to the other scenarios. By simultaneously addressing multiple sources of debris, the combination of policies reduces the replacement needs, leading to fewer launches required to sustain the optimal stock of satellites. However, even in this scenario, launches remain substantial, reflecting the ongoing challenge posed by orbital debris accumulation and the limits of passive mitigation strategies. The no-collision scenario stands out as a unique case. In this scenario, there are no satellite losses due to collisions, as the risk of orbital debris-induced damage is completely eliminated. Consequently, the trajectory for launches follows a continuously increasing trend throughout the simulation horizon, mirroring the uninterrupted growth of the optimal stock of operational satellites. In essence, with no constraints imposed by space pollution, the number of launches increases steadily in response to economic output growth and the rising demand for space-based infrastructure.

These results highlight two important insights. First, even under scenarios with mitigation policies, the need for frequent launches remains substantial due to ongoing satellite losses caused by collisions. This underscores the limitations of passive debris mitigation strategies and the need for more robust measures to address orbital debris accumulation. Second, the no-collision scenario provides a benchmark for the potential of space infrastructure development in an idealized environment free of debris risks. Achieving such an outcome would require significant advancements in collision avoidance systems, active debris removal technologies, and international coordination to ensure a sustainable orbital environment.

Figure 6 illustrates the trajectory of derelict satellites left in orbit across the different scenarios. This figure is an example of the complex in-orbit dynamics provoked by the different mitigation policies in the long-run. The dynamics of derelict satellites are closely tied to the end-of-life processes for operational satellites, with significant differences emerging depending on the implementation of de-orbiting measures. In the de-orbiting scenario, as well as in scenarios that combine de-orbiting with other mitigation measures (e.g., no-breakups and reusable launch vehicles), and the ESA zero debris approach, the stock of derelict satellites trends toward zero. This outcome is a direct consequence of the model's assumption that, in each period, de-orbiting ensures the removal of end-of-life satellites, preventing them from accumulating as space debris. By actively managing satellite disposal, de-orbiting policies eliminate this particular source of orbital pollution. In contrast, scenarios without de-orbiting such as non-intervention, no-collision, and no-breakups, allow end-of-life satellites to remain in orbit, contributing to the growing stock of derelict satellites. The no-collision scenario, in particular, stands out as the case where the stock of derelict satellites reaches its maximum. This result stems from the absence of debris-induced collisions in this scenario, which allows satellites to remain in orbit until their natural end of life. Initially, as the number of operational satellites increases over time, so too does the number of end-of-life satellites, leading to an accumulation of derelict satellites.

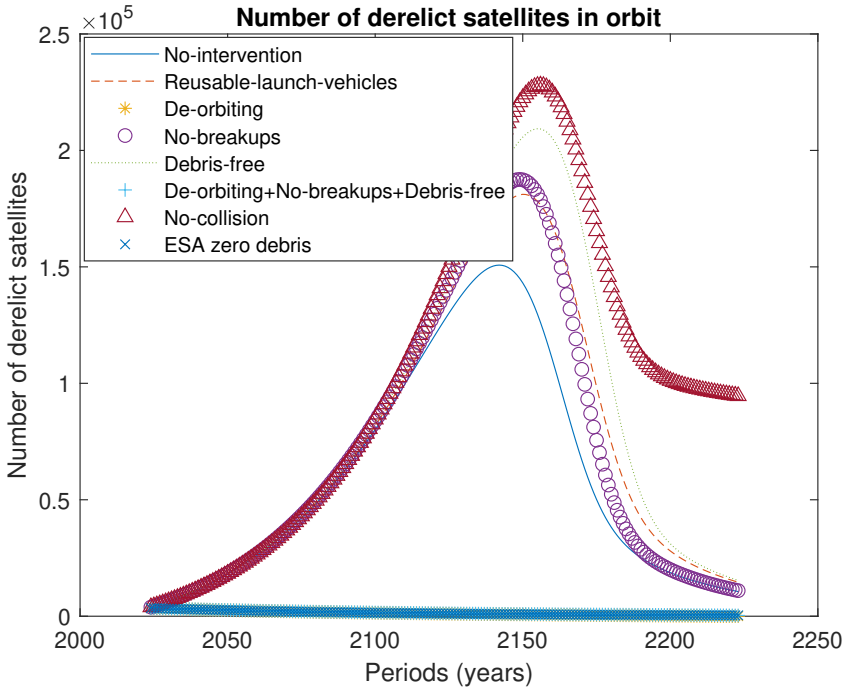


FIGURE 6. Number of derelict satellites

In the non-intervention, reusable launch vehicles, no-breakups, debris-free, and no collision scenarios, the stock of derelict satellites initially rises as the number of operational satellites grows. However, once the stock of operational satellites begins to decline due to the rising collision risk, the stock of derelict satellites also plateaus and eventually decreases. This dynamic reflects the tipping point where debris-induced collisions and damages begin to outweigh the benefits of continued satellite deployment, reducing both the flow of new operational satellites and, consequently, the number of derelict satellites entering orbit. The trajectories across scenarios highlight the critical role of de-orbiting policies in controlling the accumulation of derelict satellites. Without de-orbiting, the inactive satellite population continues to grow, contributing to orbital congestion and increasing the risk of further collisions and the production of additional debris. By contrast, scenarios incorporating de-orbiting measures demonstrate the effectiveness of active disposal strategies in mitigating this specific source of orbital debris.

Figure 7 presents the trajectories for the number of rocket bodies across the various scenarios. Rocket bodies are large debris fragments left as a by-product of traditional launch vehicle designs and they could be a significant contributor to the orbital debris population due to fragmentation. Their accumulation is directly tied to the number of launches and the disposal methods used for upper stages launch vehicles. In the reusable launch vehicles scenario, the stock of rocket bodies trends to zero. This outcome reflects the adoption of technologies that enable all components of the launch vehicle, including

spent stages, to return to Earth after deployment. By eliminating the release of rocket bodies into orbit, this technology fundamentally addresses one of the major sources of large debris. The debris-free launch systems scenario, which encompasses the reusable launch vehicles scenario, also achieves a zero stock of rocket bodies. In this case, additional measures or advanced technologies are assumed to ensure that no parts of the launch vehicle remain in orbit. This reflects a comprehensive approach to eliminating debris generation from space launches. For all other scenarios, the accumulation of rocket bodies depends on the frequency of launches. As the number of launches increases to sustain the growing stock of operational satellites, so too does the number of rocket bodies left in orbit.

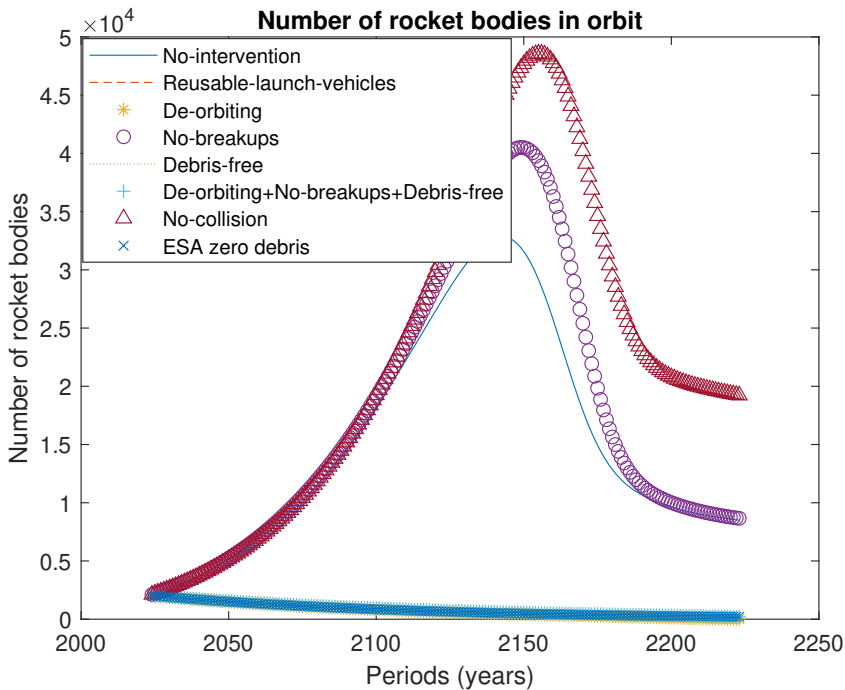


FIGURE 7. Number of upper stages rocket bodies

Damages can be calculated either as the loss value of destroyed satellites or as the number of satellites destroyed by collisions. Figure 8 shows the number of satellites destroyed by collisions, serving as a measure of the damages caused by orbital debris. As expected, the nonintervention scenario experiences the highest number of satellite losses, with over 65,000 satellites destroyed per year by the end of the simulation horizon. Similar figures are obtained for the no-breakups, reusable rockets and debris-free launch systems scenarios. This result highlights the severe consequences of inaction in mitigating orbital debris, as collisions become increasingly frequent over time. In the de-orbiting scenario the number of satellites destroyed is significantly lower compared to the previous scenarios, but the trajectories remain similar, with the damage only delayed rather than

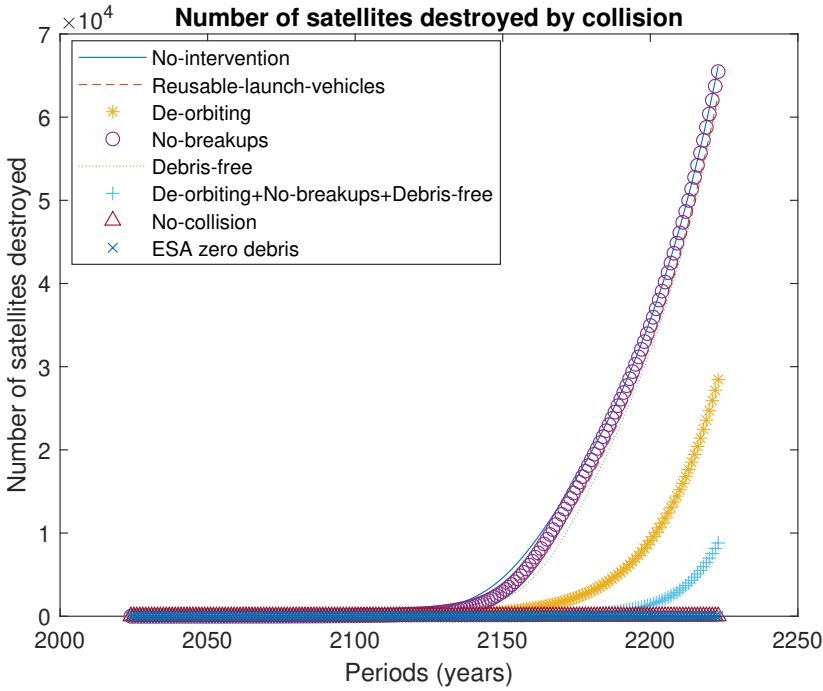


FIGURE 8. Number of satellites destroyed by collisions

fully mitigated. This delay reflects the slower accumulation of orbital debris in this scenario, resulting in fewer collisions over the medium term. However, as debris continues to accumulate, the risk of collisions increases, eventually leading to satellite destruction, albeit at a reduced rate compared to previous scenarios. The combination of de-orbiting with the no-breakups and debris-free rockets further reduces the number of satellites destroyed. The only scenario that achieves a complete elimination of satellite destruction from collisions is the collision-avoiding scenarios, where, by definition, no satellites are destroyed. This scenario assumes perfect avoidance of collisions, underscoring the theoretical ideal of fully eliminating collision risks in orbit. Notably, the combination of all mitigation measures—de-orbiting, no-breakups, reusable launch vehicles, and debris-free systems results in the most substantial reduction in satellite destruction, although it does not completely eliminate collisions.

Figure 9 plots the probability of collision for a satellite, given by $(1 - v_t)\theta D_t$. This is a measure of the likelihood of the Kessler syndrome, a catastrophic scenario where all satellites are destroyed by collision. For the baseline calibration of the model we find that under the no-intervention scenario, the probability of collision escalates up to above 50 percent at the end of the simulation horizon for the no intervention and no-breakups scenarios. The probability of collision is only slightly reduced for the scenarios of reusable and debris-free rockets. Only when a deorbiting policy is in place, it is observed a significant reduction in the probability of collision. For the combination of the previous scenarios the probability of collision at the end of the simulation horizon is of around 2.5 percent. As

expected, for the no-collision and ESA zero debris scenarios, the probability of collision is zero by assumption.

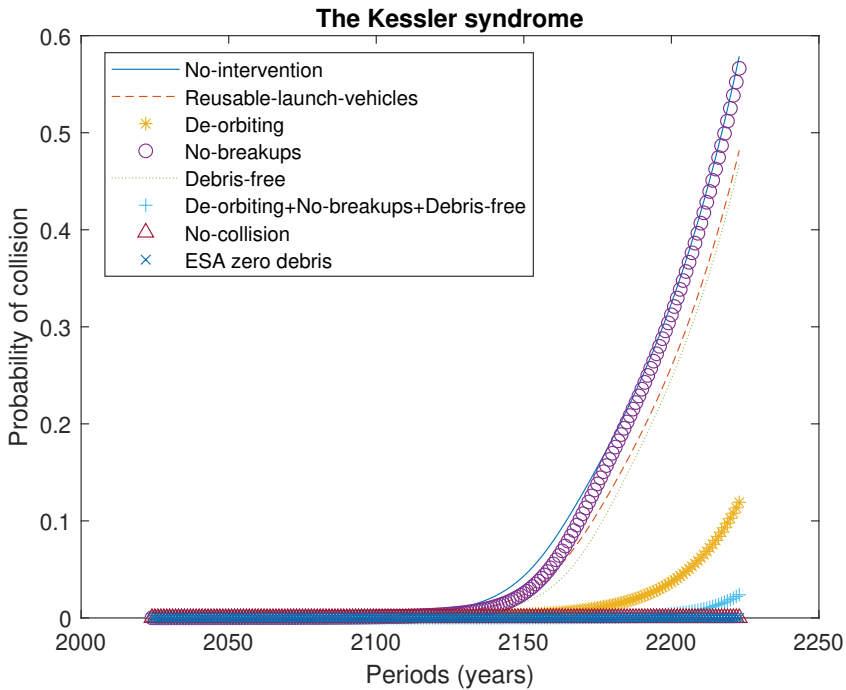


FIGURE 9. Probability of collision: The Kessler syndrome

The other way to quantify damages is looking at output. Satellites is an input in the aggregate production function, and hence, the number of satellites in orbit affects output. On the other hand, collisions of operational satellites implies a cost that affect optimal investment decisions and hence, to the accumulation process of capital. Figure 10 plots the output loss in each scenario compared to a fictitious scenario of no orbital debris. During the first 100 years the output losses are negligible, as percentage of global output. This is explained by the small relative size of the space sector compared to the rest of the economy. At the end of the simulation horizon, output losses appear evident, of around 0.6 percent of output for the no intervention and no-breakups scenarios, and of around 0.5 percent for the reusable and debris-free launch vehicles scenarios. Deorbiting reduces output losses to only 0.3 percent and to 0.2 percent if combined with no-breakups and debris-free launch vehicles. As expected, the no-collision and Esa' zero debris approach scenarios implies no output losses. Nozawa et al. (2023) find that in the horizon of 200 years, output losses are about 1.5% of GDP, whereas Bongers et al. (2024) find a small impact similar to the one presented here.

Finally, Figure 11 compares output in each scenario to output in the case of no intervention. In all cases we find output gains from the implementation of debris mitigation

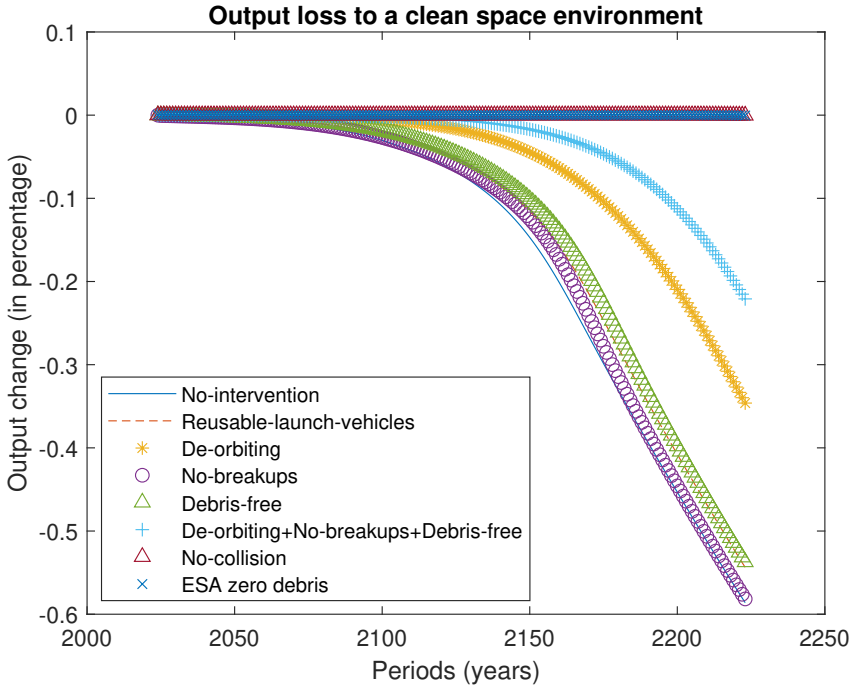


FIGURE 10. Output losses from orbital debris

guidelines, although gains are limited for some policies. Of course, the mandatory implementation of some of the debris mitigation guidelines could have some extra cost for spacefaring firms. This could be the case of de-orbiting, as extra-fuel is required for conducting de-orbiting maneuvers, increasing the weight and size of the satellite or reducing its operational life, or the case of collision avoiding systems. Nevertheless, we assume that all policies are implemented at no cost. This could be the case of reusable launch vehicles. The model does not assign any cost to the implementation of debris mitigation guidelines, so this figure shows the gross output gains. Output gains are around 0.6 percent of output for the no collision and ESA's zero debris scenarios, of around 0.25 percent for the deorbiting scenario, to negligible gains for the no-breakups scenario.

Table 2 shows a summary of the main results from the alternative scenarios for the years 2100 and 2200. The number of satellites in the year 2100 ranges from a minimum of 52,188 for the no-intervention scenario to a maximum of 57,060 in the no-collision and ESA's zero debris scenarios. For the year 2200, the number of satellites ranges between 107,720 and 482,660 for the ESA's zero debris scenario. The population of debris varies greatly across scenarios. In the year 2100, the population of debris would be of around 16 millions in the no intervention scenario (16 times the initial level of debris), to 0.99 millions in the ESA's zero debris approach. In the year 2200, the population of debris would be more than 2 billions in the non intervention, no-breakups and no collision scenarios. By contrast, the population of debris is much more smaller under the deorbiting policy, the combination of deorbiting with no-breakups and debris free, and in the ESA's zero debris

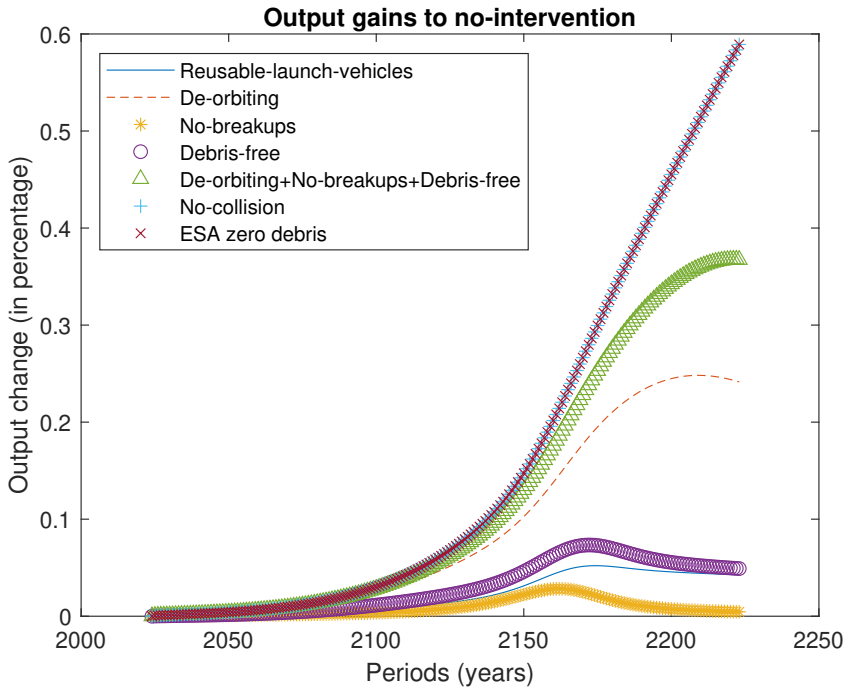


FIGURE 11. Output change with respect to the no-intervention scenario

TABLE 2. Simulations from DISE-2024.

Scenario	Satellites		Debris (Million)		Prob. of collision	
	2100	2200	2100	2200	2100	2200
No intervention	52,188	107,720	15.92	2,366.2	0.0020	0.2958
Reusable-launch-vehicles	53,370	123,800	11.72	1,874.3	0.0015	0.2347
De-orbiting policy	56,160	238,400	5.33	244.5	0.0007	0.0306
No-breakups	52,814	109,660	7.63	2,272.5	0.0010	0.2841
Debris-free launch systems	54,083	126,940	6.75	1,766.8	0.0008	0.2221
De-orbiting+no-breakups+debris-free	56,749	332,190	0.84	23.72	0.0001	0.0030
No collision	57,060	482,640	12.81	1,936.7	0.0016	0.2421
ESA Zero debris	57,060	482,660	0.99	0.58	0.0001	0.0000

scenario. The probability of collision, a measure of the Kessler syndrome, remains small for the year 2100 in all scenarios, but by 2200 reaches around 0.3 in the no intervention and no-breakups scenarios. The ESA's zero debris is the only scenario where the probability of collision is zero in the long-run, although in the deorbiting scenarios the probability of collision remains at very low values. The probability of collision in the no-collision scenario is also high (around 0.25) but in the case no damage is produced.

7. SENSITIVITY ANALYSIS

This section provides some additional results from a sensitivity analysis of the baseline calibration, and presents an on-line app for a full sensitivity analysis of all parameters. Numerical simulation of the model requires the use of a set of assumptions regarding the value of the parameters and the specification of the functions relating the variables. The literature on IAMs of climate-change economics has thoroughly investigated how results are sensitive to model specification and parameters calibration, and found that some parameters and functional forms are critical for evaluating the cost of carbon emissions and for the design of efficient environmental policies (see, for example, Miftakhova, 2021).

The projections and policy recommendations of the model simulation critically depend on the calibration of key economic and space parameters. Here, we focus only on the calibration of economic parameters. We can distinguish two main set of key economic parameters: parameters related to the exogenous sources of economic growth, and parameters affecting household utility. The first group of parameters refers to exogenous sources driving economic growth that establishes the economic conditions for the whole simulation period. This includes parameters for total factor productivity, satellite ISTC, and population growth. The second set of key parameters are those governing optimal decisions for welfare maximization. These key parameters are the social intertemporal preference parameter, and the intertemporal marginal consumption rate. Physical parameters related to the dynamics of orbital debris are also critical for the simulation of trajectories of intact objects and debris fragments, but their impact is limited to the timing where a certain population of orbital debris is reached.

This paper is accompanied by a GAMS MIRO app.¹⁶ This app solves the model using the GAMS engine and can be used for a full sensitivity analysis on all the parameters of the model. The user can modify the value of the different parameters within a predetermined scale and re-run the model to obtain the new optimal trajectories for the main variables. The app can also be used for scenarios comparison.

7.1 *Technological change and output growth*

One of the main driver of the simulation results is the underlying output growth during the periods. A characteristic of DISE-2024 is the consideration of a technological progress specific to the space capital in addition to a Hicks-neutral technological progress. These two types of technological progress in combination with the dynamics of population are the exogenous sources of economic growth. Satellite ISTC means that technological progress for space capital is faster than technological progress for the Earth capital. Greenwood et al. (1997) study the implications of ISTC in the long-run. These authors consider an economy two types of capital assets: structures and equipment, where ISTC only occurs in the later. Here, we assume that ISTC only occurs in space capital. Satellites ISTC reflects the decline in the relative price of satellites and launches. However, given the small technological parameter of satellites in the production function compared to the technological parameter of Earth capital, assumptions about the satellite ISTC process have little effect

¹⁶This app can be found at https://miro.gams.com/gallery/app_direct/dise_2024.

on the results. Labor input projection is assumed to be equal to population. Therefore, the main exogenous factor driving output growth is TFP process.

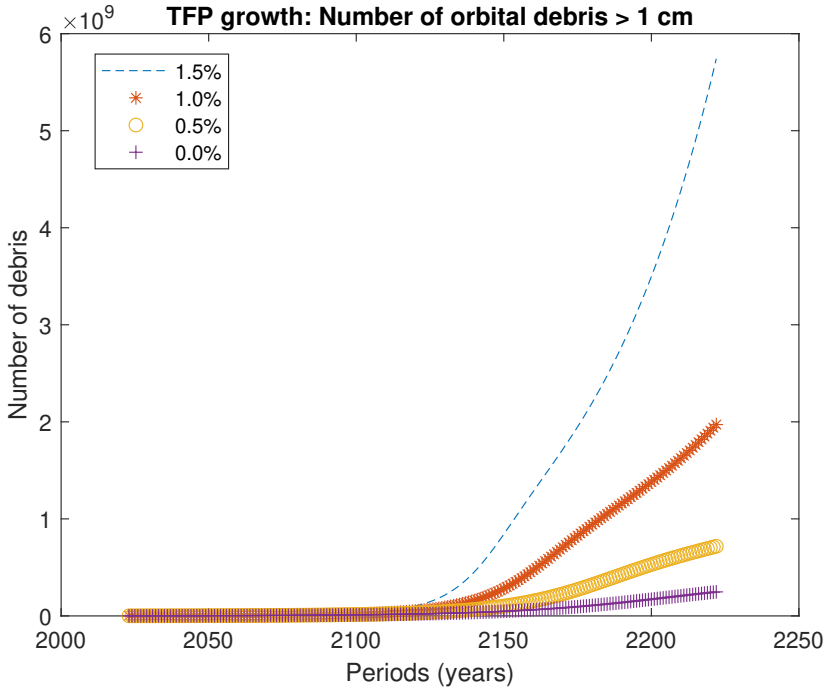


FIGURE 12. Orbital debris as a function of TFP growth

The literature has shown that long-run forecasts of output play a key role for policy and planning. Müller and Watson (2016) construct predictions for the US per capita GDP for a horizon of 75 years. Predictions are in the range 0.7 to 3.3 percent for a 90% interval. The baseline calibration of the model, with an initial TFP growth of 1.5 percent and a decay rate of 0.1 percent produces a growth of around 2.5 percent, well inside the range predicted by Müller and Watson (2016). Millner and McDermott (2016) evaluate the forecasting properties of the growth model for the US economy during the XX Century, and found that the model systematically underestimates TFP and GDP growth. Jones (2023) shows that the per capita GDP in the US over the past 150 years has been surprisingly stable at 2% per year, but growth models provide reasons that future growth can be lower or faster. In the long-run, growth is determined by the growth in the worldwide number of people searching for ideas. However, Jones (2023) indicates that declining world population growth could slow growth in the future, although the convergence of countries such as China and India provides a large number of people who could search for ideas. Jones (2022) explores a variety of reasons why future economic growth may be higher or slower than present growth rates.

Figure 12 plots the amount of orbital debris in the non-intervention scenario for different values of TFP growth, ranging from an initial 1.5 percent TFP growth to a zero TFP

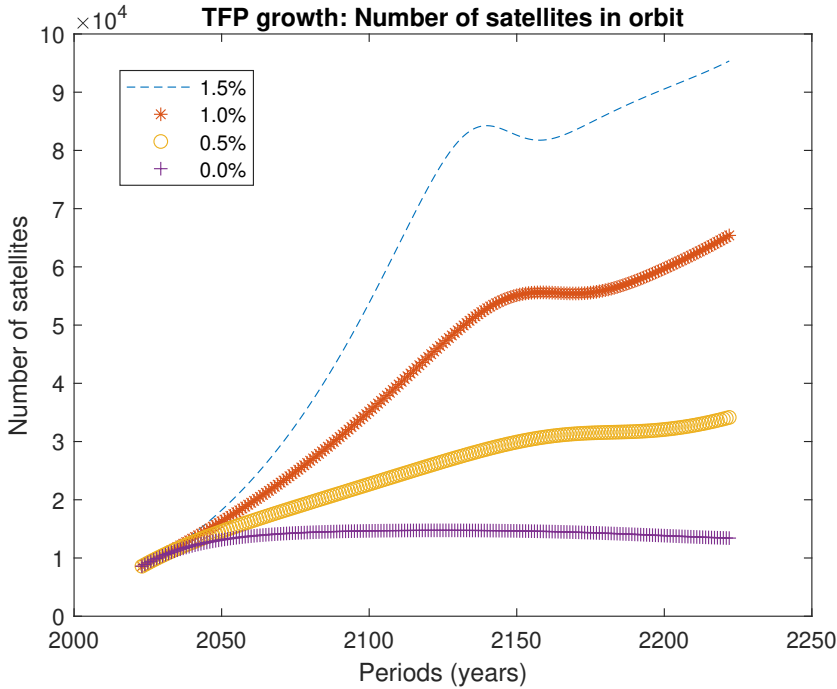


FIGURE 13. Optimal number of satellites in orbit as a function of TFP growth

growth. We can clearly observe how sensitive is orbital debris accumulation to the assumption about TFP growth, as the main driver of economic activity is. In a world with a higher initial TFP growth of 1.5%, the population of debris escalates to more than 5 billion of fragments which would implies a scenario in which the probability of collision equals to one. By contrast, reducing initial TFP growth results in a less intensive accumulation of debris; 2 billion fragments for an initial TFP growth of 1%, and less than 1 billion debris fragments for an initial TFP growth of 0.5%.

Figure 13 plots the number of satellites in orbit depending on output growth. As expected, the higher the initial TFP growth, the larger the number of satellites in orbit. The number of satellites does not only depend on economic growth but also on the accumulation of debris in each TFP growth scenario. Nevertheless, we observe that the first effect predominates the second. Even if tipping points are observed, the higher output and the particular endogenous process of debris generation by collisions, lead to further accumulation of space capital. Importantly, these simulation are obtained under the assumption that the technological parameters for the two types of capital remain constant over the simulation horizon.

7.2 The discount rate

The selection of the appropriate social discount rate is one of the more sensitive issues regarding the use of climate-change IAMs for policy analysis. The debate about the importance of the discount rate is clearly reflected by confronting the results of Stern (2006)

with Nordhaus (2008), about carbon emissions costs. Ramsey (1928) argues that there is no ethical reason for discounting the future. The discount rate reflects the marginal rate of substitution between consumption in different time periods for a society, having an important effect on the path for emissions. Here, we investigate how alternative values of the social discount rate influence on the trajectory for orbital debris and satellites.

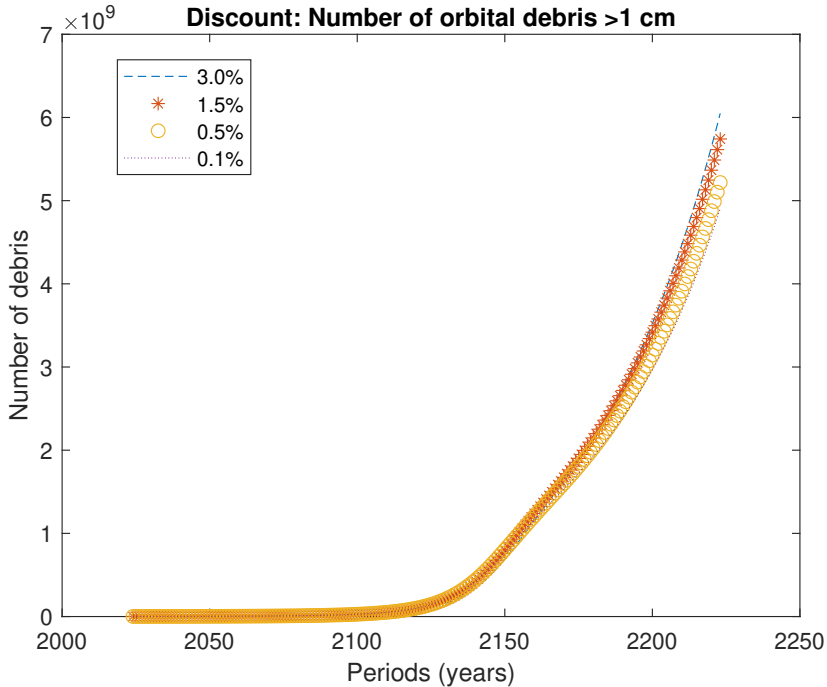


FIGURE 14. Orbital debris as a function of the discount rate

Figures 14 and 15 plot the trajectories for orbital debris and satellites for different values of the discount rate. Figure 14 plots the trajectories of orbital debris for values of the social discount rate from 3% to 0.1%. Whereas the trajectories indicate that lower the social discount rate, the lower the accumulation of orbital debris in the long-run, we find the for shorter horizons, the opposite is true. Two results are worth noting. First, we find that for the initial years, the larger the discount rate, the lower the accumulation of orbital debris and satellites. Only in the long-run, we find a positive relationship between the social discount rate and the accumulation of orbital debris. Second, contrary to the results observed in the climate-change literature, the optimal trajectories for orbital debris are not too sensitive to the intertemporal discount rate. In this sense, pollution by orbital debris is different from other pollutants in the Earth, where the path for emissions is highly sensitive to the social discount rate, and the higher the social discount rate, the larger the emissions. This distinctive result can be explained by the existence of an endogenous process of in-orbit generation of debris by breakups of intact objects and collisions. This means that emissions is the main source of debris accumulation for the first years of the horizon, but as

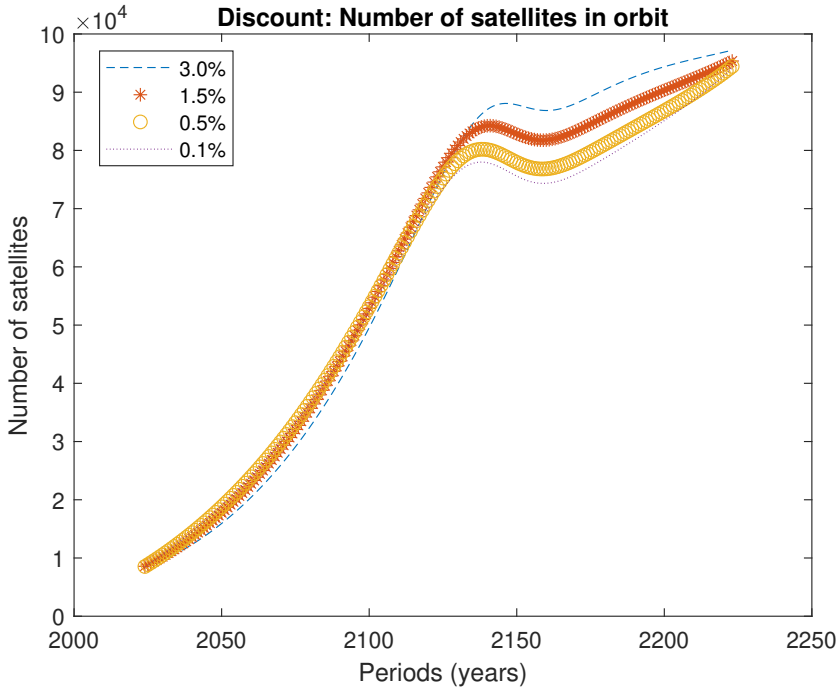


FIGURE 15. Optimal number of orbital debris as a function of the discount rate

debris accumulated, this primary source is relatively less important compared to the self-generation of debris fragments in-orbit from breakups and collisions. Figure 15 plots the trajectories for operational satellites, where a similar pattern can be observed. In the short-run, the higher the social discount rate the lower the number of operational satellites. In the long-run, that result reverses.

8. CONCLUSIONS

This paper presents an integrated space environment-economy model to study the economic implications of orbital debris and to be used for the evaluation of alternative optimal environmental policies to mitigate space junk. The space environment around Earth is a vital and complex area that influences many aspects of modern life and future aspirations in space exploration and exploitation. As human activity in space grows, addressing challenges such as space debris and orbital congestion will be essential to ensure the safe and effective use of satellite orbits. Humankind faces not only pollution on Earth, but also pollution in space in the form of orbital debris. Today, Earth's orbit is populated by millions of fragments and derelict spacecraft as a byproduct of human activity in space. Orbital debris poses a risk to human activities in space, raising a cost by the destruction of operational spacecraft and costs for monitoring and tracking orbital debris, calculation of collision probability, and collision avoiding manoeuvres. Furthermore, a catastrophic scenario, the Kessler syndrome, could be a potential result if orbital debris growth is infinity, rendering the space unusable.

The analysis done in this paper extends the standard climate-change policy evaluation framework in the environmental economics literature, as the one developed by Nordhaus (1992, 1993, 2008, 2024) combining an optimal economic growth model with a physical model relating temperature with greenhouse gas emission, to the outer space. Integrated assessment models (IAMs), such as the well-known DICE (Dynamic Integrated Climate-Economy) model, have been shown to be extremely useful tools for studying the interaction between the economy and the climate and investigating the implications of alternative environmental policies, even if these models have a number of shortcomings, and future economic dynamics is subject to large uncertainties.

The model is simulated for a centralized economy where a social planner fully internalizes the negative externality produced by orbital debris, to obtain a measure of the long-run impact of the set of debris mitigation guidelines established by international and national space agencies. We investigate the effects of mandatory implementation of debris mitigation guidelines for all spacefaring operators, assessing the following scenarios: no intervention (voluntary implementation of debris mitigation measures by each actor), use of reusable launch vehicles, de-orbiting policy, no-breakups, debris-free launch systems, avoiding collision systems, and ESA zero debris strategy. We find that some debris mitigation guidelines have little positive effects in preserving the space environment in the long-run if implemented alone. The analysis reveals that the most efficient policy is de-orbiting of derelict satellites and upper stages rocket bodies. Collision avoidance scenarios eliminate the damages but at the cost of further polluting the space. Only a strategy as the ESA's zero debris approach would restore a clean space environment in the long-run.

REFERENCES

- [1] Adilov, N., Alexander, P. J. and Cunningham, B. M. (2015). An economic analysis of earth orbit pollution. *Environmental and Resource Economics*, 60(1): 81-98.
- [2] Adilov, N., Alexander, P. J. and Cunningham, B. M. (2018). An economic "Kessler Syndrome": A dynamic model of earth orbit debris. *Economics Letters*, 166(1): 79-82.
- [3] Adilov, N., Alexander, P. J. and Cunningham, B. M. (2020). The economics of orbital debris generation, accumulation, mitigation, and remediation. *Journal of Space Safety Engineering*, 7: 447-450.
- [4] Andersson, J. A. E., Gillis, J., Horn, G., Rawlings, J. B. and Diehl, M. (2019). CasADi – A software framework for nonlinear optimization and optimal control. *Mathematical Programming Computation*, 11(1): 1-36.
- [5] Australian Space Weather Agency. 1999. *Satellite orbital decay calculations*. Sidney: Australia.
- [6] Barr, J. R. and Manne, A. S. (1967). Numerical experiments with finite horizon planning models. *Indian Economic Review*, 2(1): 1-29.
- [7] Barrage, L. and Nordhaus, W. D. (2024). Policies, projections, and the social cost of carbon: Results from the DICE-2023 model. *PNAS*, 121(13): e2312030121.

- [8] Barro, R. J. (2006). Rare disasters and asset markets in the twentieth century. *Quarterly Journal of Economics*, 121(3): 823-866.
- [9] Barro, R. J. and Jin, T. (2011). On the size distribution of macroeconomic disasters. *Econometrica*, 57(5): 1567-1589.
- [10] Barro, R. J. and Ursúa, J. F. (2008). Macroeconomic crisis since 1870. *Brookings Papers on Economic Activity*, 1: 255-335.
- [11] Béal, S., Deschamps, M. and Moulin, H. (2020). Taxing congestion of the space commons. *Acta Astronautica*, 177: 313-319.
- [12] Bernhard, P., Deschamps, M. and Zaccour, G. (2022). Large satellite constellations and space debris: Exploratory analysis of strategic management of the space commons. *European Journal of Operational Research*, 304(3): 1140-1157.
- [13] Blake, A. P. and Westaway, P. F. (1995). An analysis of the impact of finite horizons on macroeconomic control. *Oxford Economic Papers*, 47(1): 98-116.
- [14] Bonnal, C., Ruault, J. M. and Desjean, M. C. (2013). Active Debris Removal: Recent Progress and Current Trends. *Acta Astronautica*, 85: 51-60.
- [15] Bongers, A. and Torres, J. L. (2023). Orbital debris and the market for satellites. *Ecological Economics*, 209: 107831.
- [16] Bongers, A. and Torres, J. L. (2024). Star Wars: Anti-Satellite weapons and orbital debris. *Defence and Peace Economics*, 35(7): 826-845.
- [17] Bongers, A., Molinari, B., Rouillon, S. and Torres, J. L. (2024). The foundations of the economics of the outer space: A premier overview. SEWP-01-2024, Institute for Space Economics.
- [18] Bongers, A., Ortiz, C. and Torres, J.L. (2025). DISE: A dynamic integrated space economy model for orbital debris mitigation policy evaluation. *Environmental and Resource Economics*, forthcoming.
- [19] Bureau of Economic Analysis (2023). *Space Economy Data, 2012-2021*.
- [20] Caballero, R. J. and Engel, E. M. R. A. (1999). Explaining investment dynamics in U.S. manufacturing: A generalized (S,s) approach. *Econometrica*, 67(4): 783-826.
- [21] Cai, Y. (2019). Computational methods in environmental and resource economics. *Annual Review of Resource Economics*, 11: 59-82.
- [22] Cai, Y., Judd, K. L. and Lontzek, T. S. (2012). DSICE: A Dynamic Stochastic Integrated Model of Climate and Economy. RDCEP Working Paper No. 12-02.
- [23] Carrington, R. C. (1859). Description of a singular appearance seen in the Sun on September 1, 1859. *Monthly Notices of the Royal Astronomical Society*, 20: 13-15.
- [24] Cass, D. (1965). Optimal growth in an aggregative model of capital accumulation. *Review of Economic Studies*, 32: 233-240.

- [25] Chakravarty, S. (1962). The Existence of an Optimum Savings Program. *Econometrica*, 30(1): 178-187.
- [26] Christiano, L., Eichebaum, M. and Evans, C. (2005). Nominal rigidities and the dynamics effects of a shock to monetary policy. *Journal of Political Economy*, 113: 1-45.
- [27] Corrado, L., Grassi, S., Paolillo, A. and Silgado, E. (2023). The macroeconomic spillovers from space activity. *PNAS*, 120(43), e2221342120.
- [28] Farinella, P. and Cordelli, A. (1991). The proliferation of orbiting fragments: a simple mathematical model. *Science and Global Security*, 2: 365-378.
- [29] Feenstra, R. C., Inklaar, R. and Timmer, M. P. (2015). The Next Generation of the Penn World Table. *American Economic Review*, 105(10): 3150-3182.
- [30] Frisch, R. (1955). The mathematical structure of a decision model: The Oslo sub-model. *Metroeconomica*, 7(3): 111-136.
- [31] Gallois, P. 1987. Life expectancy of communication satellites, *Electronics and Power*, 33(9): 547-550.
- [32] Golosov, M., Hassler, J., Krusell, P. and Tsyvinski, A. (2014). Optimal taxes on fossil fuel in general equilibrium. *Econometrica*, 82(1): 41-88.
- [33] Greenwood, J., Hercowitz, Z. and Krusell, P. (1997). Long-Run Implications of Investment-Specific Technological Change. *American Economic Review*, 87(3): 342-362.
- [34] Grzelka, Z. and Wagner, J. (2019). Managing satellite debris in low-earth orbit: Incentivizing ex ante satellite quality and ex post take-back programs. *Environmental and Resource Economics*, 74(1): 319-336.
- [35] Guyot, J. and Rouillon, S. (2021). Designing satellites to cope with orbital debris. Bordeaux Economics Working Papers, 2021-16.
- [36] Hassell, M. P. (1975). Density-dependence in single-species populations. *British Ecological Society*, 44(1): 283-295.
- [37] Hardin, G. (1968). The tragedy of the commons. *Science* 162: 1243-1248.
- [38] Jones, C. I. (2022). The past and future of economic growth: A semi-endogenous perspective. *Annual Review of Economics*, 14: 125-152.
- [39] Jones, C. I. (2024). The outlook for long-term economic growth. NBER Working Paper 31648.
- [40] Kawamoto, S., N. Nagaoka, T. Sato, and T. Hanada. 2019. "Impact on Collision Probability by Post Mission Disposal and Active Debris Removal." First International Orbital Debris Conference.
- [41] Kellett, C. M., Faulwasser, T. and Weller, S. R. (2016). DICE2013R-mc: A Matlab/CasADi implementation of vanilla DICE2013R. arXiv:1608.04294.
- [42] Kessler, D. J. (1991). Collisional cascading: The limits of population growth in low earth orbit. *Advances in Space Research*, 11(12): 63-66.

- [43] Kessler, D. J. and Cour-Palais, B. G. (1978). Collision frequency of artificial satellites: The creation of a debris belt. *Journal of Geophysical Research*, 83(A6): 2637-2646.
- [44] Kessler, D. J., Johnson, N. L., Liou, J. C. and Matney, M. (2010). The Kessler syndrome: Implications to future space operations. AAS-10-016.
- [45] Klima, R., Bloembergen, D., Savani, R., Tuyis, K., Hennes D. and Izzo, D. (2016). Space debris removal: A game theoretic analysis. *Games* 7(3): 20.
- [46] Koopmans, T. C. (1963). On the concept of optimal economic growth. Cowles Foundation Discussion Papers 12-1-1963.
- [47] Krisko, P.H. (2007). The predicted growth of the low-Earth orbit space debris environment - An assessment of future risk for spacecraft. *Journal of Aerospace Engineering*, 221(6): 975-985.
- [48] Krisko, P.H., Johnson, N.L. and Opiela, J.N. (2001). EVOLVE 4.0 orbital debris mitigation studies. *Advances in Space Research*, 28(9): 1385-1390.
- [49] Lafleur, J.L. (2011). Extension of a simple mathematical model for orbital debris proliferation and mitigation. *American Astronautical Society*, 11-173.
- [50] Lau, M. I., Pahlke, A. and Rutherford, T. F. (2002). Approximating infinity-horizon models in a complementarity format: A primer in dynamic general equilibrium analysis. *Journal of Economic Dynamics and Control*, 26(4): 577-609.
- [51] Lemoine, D. (2020). Incentivizing Negative Emissions Through Carbon Shares. University of Arizona Working Paper 20-08.
"Extending the ECOB space debris index with fragmentation risk estimation." Proc. 7th European Conference on Space Debris, Darmstadt, Germany, 18–21 April 2017, published by the ESA Space Debris Office.
- [52] Lewis, H.G. (2020). Understanding long-term orbital debris population dynamics. *Journal of Space Safety Engineering*, 7: 164-170.
- [53] Lewis, H.G., Swinerd, G.G., Newland, R.J. and Saunders, A. (2009). The fast debris evolution model. *Advances in Space Research*, 44: 568-578.
- [54] Lifson, M., D'Ambrosio, A., Arnas, D. and Linares, R. (2022). How many satellites can we fit in low Earth orbit?: Capacity integrating Risk-based and Intrinsic Methods. AAS/AIAA Astrodynamics Specialist Conference
- [55] Liou, J. C. and Johnson, N. L. (2006). Risks in space from orbiting debris. *Science*, 311: 340–341.
- [56] Liou, J.C., Hall, D.T., Krisko, P.H. and Opiela, J.N. (2004). LEGEND - a three-dimensional LEO-to-GEO debris evolutionary model. *Advances in Space Research*, 34: 981-986.
- [57] Locke, J., Colvin, T. J., Ratliff, L., Abdul-Hamid, A. and Samples, C. (2024). *Cost and benefit analysis of mitigating, tracking, and remediating orbital debris*. Office of Technology, Policy, and Strategy. NASA.

- [58] Lucas, R. E. (1967). Adjustment costs and the theory of supply. *Journal of Political Economy*, 75(4-1): 321-334.
- [59] Macauley, M. K. (2015). The economics of space debris: Estimating the costs and benefits of debris mitigation. *Acta Astronautica*, 115: 160-164.
- [60] Mains, D. L., Peterson, G. E., McVey, J. P., Maldonado, J. C. and Sorge, M. E. (2024). Forensic analysis of recent debris-generating events. *Journal of Space Safety Engineering*, 11: 388-394.
- [61] Manne, A. S. (1970). Sufficient conditions for optimality in an infinite horizon development plan. *Econometrica*, 38(1): 18-38.
- [62] Manne, A. S. (1977). *ETA-MACRO: A Model of Energy-economy Interactions*. Electric Power Research Institute.
- [63] Manne, A. S. and Richels, R. G. (1992). *Bying Greenhouse Insurance: The Economics Costs of CO2 Emission Limits*. MIT Press, Cambridge.
- [64] Manne, A. S., Mendelsohn, R. and Richels, R. (1995). MERGE: a model for evaluating regional and global effects of GHG reduction policies. *Energy Policy*, 23(1): 17-34.
- [65] McDowell, J. C. (2018). The edge of space: Revisiting the Karman Line. *Acta Astronautica*, 151: 668-677.
- [66] McDowell, J. (2024). *Space Activities 2023*. Jonathan's Space Report.
- [67] Mercenier, J. and Michel, P. (1994). Discrete-time finite horizon approximation of infinite horizon optimization problems. *Econometrica*, 62(3): 635-656.
- [68] Miftakhova, A. (2021). Global sensitivity analysis for optimal climate policies: Finding what truly matters. *Economic Modelling*, 105: 105653.
- [69] Millner, A. and McDermott, K. J. (2016). Model confirmation in climate economics. *PNAS*, 113(31): 8675-8680.
- [70] Miyake, F., Nagaya, K., Masuda, K. and Nakamura, T. (2012). A signature of cosmic-ray increase in ad 774-775 from tree rings in Japan. *Nature*, 486(7402): 240-242.
- [71] Müller, U. K. and Watson, M. K. (2016). Measuring uncertainty about long-run predictions. *Review of Economic Studies*, 83: 1711-1740.
- [72] NASA (2007). Detection of debris from Chinese ASAT test increases; One minor fragmentation event in second quarter of 2007. *Orbital Debris Quarterly Review*, 11(3): 1-2.
- [73] NASA (2011). Fiftieth anniversary of first on-orbit satellite fragmentation. *Orbital Debris Quarterly News*, 15(3): 3-5.
- [74] NASA (2020). The tracked objects in Low Earth Orbit: 2000-2020. *Orbital Debris Quarterly Review*, 24(4): 11.
- [75] Nordhaus, W. D. (1992). An Optimal Transition Path for Controlling Greenhouse Gases. *Science*, 258(5086): 1315-1319.

- [76] Nordhaus, W. D. (1993). Rolling the 'DICE': an optimal transition path for controlling greenhouse gases. *Resource and Energy Economics*, 15(1): 27-50.
- [77] Nordhaus, W. D. (2008). *A Question of Balance: Weighing the Options on Global Warming Policies*. Yale University Press, New Haven and London.
- [78] Nordhaus, W. D. (2018). Projections and uncertainties about climate change in an era of minimal climate policies. *American Economic Journal. Economic Policy*, 10: 333-360.
- [79] Nozawa, W., Kurita, K., Tamaki, T. and Managi, S. (2023). To what extent will space debris impact the economy? *Space Policy*, 66: 101580.
- [80] OECD (2020). *Space sustainability: The economics of space debris in perspective*. OECD Science, Technology and Industry Policy Papers n. 87.
- [81] Pardini, C. and L. Anselmo. 2014. Review of past on-orbit collisions among cataloged objects and examination of the catastrophic fragmentation concept. *Acta Astronautica*, 100: 30-39.
- [82] Peck, S. C. and Teisberg, T. J. (1992). CETA: A Model for Carbon Emissions Trajectory Assessment. *Energy Journal*, 0(1): 55-78.
- [83] Percy, T. (2015). *Simplified population growth modelling for low earth orbit*. Dissertations, 76. University of Alabama.
- [84] Ramsey, F. (1928). A mathematical theory of saving. *Economic Journal*, 38: 543-559.
- [85] Rao, A., Burgess, M. G. and Kaffine, D. (2020). Orbital-use fees could more than quadruple the value of the space industry. *PNAS*, 117(23): 12756-12762.
- [86] Rao, A. and Letizia, F. (2022). An integrated debris environment assessment model. arXiv preprint 2205.05205.
- [87] Rao, A., Moretto, M., Holzinger, M., Kaffine, D. and Weeden, B. (2023). OPUS: An integrated model for satellites and orbital debris. arXiv preprint 2309.10252v.
- [88] Rao, A. and Rondina, G. (2025). The economics of orbit use: Open access, external costs, and runaway debris growth. *Journal of the Association of Environmental and Resource Economists*, 12(2): 353-388.
- [89] Rossi, A. (1997). Long term evolution of Earth orbiting debris. In *Dynamics and Astronomy of Natural and Artificial Bodies*. Wytrzyaszak and Lieske (eds.). Kluwer Academic Press.
- [90] Rossi, A., Cordelli, A., Farinella, P. and Anselmo, L. (1994). Collisional evolution of the Earth's orbital debris cloud. *Journal of Geophysical Research*, 99(E11): 23195-23210.
- [91] Rouillon, S. (2020). A physico-economic model of low Earth orbit management. *Environmental and Resource Economics*, 77(4): 695-723.
- [92] Rutherford, T. F. (1995). Extension of GAMS for complementarity problems arising in applied economic analysis. *Journal of Economic Dynamics and Control*, 19: 1299-1324.

- [93] Shiell, L. and Lyssenko, N. (2008). Computing business-as-usual with a representative agent and a pollution externality. *Journal of Economics Dynamics and Control*, 32: 1543-1568.
- [94] Space Foundation (2023). *The Space Report 2023 Q2*.
- [95] Spencer, D. B., Alary, D., Eder, V., Martinez, P., Lemmens, S., Satomi, K., Lecas, M. and Hermoso, J. M. (2025). Effective compliance to technical regulations. Why is compliance to the orbital debris mitigation rules so poor? *Acta Astronautica*, 226: 839-845.
- [96] Stern, N. (2006). *The economics of climate change: The Stern Review*, Cambridge University Press.
- [97] Stoleru, L. G. (1965). An optimal policy for economic growth. *Econometrica*, 33(2): 321-348.
- [98] Talent, D. (1992). Analytical model for orbital debris environmental management. *Journal of Spacecraft Rocket*, 29(4): 508-551.
- [99] Traeger, C. P. (2014). A 4-stated DICE: Quantitatively addressing uncertainty effects in climate change. *Environmental and Resource Economics*, 59: 1-37.
- [100] Wang, X. W. and Liu, J. (2019). An introduction to a new space debris evolution model: SOLEM. *Advances in Astronomy*, 2019: 2738276.
- [101] Weitzman, M. L. (2007). A review of the Stern Review on the economics of climate change. *Journal of Economic Literature*, 45: 703-724.
- [102] Weitzman, M. L. (2009). On modeling and interpreting the economics of catastrophic climate change. *Review of Economics and Statistics*, 91(1): 1-19. []

Appendix for OPTIMAL PATH FOR ORBITAL DEBRIS

ANELÍ BONGERS

Department of Economics, University of Malaga, Spain

JOSÉ L. TORRES

Department of Economics, University of Malaga, Spain

This version: June 2025. This is a preliminary draft and may undergo revisions

This appendix is intended to provide more detail and additional information on the derivation and calibration of the different components of the DISE-2024 (Dynamic Integrated Space Economy) model. Although this is an economic paper, we have sought to balance the explanation of the different variables and parameters of the model for both economists and space engineers. This appendix is organized into ten sections: Basic data; Initial values for the base year; Calibration of economic parameters; Calibration of physical parameters; Exogenous sources of economic growth; Launch cost; The equations of the model; Terminal conditions; Additional results; and Computer codes.

Anelí Bongers: abongers@uma.es

José L. Torres: jtorres@uma.es

APPENDIX A: BASIC DATA

DISE-2024 is a global, aggregate, dynamic integrated economy-space model (a type of Integrated Assessment Model, IAM) that encompasses both human activities in the Earth and outer space. Following the tradition of climate-change IAMs, the model consists of two interdependent modules: an economic module and a space environmental module. Human activity in space produces a negative externality in the form of orbital debris deteriorating the space environment, which in turn negatively affects economic growth. The economic module is based on the optimal neoclassical growth model by Ramsey (1928), which is extended to incorporate a space economy sector. The space environmental module is built on a three-equations dynamical system that models the accumulation of three types of orbital debris: derelict satellites, rocket bodies, and fragments. Given the diverse nature of variables and parameters in DISE-2024, we draw on a wide range of data sources, including economic databases from the World Bank, International Monetary Fund (IMF), Penn World Table (PWT), Bureau of Economic Analysis (BEA), and United Nations Population Division, as well as space activity databases from the National Aeronautics and Space Administration (NASA), European Space Agency (ESA), Union of Concerned Scientists, (UCS), Space-Track (US Space Forces), Satellite Industry Association (SIA), Space Foundation, and Jonathan C. McDowell databases.

Human activity in space began in 1957. Since then, space has been populated by an increasing number of human-made objects. A portion of these objects are operational satellites that provide a variety of services to Earth's users. However, another significant portion consists of non-functional objects, classified as orbital debris, which are by-products of launches, operational activities in orbit, and an endogenous in-orbit process of debris fragments emissions due to breakups and collisions. Regarding human activity in outer space, two key data points are fundamental: the number of launches and the number of satellites inserted into orbit, both of which are considered components of investment in the space sector.

The number of launches is a fundamental variable in the analysis for three reasons. First, launches are the current technical method by which spacecraft are inserted into orbit. While not an economic variable in themselves, launches are an integral part of the investment process in space capital. Second, the number of satellites per launch varies depending on the launch vehicle and the size of the satellites, which decouples rocket launches from the number of satellites inserted into orbit. Third, launches are the primary source of orbital debris with the current technology. Most existing launch vehicles consist

of several stages, and the upper stages of rocket bodies often remain in orbit after the payload has been deployed. Additionally, during the payload insertion phase, various pieces (such as payload fairings and connection parts between stages) are jettisoned.

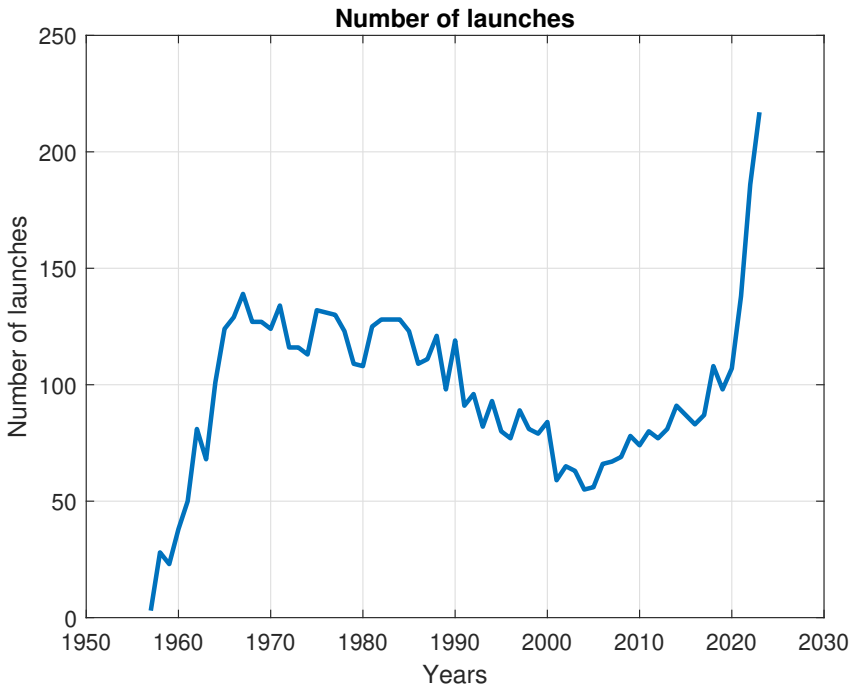


FIGURE A.1. Number of launches per year (1957-2023). Source: NASA

Figure A.1 plots the annual number of launches for the period 1957-2023. Over time, we can distinguish four stages. The first stage covers the first 10 years of space exploration, during which the number of launches increases rapidly, primarily driven by the space-race between the US and the Soviet Union. From the early 1970s to the end of the century, we observe a decline in the number of launches, as the space-race between the two super-powers lost intensity, and also due to the disintegration of the Soviet Union. The third stage begins with the new century and the entry of private firms into the market, firms that are not only satellite operators, but with launch capabilities (the new space economy). This state spans from 2000 to 2021. In 2022 launch activity experimented a sharp increase with the advent of satellite constellations, and in particular, with the activation of the Starlink satellite constellation by SpaceX, the leading and most active space firm on the World. The

number of launches in 2020 was 107, but increased to 138 in 2021, 186 in 2022, and 217 in 2023.

Figure A.2 displays the number of new satellites inserted into orbit each year. A significant change is clearly visible in the last three years of the sample period. For most of the period, the number of new satellites inserted into orbit remained relatively constant, at around 200 per year. However, this trend began to shift in 2014 with the entry of more private firms into the market, and particularly accelerated in 2022 and 2023 with the launch of large satellite constellations. Although 542 satellites were inserted into orbit in 2019, this number increased to 2,950 by 2023. The large number of satellites inserted in the last two years is mainly due to the deployment of Starlink satellite constellation of SpaceX and the OneWeb satellite constellation.

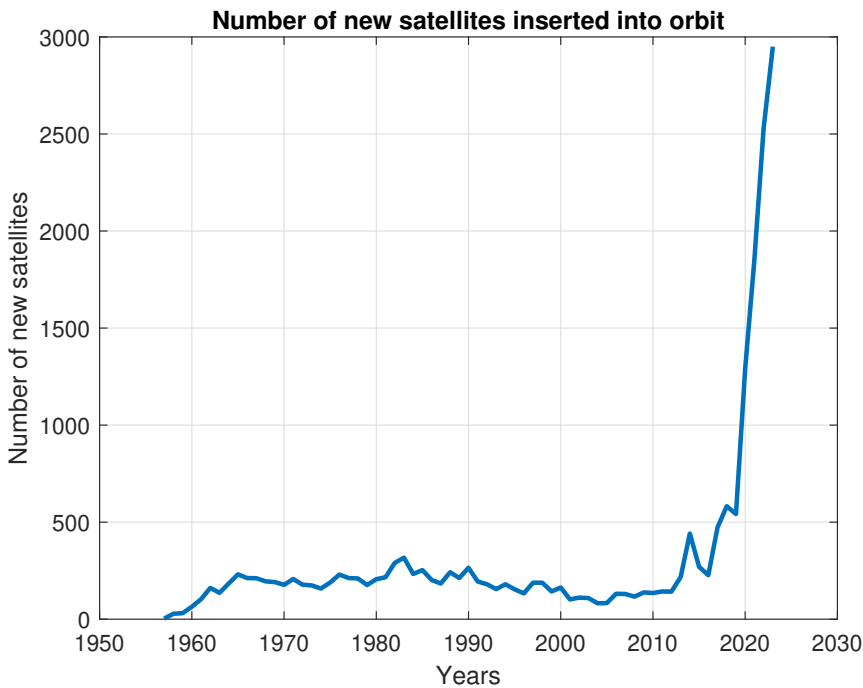


FIGURE A.2. Number of new satellites inserted into orbit (1957-2023). Source: NASA

Table A.1 shows some relevant data about human activity in Earth's orbits and the amount of debris estimated by the ESA as of December 2023. Since the beginning of space exploration until December 2023, around 6,500 successful launches have taken place. The

total number of satellites launched is 16,990, although only 11,500 remains in Earth' orbit. Of this number, around 8,500 to 9,000 are operational. As already indicated, a rocket launch can include more than one satellite or spacecraft. Indeed, the relationship between launches and new satellites in orbit is changed dramatically in recent years due to the use of small and micro satellites and the higher power and payload capacity of launch systems. The number of estimated incidents by the ESA, including break-ups, explosions, collisions, or anomalous events, resulting in fragmentation, is approximately 630. The NASA Breakups database by Anz-Meador et al. (2022) identifies a total of 268 breakup events, including collisions of intact objects with debris, deliberate collisions, self-destruction of payloads, and explosions of intact objects. One of the most significant incidents was the collision on February 10, 2009 between an active US communications satellite (*Iridium 33*) with a defunct Russian military communications satellite (*Kosmos 2251*). Both satellites were destroyed in the collision, producing around 2,200 pieces of new tracked debris measuring at least 5 cm (NASA, 2007). However, the most severe incident was intentional: an anti-satellite military test that resulted in the destruction of the *Fengyun-1C* (a Chinese satellite) on January 1, 2011, by a kinetic weapon, producing an estimated 3,037 pieces of new tracked debris (NASA, 2011). Most of the activity takes place at Low-Earth-Orbit (LEO, between 200 and 2,000 km), and at Geostationary Orbit (GEO, at 35,786 km).

The categorization of space debris is typically based on size and the availability of appropriate technology for tracking fragments in outer space. Orbital debris is tracked using Earth-based radar systems and optical telescopes. These systems can detect and monitor objects larger than 10 cm in low Earth orbit (LEO) and larger than 30 cm in geostationary orbit (GEO). In general, debris are classified according to size into three categories: Debris larger than 10 cm, debris between 1 cm and 10 cm, and debris between 1 mm and 1 cm. This classification is also based on the expected damage that can be produced by a piece of debris depending on its size. The NASA Standard Breakup model (Johnson et al., 2001) estimates that a catastrophic collision occurs when the ratio of the impactor energy to mass of the target exceeds 40 Joules (J) per gram (g). Locke et al. (2022) define a catastrophic collision as one in which two objects collide at an impact velocity above 6 kilometers (km) per second (s) and with an energy in the range 35-45 J/g, sufficient for both to break apart. For a collision speed of 10 km/s of a 10 cm impactor, Locke et al. (2022) estimate a lower bound of an impact energy of 1.3 MJ, or about 9 J/g for a large satellite and 59 J/g for a small satellite. These authors assume that the probability of a catastrophic event is 100% for a debris of 10 cm, 10% for a debris of 1 cm, and 0.01% for a debris of 1 mm. They use a

simple probabilistic model using previous figures, resulting in an average lethality probability of 21.7% for debris between 1 cm and 10 cm, and an average lethality probability of 0.09% for debris between 1 mm and 1 cm. A 3 mm of debris impacting at 10 km/s produces an energy similar to a bullet (a kinetic energy of 1.9 KJ, equivalent to 0.45 grams of TNT), and a 1 cm piece produces a kinetic energy of 70.7 KJ (equivalent to 16 grams of TNT). McKnight et al. (1992) indicate that, using data from growth test and on-orbit tests, the energy threshold for catastrophic breakups is 40 J/g of target mass. This corresponds to a target mass to projectile mass ratio of 1250 at 10 km/s (Kessler et al., 2010). Breakups models consider that fragments larger than 20 cm typically have a mass of over 1 kg and would almost always cause a catastrophic collision. The LEGEND model predicts that only 45% of the collision between cataloged objects (those larger than 10 cm) will be catastrophic, and 55% will be non-catastrophic (Johnson et al., 2001).

TABLE A.1. Basic space data

Number of rocket launches	6,500
Number of satellites inserted into orbit	16,990
Number of satellites in orbit	11,500
Number of operational satellites	9,000
Number of fragmentation events ESA	630
Number of fragmentation events NASA	268
Number of rocket bodies	2,050
Number of derelict satellites	3,500
Number of tracked objects by SSN	35,150
Estimated number of orbital debris greater than 10cm	36,500
Estimated number of orbital debris between 1cm and 10cm	1,000,000
Estimated number of orbital debris between 1mm and 1cm	130,000,000

Source: ESA and NASA. December 2023.

Based on previous information, we can conclude that debris smaller than 1 cm generally poses a low risk of catastrophic satellite damage. While their destructive power is estimated to be minimal, such debris can still significantly impair critical systems and shorten the operational lifespan of satellites. On the other hand, debris larger than 1 cm can be very dangerous due to the high speed of collisions. Therefore, in calculations the probability of destruction for operational satellites, derelict satellites, and rocket bodies, we use the population of debris larger than 1 cm.

Projections from various space debris models, such as ESA's MASTER (Meteoroid and Space Debris Terrestrial Environment Reference) model, estimate that as of December 2023, there are 36,500 pieces of debris larger than 10 cm in diameter, 1,000,000 objects between 1 cm and 10 cm, and over 130 million fragments between 1 mm and 1 cm. As of that date, the total number of debris pieces tracked by the United States Space Surveillance Network (SSN) was 35,150.

For calibration and computational reasons (particularly due to variable scaling), we first calculate the population of orbital debris larger than 10 cm, which we assume can be approximated by the number of tracked and cataloged non-operational objects. Then, using estimates from the ESA's MASTER model, we calculate the ratio between the estimated number of debris between 1 cm and 10 cm and the estimated number of debris larger than 10 cm to obtain the total number of debris larger than 1 cm, which are considered potentially fatal.

A.1 Operational satellites

Using the model's equations and historical data, we estimate key space variables, namely the number of operational satellites in orbit and the number of satellites destroyed by collisions. First, the stock of operational satellites in orbit is estimated using the following equation for $t=1957$ to 2023,

$$S_t = (1 - \delta_s)S_{t-1} + H_t - X_t \quad (\text{A.1})$$

where S_t is the stock of satellites at time t , H_t is the number of newly inserted satellites as shown by Figure A.2, X_t is the number of satellites destroyed by collision with debris, and δ_s is the depreciation rate for satellites (see Appendix C). The initial value for the stock of satellites is $S_{1957} = 3$, given that $S_{1956} = 0$ and $H_{1957} = 3$. Figure A.3 plots the estimated stock of operational satellites for the period 1957 to 2023, resulting from running equation (A.1) for the period. Whereas the number of operational satellites were around 1,000 from 1970 to 2013, from 2016 onwards, the number of satellites experienced a sharp increase, with the building of Starlink and OneWeb satellite constellations. The estimated number of operational satellites for the year 2023 is of 8,391. The ESA estimates around 9,000 operational satellites. Those figures can be compared with the number of operational satellites in the USC satellite database at May 2023 (last update) of 7,561. Based on this information, we consider that the initial stock of satellites in orbit for the simulation of the model is of 8,500. Around 84% of operational satellites are in LEO, 12% in GEO, and the rest (4%) in MEO. However, the model is an aggregate model and does not distinguish by altitude.

Notice that, to compute the number of operational satellites in orbit, we need to know the number of satellites that have been destroyed by collision with orbital debris. The number of satellites destroyed is calculated as,

$$X_t = (1 - v_t)\theta D_t S_t \quad (\text{A.2})$$

where D_t is the stock of orbital debris, v_t is the collision avoidance capability, and θ is the collision risk parameter (see Appendix D). In this expression, D_t represents pieces of debris larger than 1 cm. v_t represents the fraction of potential collisions that can be avoided by altering the orbit of the operational satellite. This depends on the tracking, alert-systems, and maneuvering capacities of the satellite. This variable will be a key factor for computing damages, and it represents a factor that disentangles the population of orbital debris with the risk of collision. In the baseline model, v_t takes a value of one for the collision avoidance and ESA zero debris scenarios, and a value of zero for the rest. This assumption

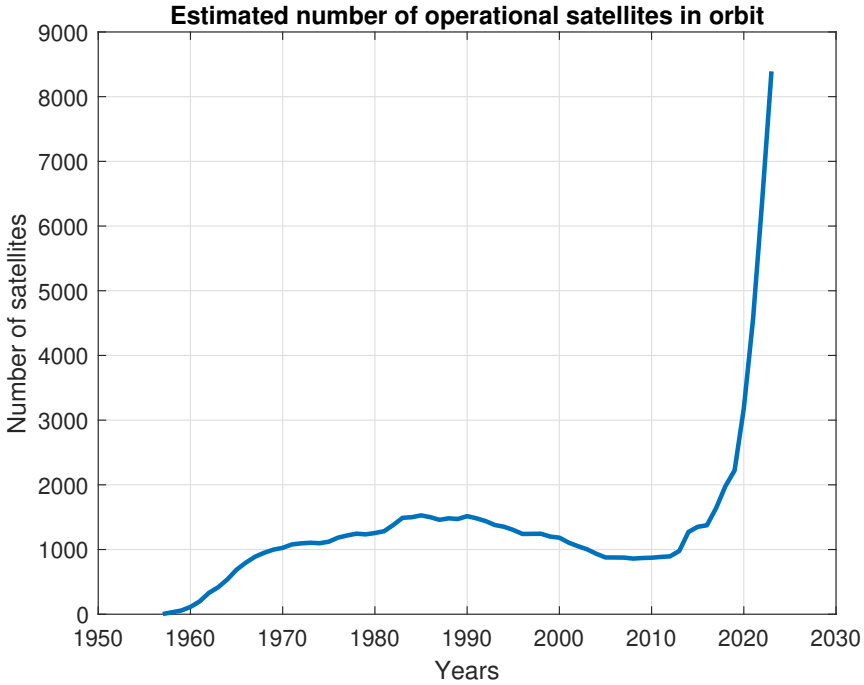


FIGURE A.3. Estimated stock of operational satellites (1957-2023)

is made for the sake of simplicity. In reality, the value of v_t is positive and increasing over time as tracking systems are developed and new satellites incorporate automatic collision avoidance systems.

Figure A.4 plots the estimated annual number of operational satellites destroyed by collisions resulting from the model for the period 1957-2023. The estimated number of fatal collisions is below 1, except for the last year of the sample period. Nevertheless, the accumulative sum of the estimation is seven for the full sample period. Estimated figures are not far from the data about losses of operational satellites by collision. Both the ESA's DISCOS database and the NASA's breakups database (Anz-Meador et al., 2022) account for a total of five collision events between operational satellites and orbital debris in each database. However, combining the two databases accounts for six different events and also includes a number of fragmentation events involving satellites for which the cause is unknown.

Many satellites have been lost or have suffered damages from impacts with micrometeoroids and orbital debris, but also due to internal failures. Some of these events are only suspected, and difficult to determine the real cause of the damages. The earliest suspected

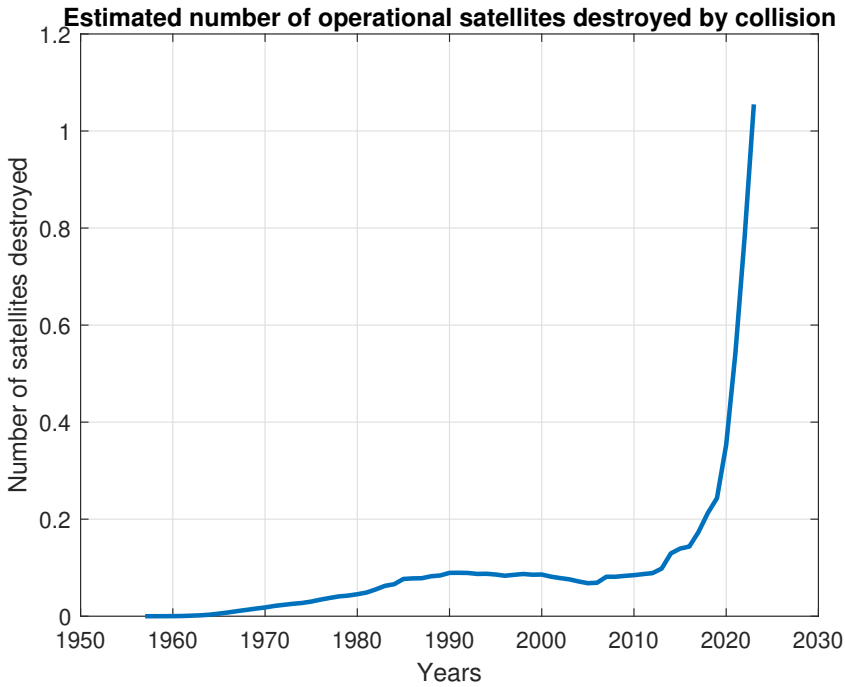


FIGURE A.4. Estimated number of operational satellites destroyed by collision

loss was of *Kosmos-1275*, a Soviet Union positioning satellite that fragmented on 24 July 1981 (a month after launch). However, there is no evidence that the destruction of this satellite was caused by a collision with orbital debris or by an internal explosion. NASA (2022a) indicates that the Russian authorities reported that the destruction of the satellite was due to a battery explosion. Tracking by NASA showed that it broke up into 479 objects. The first known collision took place on December 23, 1991 with the destruction of *Cosmos-1934*. However, the ESA's DISCOS database classifies the fail of the *Ayame-1* due to the Delta rocket fails in the insertion into planned orbit on February 6, 1979, as a collision, given that the 3rd stage of the launcher came in contact with the satellite after separation, producing 3 cataloged debris. Another collision took place on July 24, 1996, between a French microsatellite (*Cerise*) and debris from a French *Ariane-1 H-10* upper-stage rocket that had exploded in November 1986, but although the impact occurred, the satellite remained operational. The most significant known incident was the collision on February 10, 2009, between an active U.S. communications satellite (*Iridium-33*) and a defunct Russian military communications satellite (*Kosmos-2251*), resulting in the destruction of both

satellites. This collision created around 2,370 pieces of catalogued pieces of debris. On August 23, 2016, the *Sentinel-1A* was hit by a small fragments on its solar array, producing 9 cataloged debris. Finally, on November 21, 2021, the Yunhai-1-02 collided with a fragment of a Russian rocket, producing 37-38 fragments.

Table A.2 collects relevant information about operational satellite collision events as collected in the ESA's DISCOS database and in the NASA' Breakups database by Anz-Meador et al. (2022).

TABLE A.2. Operational satellite collisions

Name	Date	Cataloged debris		Apogee (Km)	Perigee (Km)
		NASA	ESA		
Ayame-1	6-Feb-1979	–	3	–	–
Cosmos-1934	23-Dec-1991	3	2	1,010	950
Cerise	24-Jul-1996	2	1	675	665
Iridium-33	10-Feb-2009	2,371	2,375	780	775
Sentinel-1A	23-Aug-2016	9	–	698	696
Yunhai-1-02	15-Nov-2021	38	37	785	780

Source: ESA's DISCOS and NASA's Breakups (Anz-Meador et al., 2022).

Apart from the confirmed events included in ESA and NASA databases, there are more suspected but nonconfirmed collisions. On March 29, 2006, the Russian *Ekspress-AM11* communications satellite was struck by an unknown object and rendered inoperable. On March 12, 2010, *Aura* lost power from one-half of one of its 11 solar panels, which resulted damaged. On January 22, 2013, *BLITS* (a Russian laser-ranging satellite) was struck by debris suspected to be from the 2007 Chinese anti-satellite missile test, changing both its orbit and rotation rate. On 22 May 2013, *GOES-13* was hit by an object, which caused it to temporarily lose track of the stars that it used to maintain an operational attitude.

A.2 Orbital debris

The stock of debris is calculated as the sum of three components: Intact objects comprising both derelict satellites and rocket bodies, and fragments. Following standard classification by ESA, fragments are defined depending on their size, considering three types: fragments larger than 10 cm, between 1 cm and 10 cm, and between 1mm and 1cm. We denote $F_{1,t}$ as the population of fragments larger than 10 cm, $F_{2,t}$ as fragments larger than 1 cm, and $F_{3,t}$ as fragments larger than 1mm. Derelict satellites and upper stages rocket bodies, including ullage motor, have sizes larger than 10 cm.

The amount of orbital debris is defined as,

$$D_{i,t} = W_t + Z_t + F_{i,t} \quad \text{for} \quad i = 1, 2, 3 \quad (\text{A.3})$$

where W_t is the stock of derelict satellites, Z_t is the stock of rocket bodies, and $F_{i,t}$ is the stock of fragments other than derelict satellites and rocket bodies, depending on their size. In our analysis, the population of debris used to calculate the risk of collision is $D_{2,t}$, that is, debris larger than 1 cm in size. The model computes fragments larger than 10 cm. Then, we assume that,

$$F_{2,t} = (1 + \Gamma)F_{1,t} \quad (\text{A.4})$$

where Γ is a scale parameter calibrated from the estimated population of debris fragments by size by the ESA (Appendix D).

In the space engineering literature, we can find a large number of orbital debris evolutionary models. In practice, several models for simulating the population dynamics of orbital debris have been developed by several authors (Farinella and Cordelli, 1991; Talent, 1992; Cordelli et al. 1993; Rossi et al. 1994; Rossi and Farinella, 1998; Lewis et al. 2009; Lafleur, 2011; Percy, 2015; Letizia et al. 2019, D’Ambrosio et al. 2022; and Lifson et al. 2022). On the other hand, debris evolutionary models have been developed by some governmental space agencies: the National Aeronautics and Space Administration (NASA), with the EVOLVE and LEGEND models; the European Space Agency (ESA), with the DELTA and MASTER models; the Japan Aerospace Exploration Agency (JAXA), with the NEODEEM model; the China National Space Administration (CNSA), with the SOLEM model; the United Kingdom Space Agency (UKSA), with the DAMAGE model, and the Centre National d’Etudes Spatiales (CNES), with the MEDEE model.

Farinella and Cordelli (1991) developed a simple model with two differential equations. Talent (1992) developed the PIB (particles-in-a-box) model. Lewis et al. (2009) developed the FADE (Fast Debris Evolution) model, consisting in a first-order differential

equation to estimate the number of new objects larger than 10 cm that are added and removed from the environment. Lafleur (2011) extended the model by Farinella and Cordelli (1991) to include collisions between intact satellites (both operational or not) and between fragments. D'Ambrosio et al. (2022) and Lifson et al. (2022) develop a debris evolutionary model for LEO with the aim of obtaining an estimate on the maximum number of satellites that can be fit in LEO. They used a PIB model based on a system of differential equations to describe the time evolution of different types of objects.

A variety of debris evolutionary models have been developed to integrate with economic models. Rouillon (2020) and Guyot and Ruillon (2023) developed a simplified model with two types of debris: large objects representing derelict satellites and rocket bodies, and small fragments. Rao and Letizia (2022) utilized a multi-shell and multi-species PIB model of the debris environment. Rao et al. (2023) developed the OPUS model. Percy (2015) and Guyot (2024) extended the two-population debris model to different layers (altitude), where atmospheric drag moves debris from upper layers to lower layers. Bongers and Torres (2023) developed a single dynamic equation with emissions related to launches and collisions. A more complex model was developed by Bongers et al. (2025).

The DAMAGE (Debris Analysis and Monitoring Architecture for the Geosynchronous Environment) model was developed by the University of Southampton (Lewis, 2020) for the UKSA. NASA developed initially the EVOLVE model in 1986 for LEO debris environment between 200 and 2000 km altitude (Krisiko et al., 2001). The EVOLVE debris model has been replaced by the LEGEND (LEO-to-GEO Environmental Debris) model (Liou et al., 2004), which reproduces the historical debris environment from LEO to GEO. The ESA has developed the MASTER (Meteoroid and Space Debris Terrestrial Environment Reference) model as a replacement for the previous DELTA model, whereas the Japan Aerospace Exploration Agency (JAXA) developed the NEODEEM (Near Earth Orbital Debris Environment Evolutionary Model) model, and the China National Space Administration (CNSA) developed the SOLEM (Space Objects Long-term Evolution Model) model (Wang and Liu, 2019).

A.3 Derelict satellites

The first type of debris is abandoned end-life satellites in orbit. This is an intact object, but the presence of residual fuels and batteries can produce an explosion and fragmentation of these objects. The law of motion of derelict satellites, W_t , is given by,

$$W_{t+1} = (1 - \delta_w - \varepsilon_w)W_t - \theta(D_{2,t} + S_t)W_t + \chi\delta_s S_t \quad (\text{A.5})$$

where δ_w is the natural orbital decay rate of derelict satellites, ε_w is the decay rate of derelict satellites due to breakups, and χ is the fraction of non-operational satellites abandoned in orbit. Values for these parameters can be found in Appendix D. The first term of the right side accounts for the reduction in the stock of derelict satellites due to natural causes or internal explosions. The second term of the right side accounts for the reduction due to collision with other debris and with operational satellites. Finally, the last term of the right side accounts for the number of non-operational satellites abandoned each period.

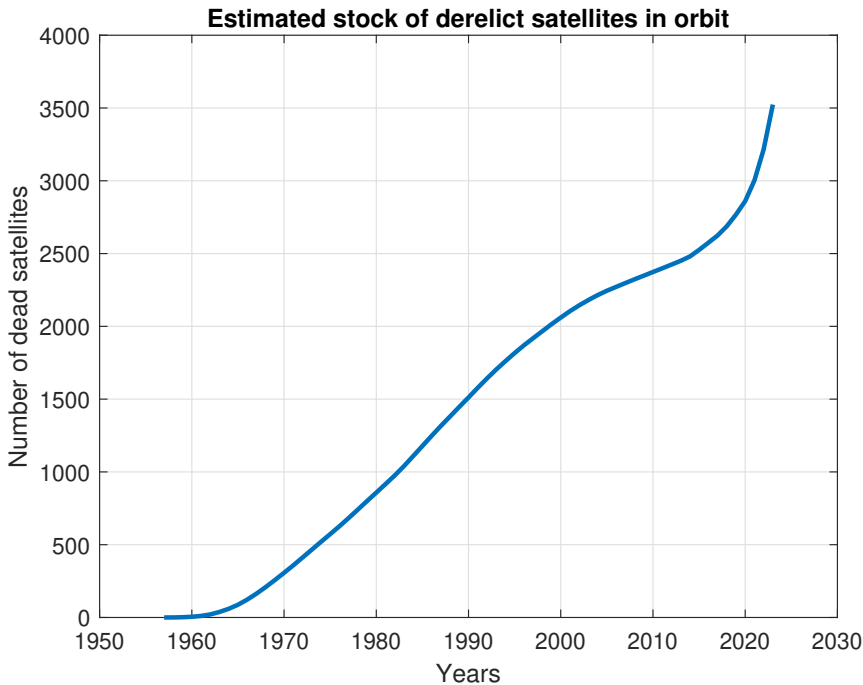


FIGURE A.5. Estimated number of derelict satellites (1957-2023)

This accumulation equation is used to estimate the stock of derelict satellites in orbit. The initial value for derelict satellites is set to zero. Accordingly to the ESA, the number

of derelict satellites in orbit as of 2023 is approximately 3,000. The DISCOS database, as of January 2025, reports a total of 13,582 payloads, encompassing both operational and non-operational satellites. Figure A.5 plots the estimated number of derelict satellites in orbit from the model for the period 1967-2023, with an estimated value of 3,524 for the year 2023.

Furthermore, it is possible to compare the estimations with NASA's estimates for the stock of spacecraft, which includes both operational satellites and derelict satellites (NASA 2024). Figure A.6 compares the values from the NASA database with the sum of estimates from Figures A.3 and A.5. For the period 1960 to 2010, the model's estimates are higher than the number of spacecraft tracked by NASA. However, the figures converge towards the end of the period, which is significant as this will be the initial value used for the model simulation. In 2023, the NASA tracked 11,860 spacecraft, whereas the model estimates 11,915.

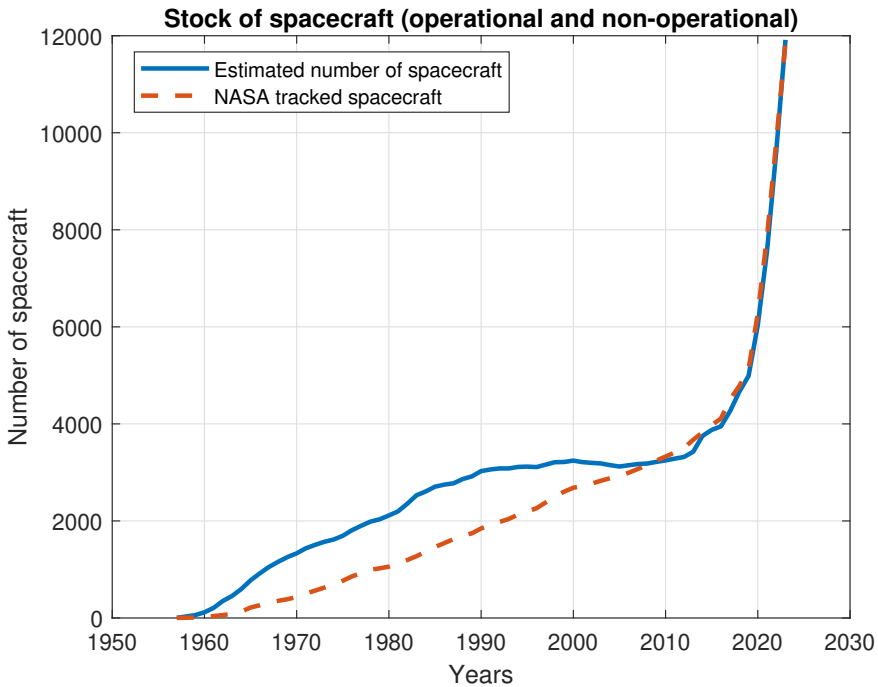


FIGURE A.6. Estimated number of spacecraft (1957-2023)

A.4 Rocket bodies

The second type of orbital debris is rocket bodies. Rocket bodies are the upper states of launch vehicle systems. Standard launch vehicles systems are composed of different stages (two to four). Whereas first stages are expended at low altitude and return to Earth, the last stage usually remains in orbit once the payload has been released if not deorbiting procedure is implemented.

As in the case of derelict satellites, rocket bodies are large intact objects that are susceptible to breakup. The final stages of launch system contain residual fuel and pressurized tanks that degrade under the extreme conditions of space, potentially leading to explosion and fragmentation of the rocket. According to Anz-Meador et al. (2022), there have been 83 rocket body breakups, resulting in a total of 8,315 tracked fragments. The first rocket body breakup occurred on 17 October 1970 with the explosion of a NASA *AGENA-D* stage. Additionally, ullage motors, relatively small rocket engines attached to the last stage of the launch system, are also intact objects subject to breakup. Anz-Meador et al. (2022) report 53 breakup events of ullage motors producing a total of 664 pieces of tracked debris.

Historically, not all final stages of launch vehicle systems have been abandoned into orbit, as some launch systems are reusable vehicles. This is exemplified by NASA's Space Shuttle program, which commenced its first flight in April 1981. The Space Shuttle was attached to a large external tank containing liquid oxygen and hydrogen, along with two solid rocket boosters (SRBs). In the first stage of flight, once the solid propellant was exhausted, the two SRBs were jettisoned and parachuted into the ocean for recovery and reuse. In the second stage, after the main engines consumed the propellants, the external tank was jettisoned, disintegrated upon reentry, and its remnants fell into the ocean. Payloads, such as satellites or other spacecraft, were deployed into orbit using a robotic arm. Upon mission completion, the orbiter vehicle re-entered Earth's atmosphere and landed for refurbishment and reuse. NASA's Space Shuttles completed 135 missions, whereas the Soviet Union's Buran shuttle completed only one flight. This type of launch vehicles can be classified as debris-free partially reusable launch vehicles. More recently, several private firms are developing reusable launch vehicles. SpaceX's Starship, although not yet operational, has completed four orbital test flights. The upcoming ninth test flight, scheduled for May 27, 2025, will mark the first time a previously flown Super Heavy booster is reused. This test is significant in advancing the development of fully reusable launch systems.

The accumulation equation of rocket bodies is a positive function of the number of launches, and a negative function of the natural decay rate, the breakups, and the collisions

with debris. The law of motion for rocket bodies, Z_t , is given by,

$$Z_{t+1} = (1 - \delta_z - \varepsilon_z)Z_t - \theta(D_{2,t} + S_t)Z_t + \varphi L_t \quad (\text{A.6})$$

whereas δ_z represents the natural decay rate of rocket bodies, ε_z denotes the fraction of rocket body breakups, φ is the fraction of rocket bodies per launch, and L_t is the number of launches at the time t . Tracked rocket bodies are included in the NASA database, Monthly objects in orbit by type.

Figure A.7 illustrates the trajectory of rocket bodies tracked by NASA along the estimates generated by the model using expression (A.6). Despite the approximation of constant parameters for natural decay and breakup rates of rocket bodies, the estimate resulting from expression (A.6) is similarly align the rocketed bodies tracked by NASA.

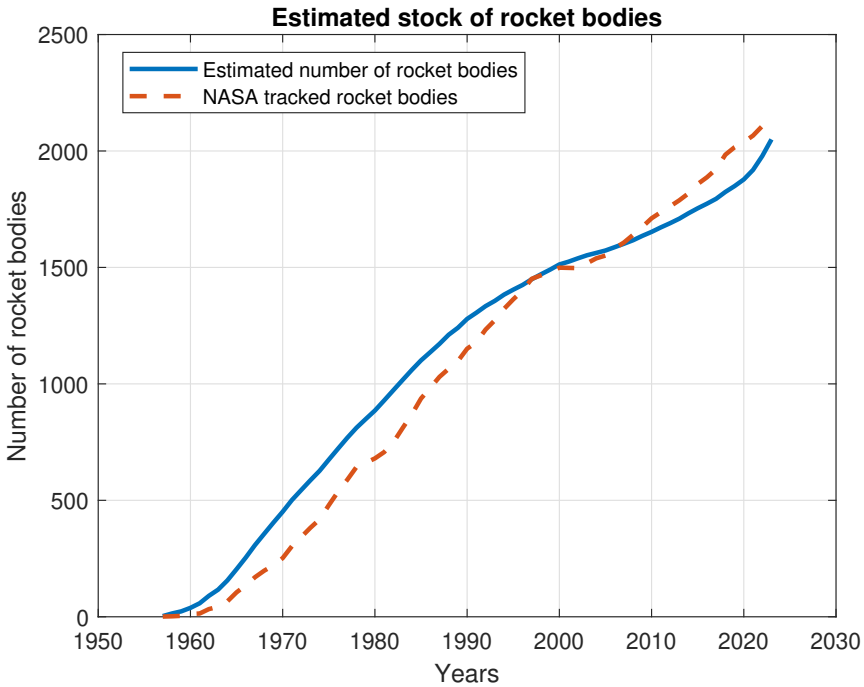


FIGURE A.7. Estimated number of rocket bodies and rocket bodies tracked by NASA

A.5 Fragments

Finally, the third type of debris is fragments. The law of motion for fragments includes two endogenous sources of orbital debris: Breakups and collisions. Formally,

$$F_{1,t+1} = (1 - \delta_f)F_{1,t} + \omega L_t + \phi_w \varepsilon_w W_t + \phi_z \varepsilon_z Z_t + \gamma_s X_t + \gamma_w \theta D_{2,t} W_t + \gamma_z \theta D_{2,t} Z_t \quad (\text{A.7})$$

where δ_f denotes the natural decay rate of fragments, ω represents the number of fragments generated per launch, ϕ_w is the number of fragment produced per derelict satellite breakup, ϕ_z is the number of fragments per rocket body breakup, γ_s is the number of fragments resulting from a collision between an operational satellite and debris, γ_w is the number of fragments from a collision between derelict satellites with debris, and γ_z is the number of fragments resulting from a collision of rocket bodies with debris.

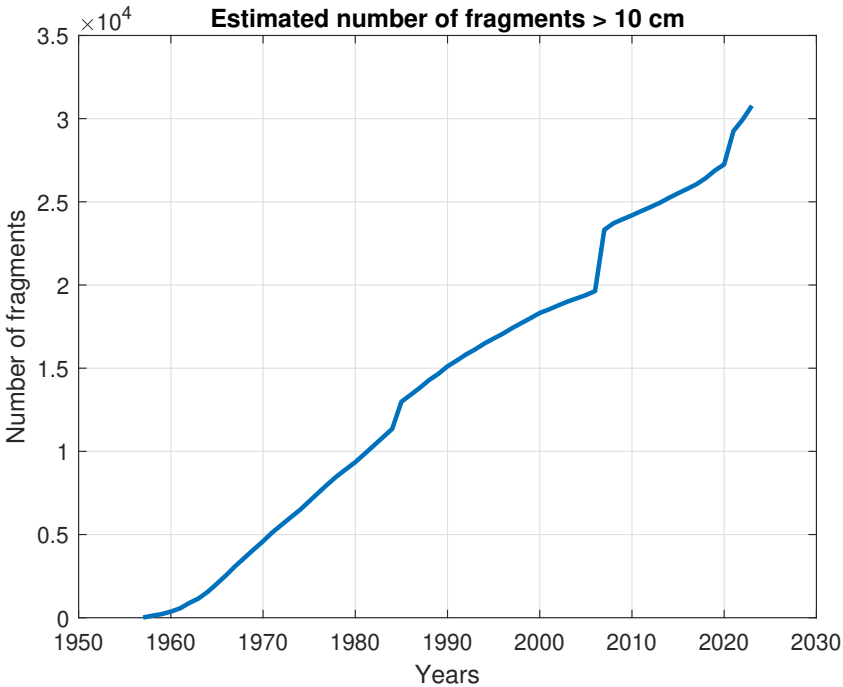


FIGURE A.8. Estimated number of fragments larger than 10 cm

A.6 Self-destruction and anti-satellite tests

A significant amount of orbital debris has been intentionally generated beyond the normal operational release of objects. This type of debris originates from the deliberate destruction of satellites. An example is a series of Soviet Union Cosmos satellites, which incorporated self-destruction explosive charges. Some Cosmos satellites, particularly military ones, were equipped with self-destruct mechanisms for security reasons. These mechanisms could be activated in cases of system failure, risk of capture by adversaries, or upon mission completion. The self-destruction typically involved an explosive charge designed to fragment the satellite into smaller pieces. According to the NASA breakups database (Anz-Meador et al., 2022), there have been 51 self-destruction events of Cosmos satellites, resulting in a total of 2,109 cataloged debris pieces.

The other intentional source of orbital debris has been the testing of direct-ascent anti-satellite (DA-ASAT) weapon systems. These systems involve modified or specialized missiles capable of reaching altitudes well above 100 km. Such missiles can either directly collide with a spacecraft (kinetic weapons) or damage it through the explosion of a warhead a broad area. Four nations: the US, Russia, China, and India, have conducted DA-ASAT tests (see Table A.3). The first true DA-ASAT tests was conducted by the US in 1959, when a missile launched from a B-47 bomber came within four miles of the Explorer VI satellite, demonstrating the feasibility of anti-satellite weapons.

TABLE A.3. Direct-ascent ASAT tests

Date	Country	Target	Altitude	Cataloged debris
13 September 1985	US	Solwind P-78	555	1,150
11 January 2007	China	Feng-Yun 1C	865	3,449
21 February 2008	US	USA-193	247	174
27 March 2019	India	Microsat-R	300	129
15 November 2021	Russia	Cosmos-1408	485	1,500

Source: Bongers and Torres (2023)

On 13 September 1985, the United States conducted a direct-ascent anti-satellite (DA-ASAT) test targeting the *Solwind P78-1*, a U.S. gamma-ray spectroscopy satellite. The satellite, weighing 850 kg and orbiting at an altitude of 555 km, was destroyed by an ASM-135 ASAT missile launched from an F-15A aircraft. The test resulted in 1,150 (initially 285) cataloged pieces of orbital debris. On 21 February 2008, the U.S. conducted another DA-ASAT test, known as Operation Burnt Frost, targeting the malfunctioning U.S. reconnaissance

satellite *USA-193*, which had a mass of approximately 2,300 kg. The satellite was intercepted at an altitude of 247 km using a modified RIM-161 Standard Missile 3 launched from a naval vessel. This test produced 174 pieces of orbital debris that were cataloged by the U.S. military.

China was the second country to test DA-ASAT weapon systems (Weeden, 2020a) as the Soviet Union focused on the development of battle-stations (*Salyut-3*), Killer satellites (Cosmos-185, 242, 375, 2521, 2536). The most important test took place on 11 January 2007, when China destroyed its own *Feng-Yun 1C* weather satellite, which had a mass of 750kg and was at an altitude of 865 km. This test resulted in the creation of 3,438 cataloged pieces of debris (NASA, 2007). On 13 November 2015, Russia conducted its first DA-ASAT test, followed by additional tests in December 2018, April 2020 and December 2020 (Kommel and Weeden, 2020). The most recent DA-ASAT test by Russia occurred on 15 November 2021, resulting in the destruction of a defunct Soviet satellite (*Cosmos-1408*) at an altitude of 485 km, producing 1,500 pieces of tracked debris according to the USSC (NASA, 2022).

Finally, the last country to join this club was India. India joined in 2019, with an DA-ASAT test in March 2019 that destroyed *Microsat-R* at an altitude of 300 km (Pfrang and Weeden, 2020b). This test created a reported 129 tracked pieces of debris, but given the low altitude of the test, the decay rate is high (Jiang, 2020).

Debris fragments have also been produced by orbital weapon systems. For instance, on 20 October 1968 a Soviet Union killer satellite (*Cosmos 252*) attacked *Cosmos-248*, producing a total of 252 tracked debris fragments (Bongers and Torres, 2023).

A.7 Debris larger than 10 cm

Debris larger than 10 cm, $D_{1,t}$, represents the population of debris estimates by the model. This includes fragments larger than 10 cm, derelict satellites, and rocket bodies. The rationale is that for calibrating the parameters of the debris evolutionary model we use information about cataloged debris. Given the existing space surveillance technology, only debris larger than 10 cm can be tracked, although some smaller pieces can also be tracked in LEO. Therefore, we assume that cataloged debris are those larger than 10 cm, and hence this is the debris type estimates by the model.

Figure A.9 plots the estimated number of debris larger than 10 cm for the period 1957-2023, including cataloged debris from ASAT tests. The jumps observed in the time series correspond to debris fragments created by DA-ASAT tests, which are totally exogenous. It can be observed that the estimated number of debris by the model is significantly larger than those reported by Space-Track or NASA.

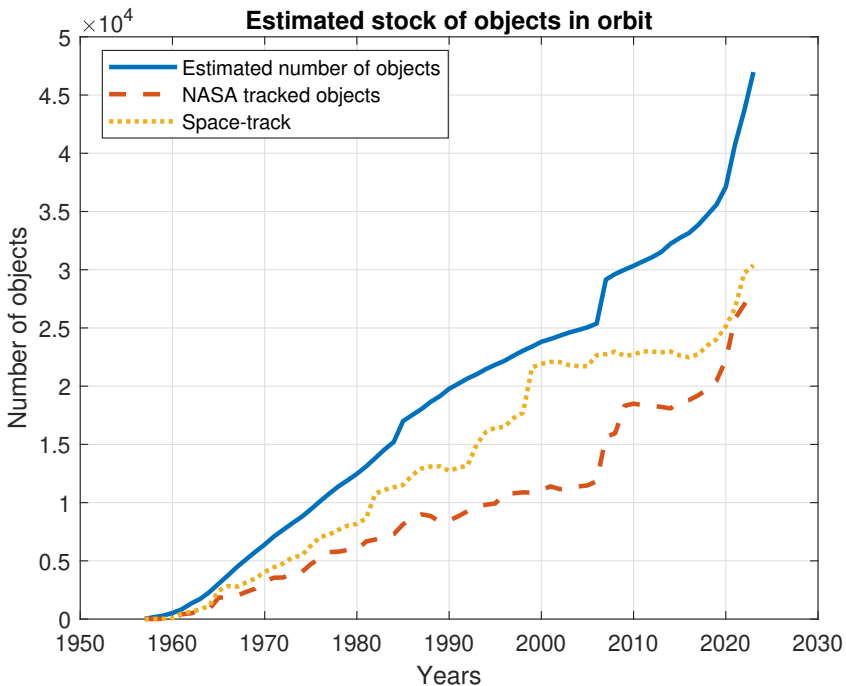


FIGURE A.9. Estimated number of objects in orbit estimated by the model, tracked by NASA, and tracked by the US Space Forces

A.8 Debris larger than 1 cm

From the estimated number of debris larger than 10 cm and using the scale factor indicated above, we obtain the estimated number of debris larger than 1 cm, which is the relevant size of debris to estimate the risk of collision. Figure A.10 plots the estimated historical trajectory debris larger than 1 cm, including fragments, rocket bodies, and derelict satellites, resulting from the calibrated model. The estimated figure for the year 2023 is 1,005,750, a number close to the 1 million orbital debris pieces larger than 1 cm estimated by the ESA by December 2023.

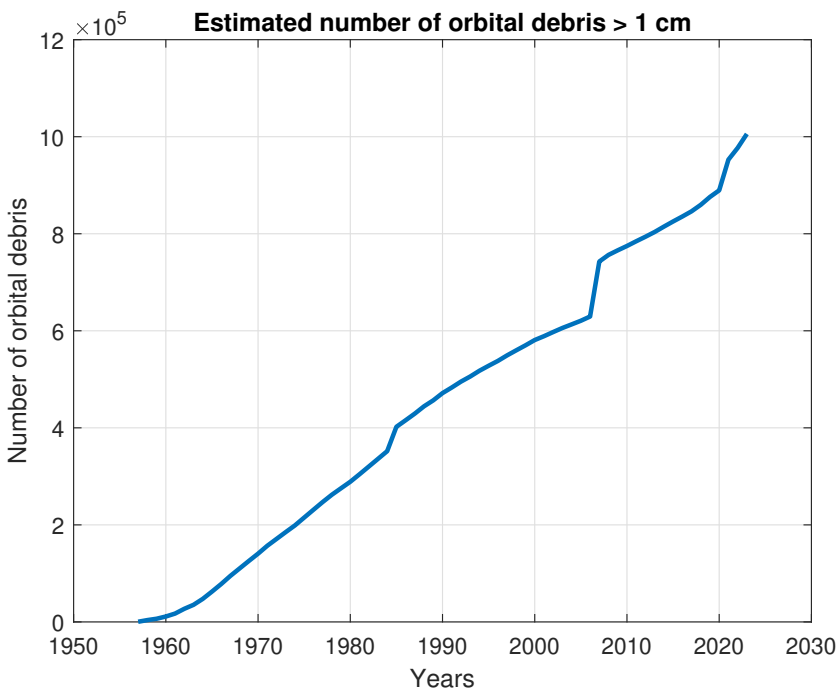


FIGURE A.10. Estimated number of orbital debris larger than 1 cm

APPENDIX B: INITIAL VALUES

The model is simulated taking 2023 as the base year. For the simulation of the trajectories of the model variables, we need initial values for the state variables and other relevant variables for the initial year. For population (i.e., labor), the figure for the year 2023 is taken from the United National Population Division (World Population Prospects, 2024), with a value of 8,056 million, and an asymptotic population value of 10,200 million. The initial value for World GDP is taken from the World Bank Economic Indicators, and is 184.65 trillions in 2023 international US\$. Other sources of World GDP estimation are the IMF and Penn World Tables. From the IMF Investment and Capital Stock Dataset, 1960-2019, World GDP was 124.2 trillions in 2017 international US\$ for the year 2019 (175.53 trillions international US\$ at current 2023 prices). This figure as estimated in the Penn World Tables (PWT 10.01, Feenstra et al. 2015), for World GDP in the year 2019 is of 125.5 trillions 2017 international US\$ (177.37 trillions in 2023 international US\$). All three estimates are fairly similar, taking into account that the estimate from the World Bank is for the year 2023, whereas the estimates from the IMF and PWT are for the year 2019.

World capital stock is taken from the IMF Investment and Capital Stock Dataset, 1960-2019, as the sum of private and public capital for the year 2019, with a value of 316.25 trillion 2017 international US\$ (446.95 trillion in 2023 international US\$). The corresponding figure from the PWT is higher 535,12 trillions 2017 international US\$, (756.27 trillion in 2023 international US\$). Comparing both databases, we find a large difference in the estimates for the capital stock. Using data from the IMF, the World capital/GDP ratio is 2.55, whereas using the PWT, the ratio is 4.26. Given that difference, we choose a middle value for the capital stock to output ratio of 3. Therefore, initial values for the year 2023 are 184.65 trillion international US\$ for GDP and 553.95 trillion international US\$ for the capital stock.

We split this figure between Earth capital and space capital, using the steady state proportion as follows. First, as indicated in appendix C, labor share is fixed to be 0.65. Given the assumption of constant returns to scale, the capital share, for Earth and space capital, is 0.35. Next, from the Euler equations for capital investment in steady state, with no risk of collision, we obtain that,

$$1 = \beta \left(\alpha_1 \frac{y}{k} + 1 - \delta_k \right) \quad (\text{A.8})$$

and

$$1 = \beta \left(\alpha_1 \frac{y(1-b)}{s} + 1 - \delta_s \right) \quad (\text{A.9})$$

for the Earth capital and space capital, respectively. Using the calibrated values for the parameters (Appendix C), and taking into account that the launch cost is 30% of total investment in space capital, we obtain that,

$$1 = 0.9852 \left(0.3479 \frac{184.65}{k} + 1 - 0.07 \right) \quad (\text{A.10})$$

and

$$1 = 0.9852 \left(0.0021 \frac{184.65 \times 0.7}{s} + 1 - 0.15 \right) \quad (\text{A.11})$$

From that we obtain that initial Earth capital stock is estimated to be $k = 552.747$, and that space (satellites) capital stock is $s = 1.203$, trillion international US dollar. The fraction of Earth capital is 99.78% of total capital, with space capital accounting for the rest 0.22%. The stock of space capital is small given the small output-satellite elasticity and the fraction of launch costs. Table B.1 summarizes the initial values for the base year (2023) used for the solution of the model.

TABLE B.1. Initial values for the year 2023

Variable	Value	Units	Source
World GDP	184.65	Trillions international US\$	World Bank
Earth Capital stock	552.474	Trillions international US\$	IMF and BEA
Space capital stock	1.203	Trillions international US\$	IMF and BEA
Launch cost	0.30	Percentage of total cost	Adilov et al. (2022)
World Population	8,056	Millions inhabitants	United Nations
Operational satellites	8,391	Units	Model simulation
Number of launches	217	Units	NASA
Derelict satellites	3,524	Units	Model simulation
Rocket bodies	2,050	Units	NASA
Orbital debris > 10 cm	36,500	Units	NASA/ESA
Orbital debris > 1 cm	1,036,500	Units	NASA/ESA

APPENDIX C: CALIBRATION OF ECONOMIC PARAMETERS

For the calibration of economic parameters, it is necessary to take into account that we are modeling the global economy, including both the Earth and space. Outer space is a global commons and any country or firm with enough financial resources and the necessary technology can access space. However, only a few countries have spacecraft launch capabilities, and not all countries operate satellites. However, services produced by satellites are consumed worldwide. The US is the absolute leading spacefaring country. Private spacefaring companies are also dominated by US companies, such as SpaceX. However, an increasing number of countries are also developing space industries and gaining spacecraft launch capabilities.

The economy module of DISE-2024 includes some standard parameters in the macroeconomic literature, although it also includes some new parameters related to the space sector. This set of parameters includes the social pure discount factor, the elasticity of marginal consumption, the technological parameters of the production function, and the physical capital and satellite depreciation rates. For that set of parameters, we use standard values from the literature. Additionally, the model includes two technological growth processes: Total Factor Productivity (TFP) and Investment-Specific Technological Change (ISTC) in satellites, and the labor growth rate (see Appendix E).

TABLE C.1. Baseline calibration of the economic parameters of DISE-2024

Parameter	Definition	Value	Source
ρ	Pure time preference parameter	0.015	Nordhaus (2008)
σ	Intertemporal marginal consumption rate	1.50	Nordhaus (2008)
α_1	Capital share	0.3479	BEA
α_2	Satellite share	0.0021	BEA
δ_k	Capital depreciation rate	0.07	Standard
δ_s	Satellite depreciation rate	0.15	NASA
μ	Conversion parameter	4,941	Internal

C.1 *The pure rate of time preference (ρ)*

The pure rate of time preference reflects how individuals value present consumption compared to future consumption. The rate of time preference indicates the degree to which people prefer to receive goods or utility sooner rather than later, that is, it is a measure of the impatience of households. This reflects individual preferences for present consumption over future consumption, indicating how much current utility is valued compared to future utility. A higher rate implies a stronger preference for the present compared to the future. The relationship between the pure rate of time preference and the social discount rate is a fundamental aspect of economic theory, particularly in the context of public policy and welfare economics. The social discount is the rate used to convert future costs and benefits into present values when evaluating public projects and policies. It represents society's preference for current benefits over future ones. Therefore, this is a key parameter for the design and implementation of mitigation policies for emissions which effects are long-lasting.

The social discount rate often incorporates the rate of time preference along with considerations for economic growth and risk. A higher rate of time preference implies a higher social discount rate, suggesting that society prioritizes present benefits over future ones. This can lead to less investment in long-term projects, such as infrastructure or environmental sustainability. Conversely, a lower rate of time preference (or higher growth expectations) may result in a lower social discount rate, allowing for greater consideration of long-term benefits. The choice of the social discount rate also has significant implications for intergenerational equity. A high discount rate may prioritize current generations at the expense of future ones, while a lower rate can promote policies that consider the welfare of future generations more equitably.

The appropriate level of the social discount rate is an important debate in macroeconomics and, especially, in environmental economics, as it is an indicator of how society values future benefits relative to present ones. Some authors argue for a lower rate to account for the welfare of future generations, while others emphasize the uncertainties associated with long-term forecasts. In the literature, we find two alternative approaches for determining the social discount rate: the prescriptive and the descriptive approaches. The prescriptive approach derives a normative social discount rate based on ethical considerations (Ramsey, 1928; Stern, 2006). The descriptive approach calculates the social discount rate based on observed interest rates. The social discount rate based on ethical considerations is obtained through surveys of academic experts and is much lower than that based

on market interest rates. In contrast, the descriptive approach relies on observed interest rates, resulting in a much higher social discount.

The social discount rate has proven to be a key parameter for assessing the implications of climate-change policies. Estimated values range between the 2% per year used by Weitzman (2007) and the 0.1% used by Stern (2006). The US Interagency Group uses a central value of 3%, with a low bound of 2.5% and an upper bound of 5%. Barro (2015) argues that the use of low discount rates is inconsistent with empirical evidence and not supported by the theoretical side.

With a CRRA instantaneous utility function, we have that in steady state $r_t = \rho + \sigma g_{c,t}$, where r_t is the discount rate (interest rate) representing the net present value of a dollar in t year, σ is the intertemporal marginal consumption rate, and $g_{c,t}$ is the growth rate. This is the so-called Ramsey equation. With a steady-state growth of 2% and a relative risk aversion parameter of 2, the discount rate ranges between 6% and 4.1%, aligning with values commonly used in standard Dynamic Stochastic General Equilibrium (DSGE) macroeconomic models. For the baseline calibration, we fix the value of ρ to be 1.5% per year.

The Ramsey equation is obtained as follows. The problem solved by an infinitely-lived representative household can be formulated as,

$$\max_{c_t} \sum_{t=0}^{\infty} \left(\frac{1}{1+\rho} \right)^t U(c_t) \quad (\text{C.1})$$

subject to the following budget constraint,

$$c_t + b_t = y_t + (1 + r_{t-1})b_{t-1} \quad (\text{C.2})$$

where b_t is the stock of savings, y_t is labor income, and r_t is the interest rate of savings. It is assumed a utility function of the Constant Relative Risk Aversion (CRRA) type, defined as:

$$U(c) = \frac{c^{1-\sigma}}{1-\sigma} \quad (\sigma \neq 1) \quad (\text{C.3})$$

where σ is the coefficient of relative risk aversion. The first-order condition for maximizing utility requires that the marginal utility of consumption is equated across time. The marginal utility of consumption at time t is given by:

$$U'(c_t) = c_t^{-\sigma} \quad (\text{C.4})$$

First order conditions are derived by solving the following Lagrange problem

$$\mathcal{L} = \left(\frac{1}{1+\rho} \right)^t \frac{c^{1-\sigma}}{1-\sigma} - \lambda_t (c_t + b_t - y_t - (1 + r_{t-1})b_{t-1}) \quad (\text{C.5})$$

First order conditions are:

$$c_t^{-\sigma} - \lambda_t = 0 \quad (\text{C.6})$$

$$-\left(\frac{1}{1+\rho}\right)^t \lambda_t + \left(\frac{1}{1+\rho}\right)^{t+1} (1+r_t) \lambda_{t+1} = 0 \quad (\text{C.7})$$

Combining both first-order conditions, we get,

$$c_t^{-\sigma} = \frac{1+r_t}{1+\rho} c_{t+1}^{-\sigma} \quad (\text{C.8})$$

taking logarithms of both sides yields:

$$-\sigma \ln(c_t) = \ln(1+r_t) - \ln(1+\rho) - \sigma \ln(c_{t+1}) \quad (\text{C.9})$$

Let $g_{c,t} = \frac{c_{t+1}}{c_t} - 1$ denote the growth rate of consumption. For small $g_{c,t}$, we have that:

$$\ln(c_{t+1}) = \ln(c_t) + \ln(1+g_{c,t}) \approx \ln(c_t) + g_{c,t} \quad (\text{C.10})$$

Substituting into the logarithmic expression:

$$-\sigma \ln(c_t) = \ln(1+r_t) - \ln(1+\rho) - \sigma(\ln(c_t) + g_{c,t}) \quad (\text{C.11})$$

Finally, assuming that r_t and ρ are small, $\ln(1+r_t) \approx r_t$, and $\ln(1+\rho) \approx \rho$, we arrive to

$$r_t = \rho + \sigma g_{c,t} \quad (\text{C.12})$$

C.2 Intertemporal marginal consumption substitution parameter (σ)

This parameter reflects the curvature of the utility function, which is the inverse of the elasticity of marginal utility of consumption. See, for instance, Szpiro (1986) and Arrow (2007), Dasgupta (2007, 2008), and Weitzman (2007, 2009). A higher σ (a lower elasticity of intertemporal substitution) means the household is less willing to substitute consumption intertemporally. The use of a CRRA instantaneous utility function makes the value of the intertemporal substitution is equal to the inverse of the coefficient of relative risk aversion, both reflecting the curvature of the utility function. Formally, the elasticity of marginal utility of consumption is defined as the curvature of the utility function,

$$\sigma = -c \frac{U''(c)}{U'(c)} \quad (\text{C.13})$$

where $U'(c_t) = c_t^{-\sigma}$ and $U''(c_t) = -\sigma c_t^{-\sigma-1}$. Typically, σ is assumed to be independent of the reference consumption path, c_t , although there is no clear reason why it should be so (Dasgupta, 2008). In standard models, for the class of utility functions in which σ is constant, the larger this parameter, the greater the curvature of the utility function. For the typical specification of the utility, $U(C)$ is bounded above but unbounded below if $\sigma > 1$, while the reverse holds if $\sigma < 1$.

In the literature, the relative risk aversion parameter σ takes values between 1 (a logarithmic instantaneous utility function) and 3. For example, Stern (2006) use a value of 1, Nordhaus (2008) uses a value of 1.5, whereas Nordhaus (2017) uses a value of 2. In our baseline calibration, we set the value of σ to 1.5 in the baseline calibration. Most studies that have quantified global climate change impacts assume $\sigma = 1$; however, there is a growing number of studies that rely on the elasticity of marginal utility of consumption above the unity (e.g., Cline (1992) assumed $\sigma = 1.5$). Evans (2005) estimates the elasticity of marginal utility of consumption for 20 OECD countries based on the structure of personal income tax rates, finding an average value of around 1.4, with a range from a value of 1.00 for Ireland to 1.82 for Australia. However, other authors use large values. For instance, Mehra and Prescott (1985) estimate values greater than 10.

The literature has developed a variety of alternative methods to estimate these parameters: Direct estimation of the consumption Euler equation (Hansen and Singleton, 1982), methods based on income tax data (Stern, 1977), approaches using asset returns data (Mehra and Prescott, 1985), direct survey-based methods (Barsky et al., 1997), or based on the labor supply distortions by tax (Chetty, 2006). Stern (1977) used income tax data for the UK and suggested a value of σ around 2, with a range between 1 and 10. Barsky et al.

(1997) surveyed 11,707 middle-aged respondents in the US to elicit measures of risk tolerance, the elasticity of intertemporal substitution, and time preference. They found that there is substantial heterogeneity in these preference parameters. In their study, they report the mean of the coefficient of relative risk aversion ranging from 0.7 to 15.8, with the average at about 4.0.

Finally, some authors relax the assumption of a time-separable utility function and instead use an Epstein-Zin utility function with dynamic preferences (Epstein and Zin, 1989). This utility function allows for the separation of the risk aversion and the intertemporal elasticity of substitution and hence makes it possible to investigate how alternative values for these two parameters affect households' intertemporal decisions. See, for example, Ackerman et al. (2013).

C.3 Output-capital elasticity parameters (α_1, α_2)

For the calibration of technological parameters, we proceed as follows. First, we assume that capital and labor income shares are fixed over time. Dynamic macroeconomic models typically assume that output-input elasticities remain constant over time. With a Cobb-Douglas technology, technological parameters representing the elasticity of output with respect to capital and labor are equal to the capital and labor income share, respectively.

We fix the labor share to be 0.65. Given the assumption of constant returns to scale, this means that the sum of the technological parameters for Earth capital and space capital is 0.35 (i.e., $\alpha_1 + \alpha_2 = 0.35$). Corrado et al. (2023) calibrate the space sector's share of the overall economy at 0.0056. The Bureau of Economic Analysis (BEA, 2023) estimates that space industry contributed 129,9 billion dollars to the US economy in 2021 (0.6% of GDP), supporting a total of 360,00 full- and part-time jobs in the private space industry. Space Foundation (2023) estimates that the global space economy had a total impact of \$546 billion for the year 2022. The satellite Industry Association (SIA, 2023) estimates that the global space economy accounted for \$384 billion for the year 2022. Using this information, we allocate the capital share between Earth capital and space capital. The elasticity of output with respect to satellites equipment is calculated as $\alpha_2 = 0.35 \times 0.006 = 0.0021$. Hence, the elasticity of output with respect to Earth capital is $\alpha_1 = 0.35 - 0.0021 = 0.3479$. Nozawa et al. (2023) calibrated a Cobb-Douglas production function including labor, capital and satellites, and used a value of 0.002 for the elasticity of output to the stock of satellites.

C.4 Capital depreciation rates (δ_k, δ_s)

Typically, dynamic macroeconomic models assume that capital stock depreciates at a constant rate over time, although some models consider a non-constant depreciation rate due to a time-varying use of capital over the business cycle or to structural changes driven by technological progress, which alter the proportion of the different types of capital assets used in the economy. Capital depreciation rates greatly vary depending on the type of capital asset (Fraumeni, 1997). Structures typically show a relatively low depreciation rate compared to equipment, while capital assets related to information and communication technologies (ICTs) usually have a much higher depreciation rates. For instance, the European Central Bank (2006) estimates an average capital depreciation rate of 4.6% per year in the Euro Area, corresponding to an average lifetime of capital stock around 20 years. By asset type, depreciation rates are approximately 2% for housing, 3% for non-residential structures, 14% for equipment, and 24% for other assets including software.

Capital depreciation rates also vary across countries, as they have different combinations of capital assets. However, depreciation rates by asset type are fairly similar, and only in extreme climate conditions can depreciation rates vary substantially. In general, it is assumed that depreciation rates increase with income levels. Gupta et al. (2014) estimate that depreciation rate of private capital ranges from 4.25% in low-income countries, 8.10% in middle-income countries, to 10.41% in high income countries. For public capital, depreciation rates range from 2.5% in low-income, 3.5% in middle-income, to 4.59% in high-income countries. In the estimation of capital stocks in the Penn World Tables (PWT), depreciation rates differ across assets, across countries and over time (Feenstra et al., 2015), with average estimated values of 2% for structures, 12.6% for machinery and 31.5% for computers and software.

In the literature, standard macroeconomic models use values in the range of 7-10% per year for aggregate capital depreciation rate (or approximately 0.025 per quarter) in the case of developed economies. For the world economy, which not only include developed economies but also developing economies, the depreciation rate would be at the lower range. Therefore, the depreciation rate of capital other than satellites (what we call Earth's capital), δ_k , is set at 0.07.

In calibrating the depreciation rate of satellites, we also take into account that they are not homogeneous and exhibit specific characteristics that influence their average operational life. The extreme conditions in outer space and technical characteristics of satellites determine their life-span, in additions to differences in design depending the mission. A

satellite's life-span depends on its type, as well as electrical, mechanical, physical and gravitational factors (Gallois, 1987). One important limitation to a satellite's operational life is fuel capacity. Indeed, some derelict satellites may remain functionally intact and capable of delivering services, but are rendered inoperable due to fuel depletion, which prevents repositioning to the target orbit. Lifespans vary significantly, from as little as 6 months for CubSats (miniaturized satellites), to up to 15 years of GEO satellites. For LEO satellites, the lifespan typically ranges from 3 to 8 years. For example, the expected lifespan of Starlink satellites is of 5-7 years. Bongers and Torres (2023) assume an average lifetime of 8 years for all satellites, leading to an annual depreciation rate of 0.1733. Nozawa et al. (2023) use a depreciation rate for satellites of 0.216, based on an assumed average lifespan of 4.64 years for LEO satellites. In this study, we assume a depreciation rate of 15% per year ($\delta_s = 0.15$).

C.5 Conversion parameter (μ)

The model includes both economic and physical measurement of the same variable. While economic variables are measured in monetary values (trillions of international dollar), physical variables are measured in units. One characteristic of the theoretical model is that for obtain a numerical solution it is necessary to work simultaneously with both output-value and physical variables. This forces the introduction of a mapping function between both types of variables. As a reference, we use the value of satellites and the number of satellites. This mapping is extended to satellites destroyed by collisions, new satellites inserted in orbit, and launches.

The conversion parameter from economics variables to physical variables is calculated internally, dividing the initial number of satellites in units, S_0 , by the initial value of the stock of satellites measured in trillions international US\$, s_0 . Hence, $\mu = 8,500/1.72 = 4,941.9$. This value is fixed throughout the simulation horizon. The inverse of this number can be interpreted as a proxy of the unit value of satellites, including the associated capital assets used in the space sector.

APPENDIX D: CALIBRATION OF PHYSICAL PARAMETERS

For the calibration of physical parameters, we primarily rely on data from NASA Breakups Database (Anz-Meador et al., 2022) and ESA’s DISCOS database (DISCOSweb), supplemented by additional sources such as the Union of Concerned Scientists (UCS) Satellite Database and Jonathan C. McDowell’s satellite datasets. To calibrate the number of fragments generated by breakup or collision events, we use information on cataloged debris. We assume that debris larger than 10 cm is adequately represented by cataloged fragments. Accordingly, the calibrated number of fragments corresponds to debris exceeding 10 cm in size. Using the proportional parameter Γ , we estimate the population of debris larger than 1 cm based on the population of debris larger than 10 cm. The calibrated physical parameters are presented in Table D.1.

TABLE D.1. Baseline calibration of the physical parameters of DISE-2024

Parameter	Definition	Value	Source
η	Satellites per launch	13.6	NASA
δ_w	Derelict satellites natural depreciation rate	0.00015	Lafleur (2011)
δ_z	Rocket bodies natural decay rate	0.00015	Lafleur (2011)
δ_f	Fragments debris natural decay rate	0.01	Lafleur (2011)
θ	Collision risk parameter	1.25×10^{-10}	ESA
χ	Fraction of abandoned satellites	0.40	ESA
φ	Body rockets per launch	0.60	ESA
ε_w	Fraction of dead satellites breakups	0.0010	ESA
ε_z	Fraction of body rocket breakups	0.0012	ESA
ω	Number of fragments per launch	4.00	ESA
ϕ_w	Number of fragments per derelict satellite breakup	40.6	ESA/NASA
ϕ_z	Number of fragments per rocket body breakup	100.2	ESA/NASA
γ_s	Number of fragments per operational satellite collision	70	ESA/NASA
γ_w	Number of fragments per derelict satellite collision	70	ESA/NASA
γ_z	Number of fragments per rocket body collision	70	ESA/NASA
v_t	Collision avoidance proportion	0	Baseline
Γ	1cm to 10 cm debris proportional parameter	32.3	ESA

D.1 Satellites per launch (η)

Current technology for inserting satellites into orbit is entirely based on rocket launch systems. Rockets launch vehicles consist in several stages (from two to four). The first stage(s) provide the initial thrust and separate after fuel is exhausted. The upper stage(s) continue to propel the satellite toward its target orbit. Typically, a single rocket carries more than one payload, depending on the rocket's capacity and the payloads' size. The number of payloads per rocket launch has significantly increased in recent years due to advancements in rocket design, more powerful launch systems, and standardization and miniaturization of satellites. Recent launch systems like SpaceX's Falcon 9 and Falcon Heavy can carry dozens or even hundreds of payloads in a single launch, driven by the rise of small satellites and cubesats as well as the enhanced power of rocket engines. This trend reflects the growing demand for cost-effective access to space and innovations in payload integration systems.

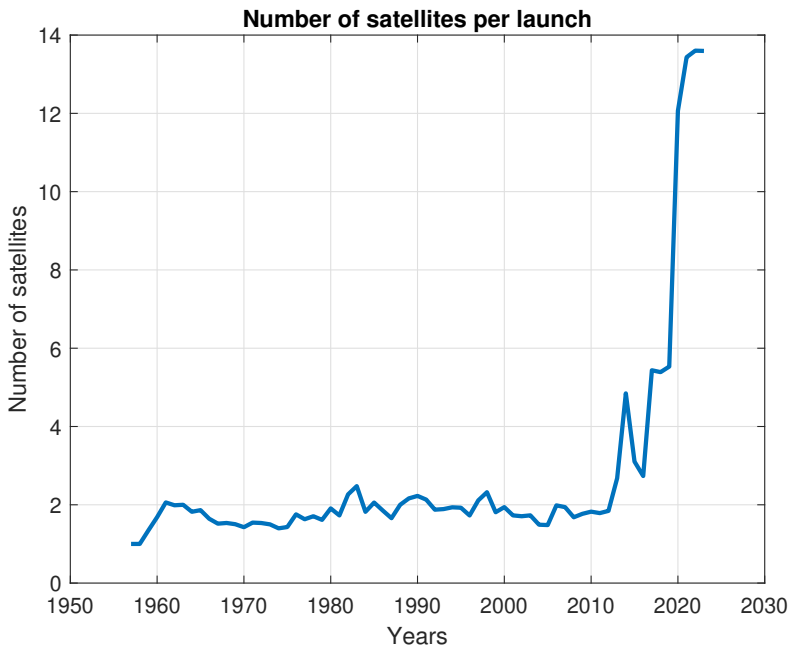


FIGURE D.1. Number of satellites per rocket launched

Figure D.1 plots the number of payload per launch for the period from 1957 to 2023. It can be observed that for most of the period, the number of satellites per launch remained almost constant around an average of 2 payloads per launch. However, this stable trend

began to change dramatically starting in 2015, increasing to more than 10 satellites per rocket in recent years, a sharp change mainly associated with the launch of the satellites of the Starlink constellation.

For the calibration of the model, instead of using the average number over the historical sample period, we use the ratio corresponding to the last year of the period, implicitly assuming that the observed change occurring in recent years will be permanent. The number of satellites inserted into orbit during the year 2023 is $H_0 = 2,950$, and the number of launches is $L_0 = 217$. Therefore, $\eta = H_0 / L_0 = 13.6$. This value is kept fixed throughout the simulation horizon, as we have no information on how this ratio will change in the future.

D.2 Fragments natural decay rate (δ_f)

The accumulation process of orbital debris critically depends on their survival time in orbit, which is a function of their natural decay rate. The computation of the decay rate of objects in orbit is a controversial issue in space engineering. The value of this parameter varies dramatically depending on the altitude of the object, making it difficult to obtain an average decay rate for the totality of objects in Earth's orbit. The decay rate of an object in orbit depends on a large number of factors, most of which are difficult to estimate accurately or are highly variable over time, even on an hourly basis. As pointed out by Niccolai and Mengali (2024), the estimation of the decay rate of an object in orbit is a very challenging task due to the difficulty to accurately modeling atmospheric properties and complex orbital dynamics. On the other hand, as pointed out by Lafleur (2011), the lifetime differs significantly between intact satellites and fragments because fragments typically have larger surface-area-to-volume ratios. Therefore, we distinguish the natural decay rate of small fragments from that of large intact objects, such as rocket bodies and derelict satellites.

The natural decay rate of orbital objects depends on several factors, including the altitude (or atmospheric density), orbit circularity, mass, area, solar radio flux, and geomagnetic index. The most important factor is the altitude due to the atmospheric drag, which results from the interaction of the object with the few air molecules present at high altitudes. This drag is very high at low altitudes but extremely low at high altitudes. Atmospheric drag tends to reduce the altitude of an object in orbit (and also circularize the orbit). The drag reduces the velocity of the object and pulls it towards the Earth. For relative low altitudes (below 1,000 km), gravitational effects of the Earth is the main factor affecting the behavior of objects. However, for high orbit, such as GEO, the gravitational effects of the sun and the moon, as well as solar radiation, are the dominant forces affecting dynamics of object at that altitude.

The force of gravity acting on an object in orbit serves as a centripetal force. Hence, in the case of a circular orbit, by applying Newton's second law along with the relationship between centripetal acceleration and the object's linear velocity, the orbital velocity of the object can be expressed as,

$$v = \sqrt{\frac{GM}{r}} \quad (\text{D.1})$$

where G is the gravitational constant ($6.674 \times 10^{-11} \text{ N} \times \text{m}^2 \times \text{kg}^{-2}$), M is the mass of the Earth ($5.98 \times 10^{24} \text{ kg}$), and r is the radius of the trajectory (the distance of the object to the center of the Earth), with the Earth's radius equal to 6,378 km. As a result of previous

expression, the conserved mechanical energy of the system (without considering any form of mechanical energy dissipation), is given by,

$$E = -\frac{GMm}{r} + \frac{1}{2}mv^2 = -\frac{GMm}{2r} \quad (\text{D.2})$$

where m is the mass of the object measured in kg . Atmospheric models based on previous calculations are used to predict the decay rate of objects. The decay rate of an object in orbit is a function of atmospheric density at each point along the orbit, the effective cross-sectional area perpendicular to the direction of motion, A , the mass m , and the drag coefficient C_D , which usually estimated from a free molecular flow model. C_D is generally assumed to be equal to 2.2 (Cook, 1965; Jacchia, 1972), although this can vary depending on altitude. The combination of these three parameters results in the so-called ballistic coefficient (King-Hele, 1987). The drag force F_D , is calculated as,

$$F_D = \frac{1}{2}C_D A \rho v^2 \quad (\text{D.3})$$

where ρ is the atmospheric density (a function of altitude, latitude, longitude, the season and time of the day, temperature, thermosphere composition, and the solar and geomagnetic activity), measured in kg/m^3 , and v is the velocity measured in m/s . On average, for a given altitude, atmospheric density can be approximated as a function of two parameters: the solar 10 cm radio flux (F_{10}), and the geomagnetic index A_p . Most drag models use solar radio flux at 10.7 cm wavelength as a proxy for solar ultraviolet flux. The solar 10 cm radio flux varies between 70 (solar minimum conditions) and 250 (solar maximum conditions). The rate of energy loss due to drag can be calculate as,

$$\frac{dE}{dt} = -F_D v \quad (\text{D.4})$$

Substituting for F_d , we have,

$$\frac{dE}{dt} = -\frac{1}{2}C_D \rho A v^3 \quad (\text{D.5})$$

For the case of near-circular orbits, the semi-major axis a is approximately equal to the radius of the central body plus the altitude ($a \approx r + h$). The semi-major axis is defined as the distance from the center of an ellipse to the farthest point along its major axis. As energy is lost due to atmospheric drag, the semi-major axis gradually decreases, leading the object to spiral closer to Earth,

$$\frac{da}{dt} = \frac{1}{GMm} \frac{dE}{dt} = -\frac{1}{2GMm} C_D \rho A v^3 \quad (\text{D.6})$$

For a near-circular orbit we have that $dh/dt \approx da/dt$, and therefore, the rate of altitude loss can be calculated as,

$$\frac{dh}{dt} = -\frac{1}{2GMm} C_D \rho A v^3 \quad (\text{D.7})$$

The object acceleration on the decay orbit, is then calculated as,

$$Drag = \frac{1}{2} \frac{C_D \rho A}{m} v^2 \quad (\text{D.8})$$

Doornbos et al. (2013) indicate that for the case of orbital debris, where both the mass and the area are unknown, it is more appropriate to estimate the inverse of the ballistic coefficient rather than the drag coefficient. The inverse of the ballistic coefficient, B , is defined as,

$$B = \frac{C_D A}{m} \quad (\text{D.9})$$

Calibrating of the debris natural decay rate is a key issue in this analysis, as this parameter determines the natural reduction in the stock of debris and, hence, also affects the distribution of debris as a function of altitude is not homogeneous. The spatial density of debris shows that it is concentrated in the range 700-900 km (NASA, 2020). Bongers and Torres (2023) use the average of this figure as a reference, and therefore estimate the average lifetime of debris at around 150 years. Assuming straight-line decay, this implies an annual decay rate of 0.0067. This is consistent with the value for the general atmospheric decay parameter of 0.0062 used by Lewis et al. (2009) in the Fast Debris Evolution (FADE) model.

The Australian Space Weather Agency (1999) estimated that the lifetimes of space objects vary significantly with altitude: approximately 1 day at 200 km, 1 month at 300 km, 1 year at 400 km, 10 years at 500 km, 100 years at 700 km, and 1000 years at 900 km. Rao and Rondina (2023) use data from ESA regarding the residence time of objects in orbit and calculate a share-weighted decay rate of 7.4% per year for the 600-650 km shell, 5% for the 650-700 km shell, and 3% for the 700-750 shell. Lafleur (2011) calculates an average debris decay rate for objects in LEO (up to 2,000 km) using the ballistic coefficient, assuming a representative value of 1.8 kg/m^2 for fragments. Based on this, he derives drag coefficient under both solar-maximum and the solar-minimum conditions, weighted by the distribution of objects at different orbit altitudes. Under the solar-maximum conditions, the average lifetime of debris fragment is of 46.9 years (a decay rate of 0.021), whereas under solar-minimum conditions, the average lifetime extends to 332.8 years (a decay rate of 0.003), resulting in a mean decay rate of 0.012 for LEO debris.

As an example, using the NASA's breakups database (Anz-Meador et al., 2022), we calculate the debris decay rate following the collision between *Iridium-33* and *Kosmos-2251* collision on February 10, 2009, was 1,347. This collision occurred at an altitude of 780 km. By January 1, 2011, 1,273 pieces of debris remained in orbit, representing 94% of the original debris, implying a decay rate of approximately 6% over two years, or about around 0.03 per year, assuming linear decay. Similarly, *Iridium-33* produced 528 cataloged fragments, with 492 pieces remaining in orbit by January 1, 2011 (or 93%), which corresponds to a decay of 7% in two years, or an annual decay rate of approximately 0.035. In contrast, the intentional destruction of *Fengyun-1C* during a military test on January 11, 2007, generated 3,037 pieces of cataloged debris. As of January 1, 2011, 2,932 pieces were still in orbit, 97% of the initial total. This implies a decay rate of just 3% over four years, or approximately 0.0075 per year. These differences in decay rates are mainly due to the altitude at which the debris was generated. While *Iridium-Kosmos* collision occurred at approximately 776 km, the *Fengyun-1C* even took place at a higher altitude of 860 km, where atmospheric drag is significantly lower, leading to slower orbital decay.

Table D.2 presents examples of the decay rate derived from NASA's breakups database, focusing on five fragmentation events. The first two cases correspond to debris generated by collision, while the remaining three involve breakups, two from rocket bodies (R/B) and one from a satellite. Even when the collision occurs at the same altitude, different decay rates are observed. For example, fragments from *Iridium-33* show a decay rate of 0.0557, whereas those from *Cosmos-2251* decay at a slower rate of 0.0389. These discrepancies highlight the role of orbital characteristic, particularly circularity, that is, the difference between the apogee and perigee, in influencing decay rate. In the case of the *Arabsat-4* rocket body breakup, a relatively low decay rate of 0.0065 is estimated, despite a perigee of just 495 km. For comparison, fragments from the *Telecom-3* rocket body breakup exhibit a much higher decay rate of 0.1863, even though the orbit ranges from a perigee of 265 km to an apogee of 5,010 km. This sharp contrast is likely driven by the low perigee, which exposes the debris to significant atmospheric drag. Finally, the breakup of a satellite in higher, more stable orbit, ranging between 960-1,015 km, results in a decay rate of 0.033, consistent with expectations for such altitudes.

Locke et al. (2024) assume that all fragments are spherical and model atmospheric drag using a simplified atmospheric density profile based on the ballistic coefficient, without accounting for solar radiation pressure. For small debris, they assume that a constant drag coefficient is 2.2. Prieto et al. (2014) provide a comprehensive review of existing methods for estimating drag coefficient.

TABLE D.2. Decay rates for selected case of the NASA's breakups database

Satellite	Apogee (Km)	Perigee (Km)	δ_f
Iridium 33	780	775	0.0557
Cosmos 2251	800	775	0.0389
Arabsat 4 Briz-M R/B	14,705	495	0.0065
Telecom 3 express MD2 Briz-M R/B	5,010	265	0.1863
Cosmos 1275	1,015	960	0.0033

An online calculator for satellite orbital decay, develop by the Australian Space Weather Agency, is available at https://www.lizard-tail.com/isana/lab/orbital_decay/. Below, we present a MATLAB code adapted from the original QBASIC implementation provide by Australian Space Weather Agency for estimating decay rates of satellites in circular orbits below 500 km.

```
% *****
% ORBITAL DECAY
% Adapted from the QuickBasic code of the Australian Space Weather Agency
% Optimal path for orbital debris
% *****
% Get required input parameters
M = input('Mass (kg): ');
A = input('Area (m^2): ');
H = input('Altitude (km): ');
F10 = input('Solar Radio Flux (SFU) (40-400): ');
Ap = input('Geomagnetic A index (0-280): ');
% Print information
fprintf('ORBITAL DECAY - Model date/time: %s\n', datestr(now));
fprintf('Mass = %.1f kg\n', M);
fprintf('Area = %.1f m^2\n', A);
fprintf('Initial height = %.1f km\n', H);
fprintf('F10.7 = %.1f, Ap = %.1f\n', F10, Ap);
% Column headings
fprintf('TIME          HEIGHT          PERIOD          MEAN MOTION          DECAY\n');
```

```

fprintf('(days)      (km)          (mins)      (rev/day)      (rev/day^2)\n');
% Constants
Re=6378000;          % Earth radius in km
Me=5.98e24;          % Earth mass in kg
G=6.67e-11;          % Gravitational constant
pi=3.1416;
T=0;                 % Initial time in days
dT=0.1;              % Time increment in days
D9=dT*3600*24;       % Time increment in seconds
H1=10;               % Height decrement for printing
H2=H;                % Initial height for tracking
R=Re+H*1000;         % Orbital radius in meters
P=2*pi*sqrt(R^3/(G*Me)); % Orbital period in seconds
% Iteration for orbital decay
while H > 180 % Loop until satellite re-entry
    % Atmospheric scale height and density
    SH=(900+2.5*(F10-70)+1.5*Ap)/(27-0.012*(H-200));
    DN=6e-10*exp(-(H-175)/SH); % Atmospheric density
    % Change in orbital period
    dP=3*pi*A/M*R*DN*D9;
    % Print results when height decreases by H1
    if H <= H2
        Pm=P/60;          % Period in minutes
        MM=1440/Pm;        % Mean motion in rev/day
        nMM=1440/((P-dP)/60); % New mean motion
        Decay=dP/dT/P*MM; % Decay in rev/day$ \hat{} $2
        fprintf('%6.1f %8.1f %8.1f %10.4f %10.5f\n', ...
            T, H, Pm, MM, Decay);
        H2=H2-H1;          % Update print height
    end
    % Update values for next iteration
    P = P-dP;              % Update period
    T = T+dT;              % Update time
    R = (G*Me*P^2/(4*pi^2))^(1/3); % Update orbital radius
    H = (R-Re)/1000;       % Update height in km
end

```

44

end

\% Print estimated lifetime of the satellite

```
fprintf('Re-entry after \%.1f days (%.2f years)\n', T, T/365);
```

D.3 *Derelict satellites natural decay rate (δ_w)*

The natural decay rate of intact objects in orbit differs significantly from that of orbital fragments. Fragments typically have a much larger surface-area-to-volume ratio compared to intact objects such as derelict satellites or rocket bodies. This characteristic leads to a smaller ballistic coefficient for fragments, which in turn results in much shorter orbital lifetime at a given altitude compared to intact objects. Conversely, intact objects have higher ballistic coefficients and thus remain in orbit for longer periods under similar conditions. Moreover, the drag coefficient also varies between fragments and intact objects. For example, Locke et al. (2024) report that the space drag coefficient for intact spacecraft ranges from $C_D = 10$ for a 6U cubesat to $C_D = 35$ for a larger NOAA-20 type satellite. These values reflect the variation in size, shape, and surface properties that affect how objects interact with the residual atmosphere in low Earth orbit.

Lafleur (2011) estimates an average debris decay rate for intact objects in LEO (up to 2,000 km) using the ballistic coefficient value of 110 kg/m^2 as an approximate representation for satellites. From this, he derives the drag coefficient under both solar-maximum and the solar-minimum conditions. The values are weighted according to the distribution of satellites across different orbit altitudes. Under solar-maximum conditions, the average lifetime of derelict satellites is approximately 3,990 years (a decay rate of 0.00025), whereas under solar-minimum conditions, the average lifetime extends to about 24,850 years (a decay rate of 0.00004), resulting in a mean value for the natural decay rate of satellites in LEO of 0.000145. In calibrating δ_w we take Lafleur's (2011) estimated mean value for the natural decay rate as a reference. However, since the model incorporates all orbital regimes, the actual average natural decay rate is likely to be even lower. In the baseline calibration, this parameter has been fixed to 0.00015.

D.4 *Rocket bodies natural decay rate (δ_z)*

Natural decay rate of rocket bodies is calculated in a similar way to that for derelict satellites. Rocket bodies are intact objects and, therefore, their natural decay rate is lower than that of fragments. For rocket bodies, Locke et al. (2024) assume a drag coefficient of $C_D = 60$. This implies that the natural decay rate of rocket bodies is even lower than that of derelict satellites. However, Lafleur (2011) does not distinguish between derelict satellites and rocket bodies and instead uses an average mass-to-surface ratio for all intact objects. As no additional information is available, we adopt the average value estimated by Lafleur (2011), and hence, $\delta_z = 0.00015$.

D.5 Risk of collision (θ)

In the history of activity in outer space, a number of collisions have been reported. Collisions can occur between pieces of debris themselves or between debris and operational satellites. A risk of collision between operating satellites also exists, but in some cases they can be avoided by maneuvering, although many satellites have limited or no maneuvering capabilities. Several collisions with human-made debris have been reported in recent years, but some incidents likely remain undocumented. On February 10, 2009, an active US communications satellite (Iridium 33) collided with a non-operating Russian military communications satellite (Kosmos 2251). On January 22, 2013, a Russian small satellite (BLITS) was destroyed by a piece of debris from Fengyun-1C. On May 22, 2013, two CubeSats collided with debris (Ecuador's NEE-01 Pegaso and Argentina's CubeBug-1). A large number of potential collisions are avoided through frequent satellite and spacecraft maneuvering. Krisko (2007) estimated an average number of catastrophic collisions (involving a target and impactor larger than 10 cm) of 0.9, whereas the estimation from the DAMAGE model (Lewis et al, 2009) is 1.5, both covering the period 1957-2006. As a result of these collisions, numerous pieces of debris have been generated. Farinella and Cordelli (1991) estimated a value of $\theta = 3 \times 10^{-10}$, based on an estimated quantity of debris of 50,000.¹ This implies a number of satellite destruction per year of 0.2, given a collision probability ($\theta \times 50,000$) of 1.5×10^{-5} . Kawamoto et al. (2019) estimated that the current probability of collision is substantially higher. The total probability of collision of objects larger than 10 cm is approximately 0.1 for 800-900 km orbits, 0.05 for 900-1,000 km orbits, and 0.025 for 600-700 km orbits. Following Farinella and Cordelli (1991) we adopt a total probability of 0.2 (i.e., one fatal collision every 5 years) as the reference, which aligns with observed number of incidents (four collisions occurred in the period 1991 to 2009), resulting in a collision probability $\theta \times D = 6.6 \times 10^{-5}$. Pardini and Anselmo (2014) estimate that the risk of collision in LEO increased by a factor of 4.5 between 1980 and 2010.

Lafleur (2011) estimates a value of $\theta = 6.895 \times 10^{-10}$. Percy (2015) estimates a value of $\theta = 6.37 \times 10^{-10}$. Guyot and Rouillon (2024) use a value of $\theta = 4 \times 10^{-10}$. Bongers and Torres (2023) estimate a value of $\theta = 6.37 \times 10^{-11}$. In this paper, following Bongers et al. (2025), we adopt a value of $\theta = 1.25 \times 10^{-10}$, based on the observed number of registered collisions.

¹Farinella and Cordelli (1991) estimate the number of collisions per unit cross section per year as the average collision velocity (10 km/s) divided by the volume of the circumterrestrial shell ($1,800 \text{ km} \times 6 \times 10^8 \text{ km}^2$).

D.6 Fraction of abandoned satellites (χ)

Defunct satellites abandoned in orbit is observed to be an important source of orbital debris. The operational life of satellites is typically short (just a few years). Once they are no longer operational, they effectively become debris if they remain in orbit. In most cases, satellites reach the end of their life after running out of fuel. Derelict satellites may still be functionally intact, but without fuel, they cannot be maneuvered to remain in their designated orbit. This means they lack maneuvering capacity. In such cases, they are abandoned in orbit, posing a risk of breakup due to residual fuel or battery explosions. In the early years of space exploration, the fraction of abandoned satellites was high. Over time, growing concerns about this practice have reduced the proportion of satellites left in orbit. Today, most spacefaring entities implement post-mission disposal (PMD) plans to either deorbit satellites or move them to a graveyard orbit at the end of their mission life.

This occurs when satellites exhaust their fuel reserves and can no longer be moved to graveyard orbits. Such cases were relatively common during the early stages of space exploration. Abandoned satellites pose a significant risk due to their size and mass. Indeed, one of the most damaging incidents was the collision between Kosmos 2251 with Iridium 33 in February 2009. However, the number of abandoned satellites is small compared to other types of orbital debris. Furthermore, new international standards for spacefaring nations and companies emphasize the importance of including reserve fuel for end-of-life deorbiting maneuvers. As a result, it is expected that the number of derelict satellites abandoned in orbit will decline over time, particularly as concerns about orbital debris continue to grow.

For the calibration of this parameter, we proceed as follows, using data from the ESA. As of December 2023, the total number of satellites launched is of 16,990, of which 11,500 remain in orbit. Hence, the difference ($16,990 - 11,500$) corresponds to end-life satellites that have been deorbited, either naturally or intentionally, or have fragmented, totaling 5,490. In addition, the number of derelict satellites abandoned in orbit as of December 2023 is estimated at 3,500. Therefore, the total number of end-life satellites over the sample period, including the current stock of derelict satellites, amounts to $5,490 + 3,500 = 8,990$. Assuming that the accumulated number of derelict satellites corresponds to the number of abandoned end-life satellites, the lower bound for the fraction of satellites, the lower bound for the fraction of satellites abandoned in orbit can be approximated as: $\chi = 3,500/8,990 = 0.389$. Hence, we fix this parameter to be 0.4.

D.7 Fraction of rocket bodies abandoned in orbit (ϕ)

Rocket bodies represent another source of intact debris objects. Rocket bodies are large, with a substantial surface area and mass. Standard launch systems are composed of multi-stage rocket vehicles, typically two to four stages, to generate the necessary thrust to reach the target altitude. It is the upper stages of these rockets that are commonly left in orbit. Although some upper stages are brought back to Earth in a controlled manner, most are abandoned in orbit, as spacefaring agencies maximize the lifting capacity of rockets and typically do not reserve fuel for deorbiting maneuvers. Historically, not all launches have resulted in upper stages remaining in orbit. This is primarily due to the NASA Space Shuttle program. NASA's shuttle fleet flew 135 missions, while the Soviet Union's Buran shuttle completed only one. Although the Space Shuttle developing reusable launch systems. For example, the SpaceX's Starship is not yet fully operational but has already completed four orbital test flights. On the other hand, some spacefaring operators systematically conduct upper stages disposal. For example, this is the case with SpaceX's Falcon-9 vehicles (a two-state rocket), where the second stage is deorbited after releasing its payloads. Jonathan McDowell's annual reports on Space Activities (the last one for the year 2024) provide detailed information about the disposal of launch vehicle upper stages. See also Byers and Boley (2023) and Wright et al. (2024) on this issue, who indicate that over 60% of launches to LEO resulted in at least one rocket body being abandoned in orbit. For the year 2018 (McDowell, 2019), the number of launches with upper stages disposal was of 33 out of 112, whereas the number of stages left in orbit was 89 out of 112 launches. Therefore, the ratio of abandoned rocket bodies in orbit to launches was of 0.795. The number of upper stages disposed of corresponds to the Falcom-9, SAST CZ-2D, and Vega-C vehicles. For the year 2019 (McDowell, 2020), the number of launches with upper stages disposal was 21, and the number of stages left in orbit was 86 out of 97, with a rocket body abandonment rate of 0.887. For 2020, there were 39 launches with upper stage disposal and 71 upper stages left in orbit out of 104 launches, resulting in an abandon rate of 0.683. According to Wright et al. (2024), in 2021, 97 out of 136 successful launches (71.3%) left rocket bodies in orbit. In 2022, the figure was 129 abandoned rocket bodies out of 180 launches, which represents a ratio of 71.7% (McDowell, 2023). For 2023, there were 122 rocket bodies abandoned from 212 successful launches, resulting in an abandonment rate of 57.5%, largely due to the high number of Falcon-9 launches, whose second stage are routinely deorbited (McDowell, 2024). Given this data, we adopt a baseline calibration of the model we used a value of $\phi = 0.60$, reflecting the recent trend in upper stages rocket body management.

D.8 Fraction of dead satellites breakups (ϵ_w)

A dead satellite abandoned in orbit is not only a big intact piece of debris, but also poses a significant risk of breaking up into thousands of fragments. The probability of such a breakup depends on several factors: the satellite's design, the presence of residual energy sources (such as unspent fuel or unpassivated batteries), and the duration of exposure to the harsh conditions of space, which deteriorate spacecraft components over time.

Accordingly to NASA's breakups database (Anz-Meador et al., 2022) a total of 47 satellite breakups had occurred by 2022, excluding deliberate destruction events. Of these, one involved an operational satellite, while the remaining 46 were derelict satellites. We estimate the value of this parameter by dividing the number of breakups by the estimated cumulative number of derelict satellites, W_t , calculated in Figure A.5. The cumulative number of derelict satellites for the period 1957-2023 is of 130,066. This gives a value of $46/130,066 = 0.00035$. In the baseline calibration of the model we use a value of $\delta_w = 0.001$.

D.9 *Fraction of rocket bodies breakups (ϵ_z)*

Rocket bodies (last stages of launch systems) contain engines and residual propellant tanks. As the rocket bodies spend extended periods in orbit, harsh environmental conditions can degrade their components, potentially causing explosions and fragmentation. These events are typically triggered by residual fuel, pressure changes in chemical tanks, or other physical and chemical processes. Kessler et al. (2010) indicate that in the initial years of space exploration, upper stages rocket bodies often tended to explode in orbit after a mission completion. However, since the early 1980's, design improvements and revised operational procedures have significantly reduced this risk.

According to NASA's monthly database on the number of objects in orbit, the number of rocket bodies as of December 2023 was 2,129. In NASA's breakups database (Anz-Meador et al., 2022), a total of 83 rocket body breakups have been recorded. The cumulative number of rockets launched is 6,508, and the cumulative number of rocket bodies abandoned in orbit over the full period is 70,282. Dividing the number of breakups by the total number of rocket bodies abandoned in orbit, we estimate that $\delta_z = 83/70,282 = 0.00118$.

D.10 *Number of fragments of debris per launch (ω)*

Launch activity is the primary source of debris generation, and the parameter ω represents the number of fragments generated per launch, excluding rocket bodies. This parameter includes only parts of launch vehicles discarded during the process of inserting a satellite into the target orbit, explicitly excluding expended rocket bodies. This is the case of payload fairings, connecting parts among rocket stages, adapter rings covers for optical instruments.

Jonathan McDowell's Space Activity reports offer detailed information on the number of debris pieces, excluding upper stages, released by launches for the years 2018 to 2023. According to this data, in 2018, there were 112 launches, producing 68 pieces of debris, approximately one piece for every two launches. In 2019, there were 97 launches and 38 pieces of debris. In 2020, 106 launches produced 61 debris pieces. In 2021, 136 launches resulted in 105 debris fragments. In 2022, 180 launches producing 143 pieces of debris. Finally, in 2023, 212 launches generated 61 debris items. Thus, over the 2019-2023 period, the number of debris pieces per launch remained below one, indicating a trend toward reduced debris generation during launch activities.

Lewis et al. (2009) estimated that an average of 2.75 intact objects are introduced into the space environment per launch. At a minimum, 2 fragments are released per launch, as payload fairings typically split into two halves, but additional objects are often expected to remain in orbit. Based on this, We assume that each launch produces a total of 4 fragments.

D.11 Number of fragments per derelict satellites breakup (ϕ_w)

Derelict satellites abandoned in orbit constitute intact objects that may breakup. These events occur when inactive satellites suddenly fragment due to explosions caused by residual fuel or ruptures in onboard batteries.

For the calibration of this parameter, we use information on recorded satellite breakups from Anz-Meador et al. (2022) and the DISCOS database. Some of these satellite breakups were intentional, such as several Soviet Union satellites that were deliberately destroyed.

In the NASA's brakups database (Anz-Meador et al., 2022), a total of 47 satellite breakups are recorded up to 2022, excluding deliberate destruction events (Table D.3). These breakups are mainly due to unknown causes (36 out of 47), although some of them could be associated with satellite inspectors (Killer satellites, such as the *Cosmos-252*, *Cosmos-375*, and *Cosmos-2535*) that, for unknown reasons, release debris when attacking the target satellite. In other cases, the confirmed cause is battery explosion (9 cases), and propulsion-related failures (2 cases).

TABLE D.3. Satellite breakups and cataloged debris. Source: Anz-Meador et al. (2022)

Cause	Number	Cataloged debris	Cataloged debris per breakup
Unknown	36	1,248	34.7
Battery	9	1,030	114.4
Propulsion	2	41	20.5
Total	47	2,319	49.3

The DISCOS database includes 12 fragmentation events involving satellites due to battery explosions, resulting in a total of 979 cataloged debris items (an average of 81.6 fragments per event). Additionally, there are three fragmentation events caused by accidental factors, which produced a total of 35 cataloged debris items, or approximately 11.7 fragments per event.

Another type of satellite fragmentation results from self-destruction using explosive charges, such as in the case of the *Cosmos-862* series. According to DISCOS, a total of 22 fragmentation events due to explosives are recorded, producing 173 cataloged fragments, which corresponds to an average of about 8 fragments per explosion.

D.12 Number of fragments per rocket body breakup (ϕ_z)

As with the previous parameter, we use the information from Anz-Meador et al. (2022) and the DISCOS database on rocket body breakup events and the corresponding number of debris generated. This database records a total of 83 rocket body breakups, resulting in 8,315 cataloged debris, which corresponds to an average of 100.2 fragments per event. The NASA database also includes ullage motor breakups, with 53 events producing 664 cataloged fragments, or 12.5 pieces per event. However, ullage motors are significantly smaller than standard rocket bodies and are no longer in use, making their contribution less relevant for current modeling purposes. Hence, we fixed $\phi_z = 100.2$.

Fragments resulting from the breakup of rocket bodies is highly dependent on the type of rocket. For example, according to DISCOS, the *Titan Transtage* experienced four breakup events, generating 194 cataloged fragments, for an average of 48,5 per breakup. In contrast, the Delta upper stage accounts for 15 breakups, producing a total of 1,959 cataloged debris, which represents an average of 130.6 fragments per event. The number of fragmentation events by *CZ-6A* recorded is of four, with an average number of 390.5 piece of debris fragments. For the *Ariane* rocket, a total of 30 breakups events, producing a total of 845 pieces of debris (an average of 28.3 debris fragments per event).

D.13 Number of pieces of debris per operational satellite collision (γ_s)

The number of new debris fragments generated by collisions between an operational satellite and a piece of orbital debris could vary significantly, primarily depending on the masses and relative velocities of the colliding objects. The most significant recorded incident occurred on 10 February 2009, involving the collision of an active US communications satellite (*Iridium-33*) with a defunct Russian satellite (*Kosmos-2251*). This event produced an estimated 2,371 cataloged debris fragments (Anz-Meador et al., 2022) while the ESA's DISCOS database lists 2,375 fragments for the same incident. In contrast, the collision involving *Sentinel-1A* resulted in only 9 cataloged fragments. However, this incident is not classified as a collision in the DISCOS database. The most recent recorded collision occurred 18 March 2021, when the Chinese satellite *Yunhai-1-02* collided with a piece of debris producing a total of 38 cataloged debris (37 according to DISCOS).

According to the NASA's breakups database (Anz-Meador et al., 2022), 7 confirmed collision events have been recorded to date, generating a total of 2,430 cataloged debris, averaging 347 fragments per collision. In addition, the database includes 67 events of unknown cause, which have produced 3,436 cataloged debris, averaging 51 pieces per event. According to the DISCOS database, a total of 6 fragmentation events due to collisions have been recorded. Five correspond to collision between operational satellites and pieces of orbital debris (*Cosmos-1934*, *Iridium-33*, *Cerise*, *Ayame-1*, and *Yunhai-1-02*). The sixth event corresponds to the collision of an upper stage motor (*Star-26B*) with a debris fragment on 17 January 2005, resulting in six cataloged debris fragments. When considering only the 5 events involving operational satellites, the average number of cataloged fragments per event is approximately 483.6.

On the other hand, a total of 51 deliberate self-destruction events, all attributed to Soviet Union satellites, are registered in the database. These events produced a combined 2,109 pieces of cataloged debris, yielding an average of 41 fragments per event. To estimate the total number of debris fragments larger than 1 cm, we extrapolate from the cataloged fragments (which represent objects larger than 10 cm) using the ratio of estimated debris: larger than 10 cm (36,500) and between 1 cm and 10 cm (1,000,000). The resulting figures are an average of 9,855 ($347 + 347 \times 27.4$) pieces of debris larger than 1 cm from collisions between operational satellites and debris, an average of 1,448 for the unknown events, and an average of 1,164 for self-destruction.

Farinella and Cordelli (1991) estimated this debris generation from hypervelocity impacts based on the typical mass distribution of fragments. Their findings suggest that a

catastrophic collision, where the largest surviving fragment is around 10 kilograms, produces approximately 10,000 fragments with masses exceeding a few grams. Similarly, Lewis et al. (2009) found that the number of pieces of debris per catastrophic collision is 625 (collision with debris larger than 10 cm) and 25 for a damaging collision (collision with debris between 1 and 10 cm). Applying the scaling factor used to estimate debris larger than 1 cm, the results is 17,750 for catastrophic collision and 710 in the case of a non-catastrophic collision. The NASA Standard Breakup model further refines these estimates by modeling fragments production based on mass and energy transfer in collisions, calibrated through laboratory hypervelocity impact experiments. Jonhson et al. (2001) found similar outcomes between two objects with a combined mass of of 1,260 kg, which is comparable to the average mass of a medium-class satellite (Bryce, 2020). Assuming a uniform collision probability across debris size classes, the final calibrated estimate for the number of fragments larger than 1 cm per collision event is 1,309, a figure closely aligned with those derived from observed accidental explosions. Based on all previous information, we fixed $\gamma_s = 70$ as the baseline.

D.14 Number of fragments from derelict satellites collision (γ_w)

Derelict satellites are non-operational satellites that have reached the end of their service life (i.e., have run out of fuel) and remain in orbit without any form of control. These uncontrolled objects pose a collision risk to both operational satellites and other pieces of orbital debris. The only registered collision involving a derelict satellite was a collision with an operational satellite (the collision of the derelict satellite *Cosmos-2251* with the operational satellite *Iridium-33*). Anz-Meador et al. (2002) indicate that this collision produced a total of 2,371 cataloged fragments. However, this collision involved two large objects, and we can expect a lower number of fragments in the case of collision with a small piece of debris.

Although data is limited, derelict satellites have the same characteristics as operational satellites. Therefore, in case of collision, we can argue that they will be fragmented in a similar way to the rest of the operational satellites. This means that the calibration of the parameter γ_w takes the same value as the parameter γ_s , although the model allows for using a different fragmentation coefficient than that of operational satellites. Therefore, we fix $\gamma_w = 70$.

D.15 Number of fragments from rocket bodies collision (γ_z)

Given the differences in mass and size between rocket bodies and satellites, we might expect a different fragmentation behavior in the event of a collision between these two types of objects. Kessler et al. (2010) indicate that, whereas a number of tests have been conducted to understand the size distribution from the collision of a payload, none have been conducted on rocket bodies, and the standard assumption in breakups models is that payloads and rocket bodies fragment under identical conditions and produce identical fragment distribution. However, as Kessler et al. (2010) point out, the large tank of rocket bodies may not absorb all the energy of a collision, or, by contrast, could dissipate the energy of a collision over the opposite tank wall, acting like a Whipple shield. Therefore, it remains unclear whether a rocket body collision would generate more fragments or fewer fragments than a satellite collision.

The source for the calibration of this parameter is Anz-Meador et al. (2022). However, there is only one collision in January 2005 between a rocket body (*DMSP-5B-F5 Thor-Burner 2A rocket*) and other debris from a Chinese ASAT test, producing 5 cataloged debris fragments. Another collision was deliberate (the collision of USA-19 with the upper stage of USA-19), resulting in the fragmentation of USA-19 in 13 cataloged debris fragments and the fragmentation of the rocket body into 5 cataloged debris fragments. Given the lack of available data, we adopt the same assumption as the LEGEND model: that both payloads and rocket bodies produce identical fragment distributions in case of collision. Therefore, we assume that $\gamma_z = 70$.

There is more extensive data available from upper stage explosions in orbit (parameter ε_z). As noted by Kessler et al. (2010), collisions release significantly more energy than explosions, and thus we would expect the number of fragments produced by a collision to be larger than that the produced by an explosion. Previously, the parameter representing cataloged fragments from rocket bodies breakups was estimated to be 100, based on the information from the NASA breakups database, which is larger than the number of fragments produced by satellite breakups. However, based on the Kessler et al. (2010) arguments, we take a conservative perspective, and assume a number of fragments from rocket bodies collisions as for derelict satellites collisions.

D.16 *Collision avoidance fraction (v_t)*

The damage function incorporates an additional variable to account for collision avoidance operations. Operational satellites, except for small cubsats in LEO, are capable of performing maneuvers to prevent collisions. When such maneuvers are successfully executed, collisions, and the resulting destruction of the satellite, are avoided, thereby preventing the generation of debris fragments that would otherwise occur. This variable is assumed to be determined exogenously. In the baseline scenario, the fraction of avoided collisions is set to zero. In the no-collision scenario, the value of v_t is set to one. However, the model can be simulated for any value of the collision avoidance fraction up to one. Alternatively, v_t can be modeled as a time-varying, increasing function, which could be justified by technological advancements in tracking orbiting objects, improved conjunction assessments, and enhanced spacecraft maneuverability. This is left for a future extension of the model.

D.17 Size debris proportional parameter

The model considers different types of debris depending on their size, following standard classification by the ESA: debris between 1 mm and 1 cm, debris between 1 cm and 10 cm, and debris larger than 10 cm. Whereas DISE-2024 consider that debris larger than 1 cm can be catastrophic in case of collision, for the calibration of the different parameters of the model, available information refers to tracked or cataloged debris, which usually have larger than 10 cm in size. Therefore, whereas the debris module calculates debris larger than 10 cm, the collision probability and the damage functions require the population of debris larger than 1 cm.

Mains et al. (2024) use the IMPACT satellite fragmentation model (Mains and Sorge, 2022) to study four fragmentation events, including two collision (*Cosmos-1408* ASAT test and *SL-14* rocket body), a rocket body breakup (*Long March 6A*), and a satellite breakup (*Resur-01*). The IMPACT model is used to predict the number of fragments larger than 10 cm and larger than 1 cm. A summary of the results is shown in Table D.4, including the number of cataloged objects and the estimated number of fragments larger than 10 cm and 1 cm. The average proportion across the three events is 63.21. Nevertheless, this is a limited sample, and difficult to extrapolate to the whole debris environment.

TABLE D.4. IMPACT model estimations

Object	Cataloged	Fragments > 10 cm	Fragments > 1 cm	Ratio
Cosmos-1408	1,600	1,320	200,000	151.50
CZ-6A R/B	500	734	20,000	27.24
Resur-01	100	147	1,600	10.88
<i>Average</i>	733.33	733.66	73,866.66	63.21

Source: Mains et al. (2024).

Based on the population of debris of different sizes estimated by the ESA, to compute the number of debris larger than 1 cm, we use the scaling factor as follows,

$$\Gamma = \frac{1,000,000}{(36,500 - 2,050 - 3,500)} = 32.3 \quad (\text{D.10})$$

where 1 million is the population of debris between 1 cm and 10 cm at December 2023 estimated by the ESA, 36,500 is the population of debris larger than 10 cm by ESA, 2,050 is the number of rocket bodies and 3,500 the number of derelict satellites.

APPENDIX E: EXOGENOUS SOURCES OF GROWTH

The economy module of DISE-2024 incorporates three exogenous sources of growth: Two types of technological progress, one aggregate and other specific to the space sector, and world population (i.e., labor) growth. The assumptions about these processes remain key, as economic growth is the main determinant of the space environment. Table E.1 shows the selected values for the parameters of the processes for TFP, satellite-ISTC, and population growth.

TABLE E.1. Baseline calibration of exogenous sources of growth of DISE-2024

Parameter	Definition	Value	Source
g_a	TFP growth rate	0.015	Assumption
g_q	Satellite ISTC growth rate	0.030	Assumption
δ_a	TFP growth decay rate	0.001	Assumption
δ_q	ISTC growth decay rate	0.005	Assumption
ζ	Population growth parameter	0.05	Assumption

E.1 Total Factor Productivity (a_t)

As is standard in growth models, aggregate technical progress is represented by a Hicks-neutral technological change. This is an important source of output growth. We assume that Total Factor Productivity (TFP) follows an exogenous process defined as follows,

$$a_{t+1} = \exp(g_{a,t})a_t \quad (\text{E.1})$$

where $g_{a,t}$ is the growth rate of TFP defined as,

$$g_{a,t} = g_{a,0} \exp(-\delta_a t) \quad (\text{E.2})$$

where $g_{a,0}$ is the TFP growth rate in the base period ($t = 0$, which corresponds to the year 2023) and δ_a is the decay rate of the TFP growth rate.

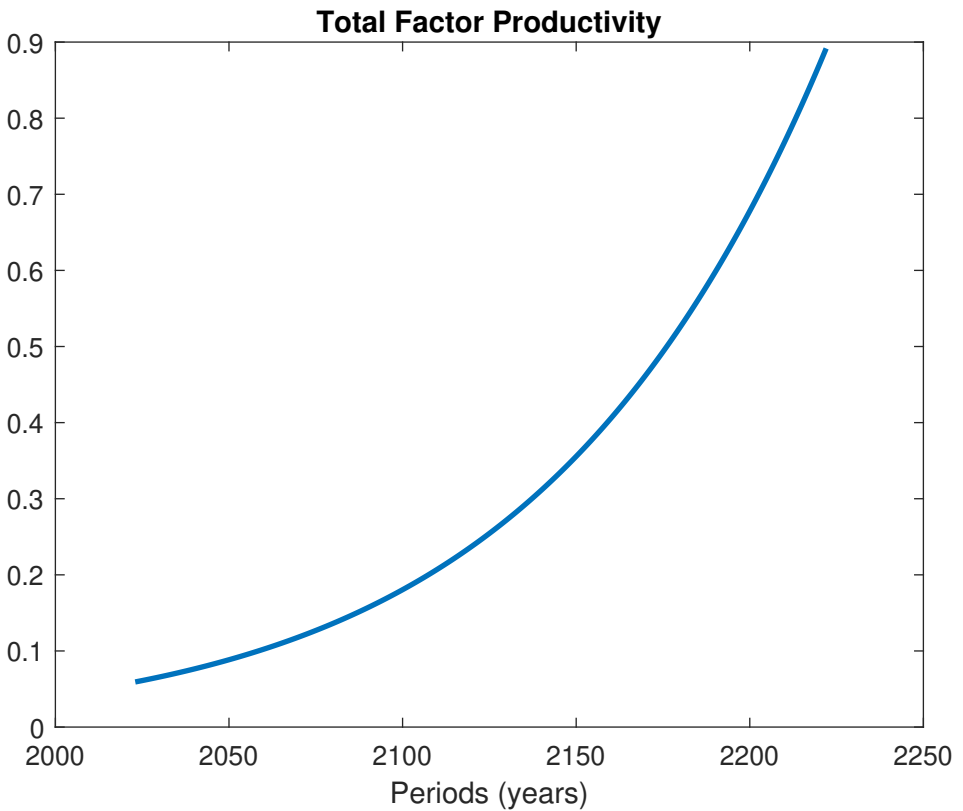


FIGURE E.1. Total Factor Productivity

Initial value for TFP is calculated as:

$$a_{2023} = \frac{y_{2023}}{k_{2023}^{\alpha_1} s_{2023}^{\alpha_2} N_{2023}^{1-\alpha_1-\alpha_2}} = \frac{184.65}{552.474^{0.3479} 1.203^{0.0021} 8,056^{0.65}} = 0.0593. \quad (\text{E.3})$$

We assume an initial TFP growth rate of 1.5% per year, with a decay rate in the growth rate of 0.1% per year. For comparison, DICE-2023 assumes an initial TFP growth of 0.066 (per 5 years), with a decline rate of 0.0015 (per 5 years). Roughly, this is equivalent to an initial annual TFP growth rate of 0.0132, and a decline rate of 0.003, values which are similar to the ones used in DISE-2024.

Figure E.1 plots the time path of TFP over the simulation horizon. Although TFP growth rate is decreasing (Figure E.2), the accumulation process results in an exponential path.

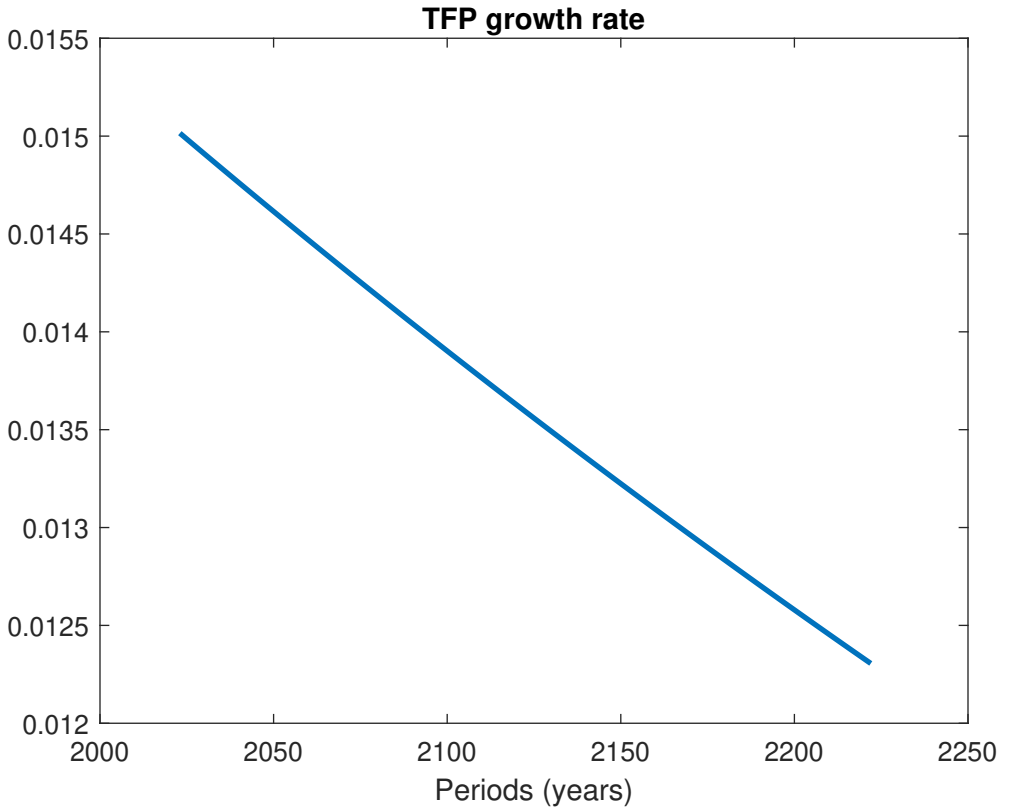


FIGURE E.2. Growth rate of Total Factor Productivity

E.2 Satellite investment-specific technological change (q_t)

In the model economy represented by DISE-2024, technological change is not only represented by a Hicks neutral technological change represented by TFP, but also for embodied-technological progress. We consider an additional technological progress specific to satellites, following Greenwood, Hercowitz and Krusell (1997). Greenwood et al. (1997) introduce ISTC in a growth model with two capital assets: structures and equipment, where ISTC applies over equipment. DISE-2024 incorporates ISCT for space capital, reflecting the assumption that space assets will experience a higher rate of technological progress compared to Earth capital assets. This is equivalent to assume that the price of space assets will be cheaper in the future at a higher rate than the prices of Earth capital assets.

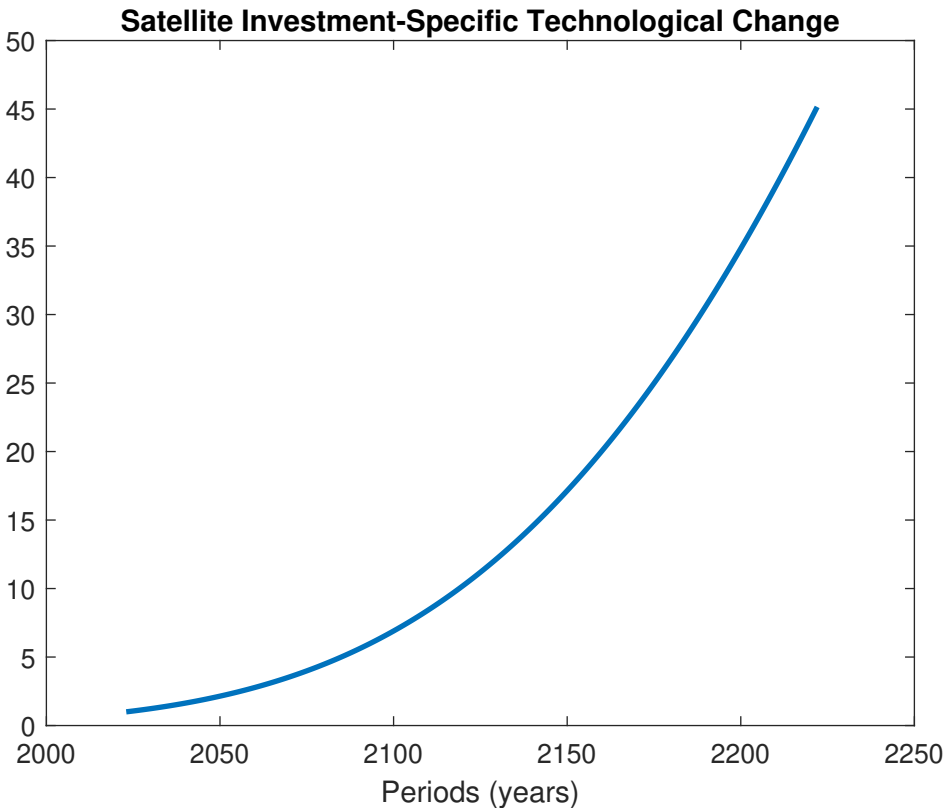


FIGURE E.3. Satellite Investment-Specific Technological Change

Similarly to TFP, we assume that ISTC follows an exogenous process given by,

$$q_{t+1} = \exp(g_{q,t})q_t \quad (\text{E.4})$$

where $g_{q,t}$ is the growth rate of ISTC defined as,

$$g_{q,t} = g_{q,0} \exp(-\delta_q t) \quad (\text{E.5})$$

where $g_{q,0}$ is the ISTC growth rate in the base period and δ_q is the decay rate of the TFP growth rate.

Initial value for ISTC is normalized to one ($q_{2023} = 1$). It is assumed that the initial growth rate of ISTC is 3% ($g_{q,0} = 0.03$), where the growth rate decays at 0.5% ($\delta_q = 0.05$). Results are plotted in figures E.3 and E.4.

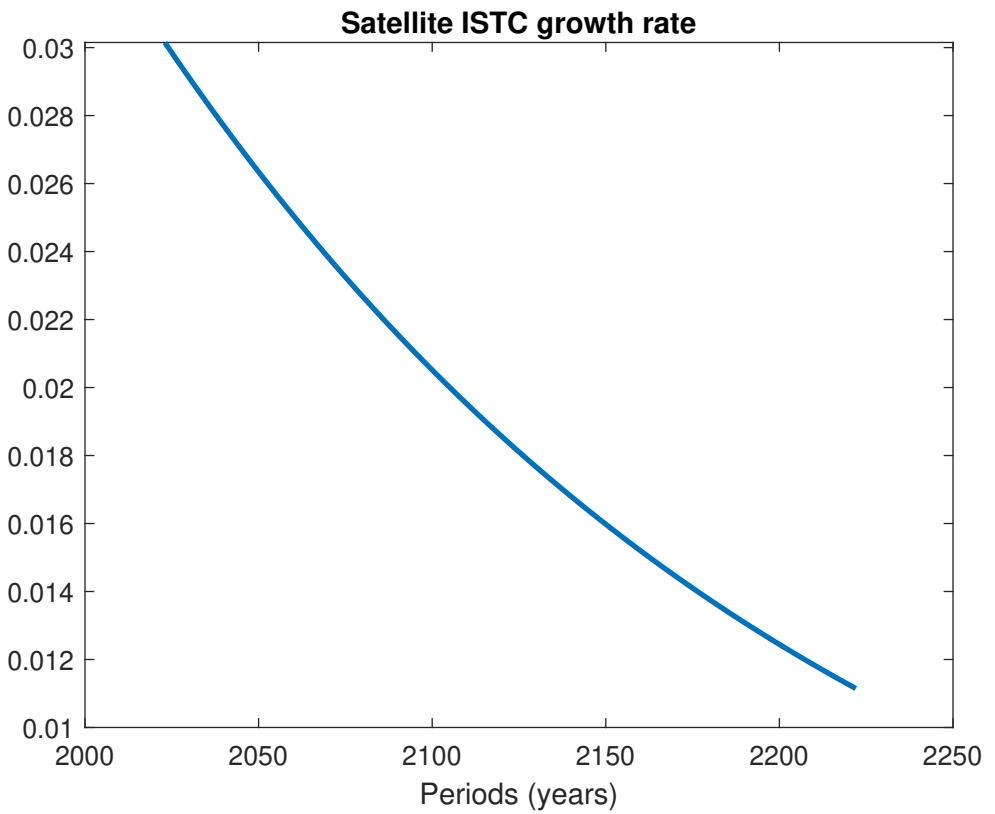


FIGURE E.4. Growth rate of satellite ISTC

E.3 Population (N_t)

Another source of economic growth is population growth. This is because production input labor is assumed to be equal or proportional to population. Hence, population is an additional production factor to Earth capital and space capital, and output growth is a function of population growth. In DISE-2024, we use data from World Population Prospects 2024 (UN, 2024) which includes projections to the year 2100. Using those projections, we extend population to the year 2222 assuming that from 2100 onward population growth is almost zero. The base year (2023) for the world population is 8,056,505 thousand. The asymptotic population is 10,200 million (see Figure E.5). Population contributes to output growth until approximately the year 2100, being zero for the last years of the simulation period.

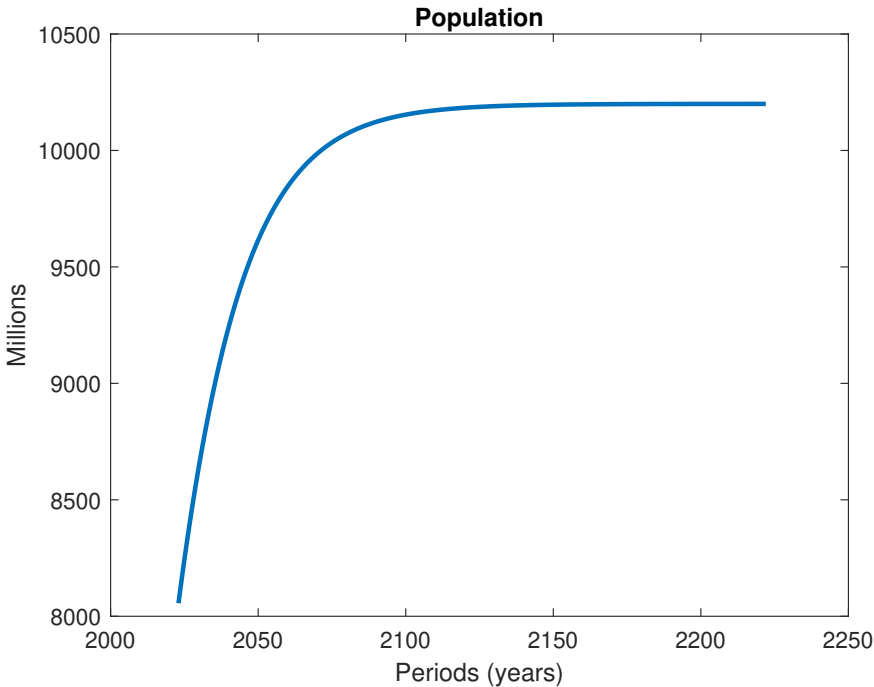


FIGURE E.5. Population projections. Based on World Population Prospects 2024, Medium fertility variant, 2024-2100, extended to 2222.

Formally, world population is calculated as,

$$N_{t+1} = N_t \left(\frac{N^*}{N_t} \right)^\zeta \quad (\text{E.6})$$

where N^* is an asymptotic population and the parameter ζ is a parameter driving the growth rate of population to the asymptotic population. Initial growth rate is around 1.2%, decreasing to zero by the year 2150 (Figure E.6).

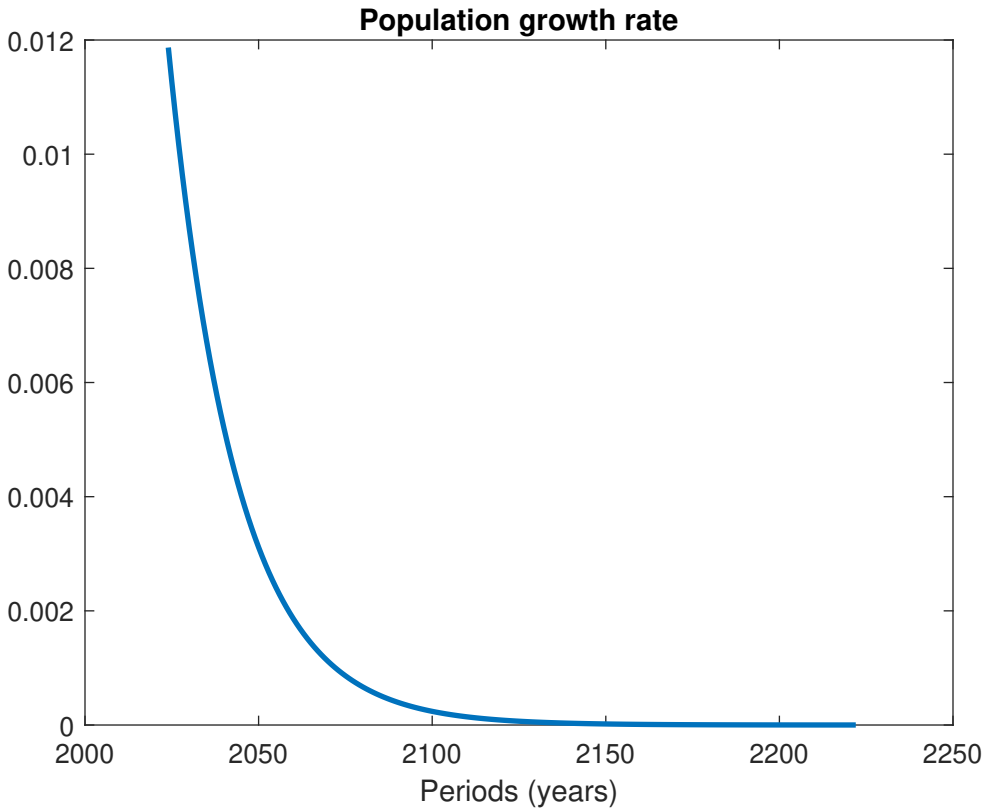


FIGURE E.6. World population growth rate

E.4 GDP growth

As shown previously, the model has three exogenous sources of growth: neutral technological change, satellite ISTC, and population (employment) growth, and two endogenous sources of growth: accumulation of Earth and space capital. To show how calibration of these exogenous process affects output growth, we simulate the model in a sci-fi scenario with no orbital debris. Figure E.7 plots the result of the output growth in the simulation horizon for the clean space environment scenario. It can be seen that the initial output growth is around 3%, which decreases to less than 2% at the end of the simulation period.

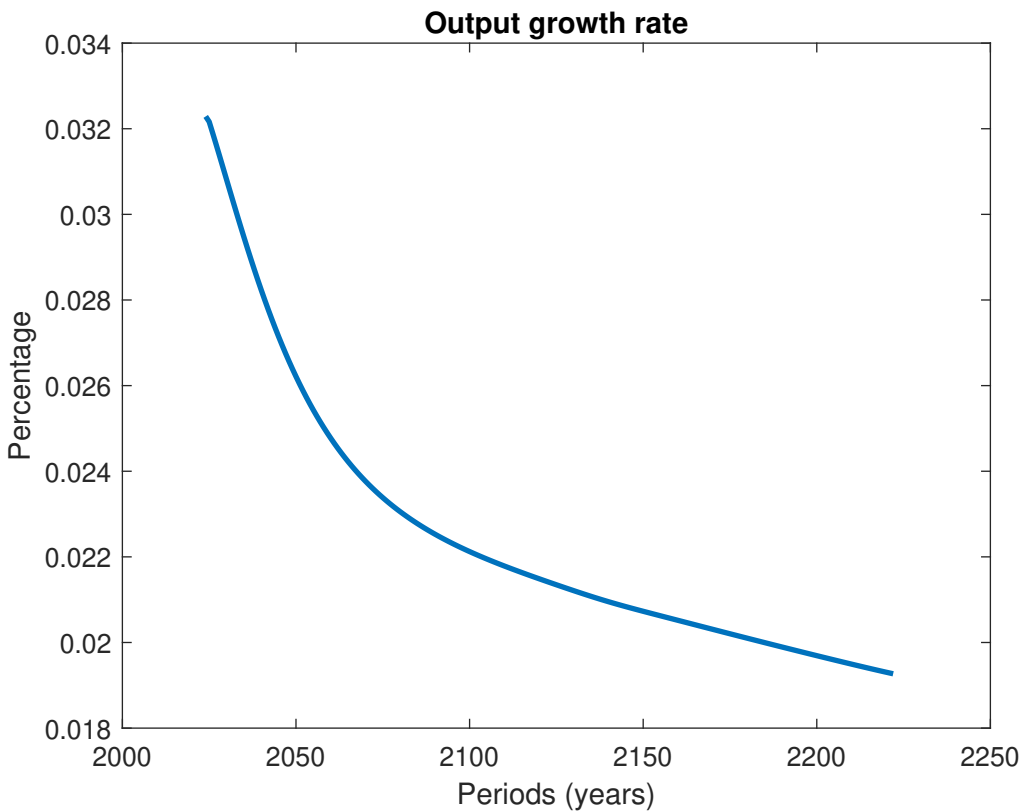


FIGURE E.7. GDP growth rate

APPENDIX F: LAUNCH COST

When computing investment in space capital, the model takes into account the existence of an installation cost, i.e., and investment adjustment cost to effectively accumulate investment into space capital. This installation cost is represented by launch costs. Making operational a satellite, even if the satellite is completed manufactured, is not a direct process, as the satellite have to be moved from the Earth to outer space. For inserting a satellite in orbit, it is necessary a launch vehicle, which is costly. This means that a fraction of investment in space capital is loss in the process of installation of the satellite into orbit. The model assumes that the launch cost is a constant fraction of the total investment cost and that the initial launch cost is 30% ($b_0 = 0.3$) of total investment in space capital, and hence, only the 70% of gross investment accumulates into satellite assets. This cost, together with a high depreciation rate, result in a high rate of return of satellites.

The model also assumes that the launch cost is decreasing over time. Adilov et al. (2022) estimate that from 2000 to 2020 the per-kilogram launch costs decreased at an average annual rate of 5.5% (a 4.4% if altitude-adjusted). Adilov et al. (2022) report that between 2000 and 2020, launch costs per kilogram to low Earth orbit declined significantly, driven by decreasing satellite masses, with projections indicating they will drop below \$1000/kg between 2045–2076 and \$100/kg by the next century.

For simulating the trajectory of the fraction of the launch cost, we use the following specification,

$$b_{t+1} = \exp(g_{b,t})b_t \quad (\text{F.1})$$

where $g_{b,t}$ is the (negative) growth rate of launch cost,

$$g_{b,t} = g_{b,0} \exp(-\delta_b t) \quad (\text{F.2})$$

where $g_{b,0}$ is the change in launch cost in the base year and δ_b is the decay rate of the change in launch cost.

Figure F.1 plots the fraction of launch cost over total investment in space capital, reflecting a decline in the launch cost, as a fraction of total cost, over time. Following estimates by Adilov et al. (2022), we assume that the initial decline in launch cost is of 5% ($g_{b,0} = -0.05$), and that the decline in the growth rate is of 1% ($\delta_b = 0.01$). Based on that figures, the fraction of launch cost reduces to 15% of total cost by 2050, and to only 5% by about 2100. The decreasing launch cost can be justified by a number of factors, including learning-by-doing process in the launching industry, technological progress in launch

vehicles, reduction in the size and mass of satellites, and commercial use of low altitude orbits.

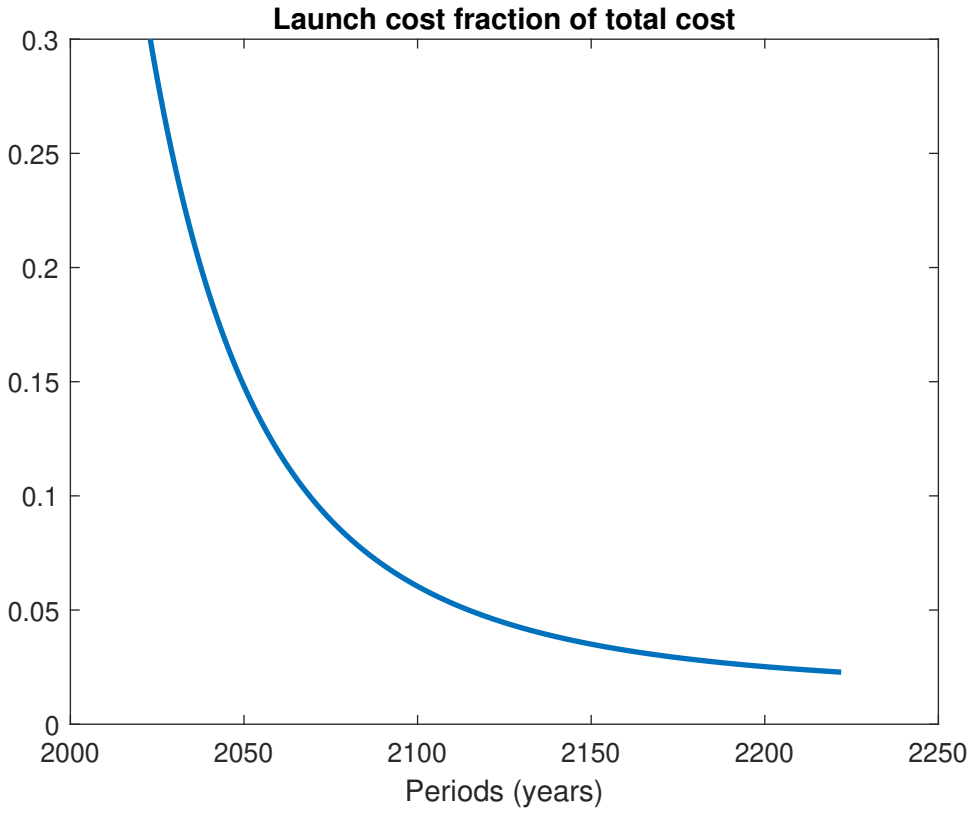


FIGURE F.1. Fraction of launch cost over total cost of space capital investment

APPENDIX G: THE MODEL

This appendix collects the equations of the DISE-2024 model. The economic sub-model is formed by the following equations:

$$\max_{\{c_t\}_{t=0}^{\infty}} \sum_{t=0}^{\infty} \left(\frac{1}{1+\rho} \right)^t U(\hat{c}_t, N_t) \quad (\text{G.1})$$

$$c_t + i_t^k + i_t^s = y_t \quad (\text{G.2})$$

$$y_t = a_t f(k_t, s_t, N_t) \quad (\text{G.3})$$

$$k_{t+1} = (1 - \delta_k)k_t + i_t^k \quad (\text{G.4})$$

$$i_t^s = h_t + l_t \quad (\text{G.5})$$

$$l_t = b_t i_t^s \quad (\text{G.6})$$

$$s_{t+1} = (1 - \delta_s)s_t + q_t h_t - x_t \quad (\text{G.7})$$

The damage function linking the economic sub-model with the debris sub-model is the following,

$$x_t = (1 - v_t)\theta D_{2,t} s_t \quad (\text{G.8})$$

The debris sub-model is given by,

$$D_{i,t} = W_t + B_t + F_{i,t} \quad i = 1, 2, 3 \quad (\text{G.9})$$

$$W_{t+1} = (1 - \delta_w - \varepsilon_w)W_t - \theta(D_{2,t} + (1 - v_t)S_t)W_t + \chi\delta_s S_t \quad (\text{G.10})$$

$$Z_{t+1} = (1 - \delta_z - \varepsilon_z)Z_t - \theta(D_{2,t} + (1 - v_t)S_t)Z_t + \phi L_t \quad (\text{G.11})$$

$$\begin{aligned} F_{1,t+1} &= (1 - \delta_f)F_{1,t} + \omega L_t + \phi_w \varepsilon_w W_t + \phi_z \varepsilon_z Z_t + \\ &\quad \gamma_s X_t + \gamma_w \theta D_{2,t} W_t + \gamma_z \theta D_{2,t} Z_t \end{aligned} \quad (\text{G.12})$$

The mapping between economic and physical variables is given by,

$$S_t = \mu s_t \quad (\text{G.13})$$

$$X_t = \mu x_t \quad (\text{G.14})$$

$$H_t = \mu q_t h_t \quad (\text{G.15})$$

$$S_{t+1} = (1 - \delta_s)S_t + H_t - X_t \quad (\text{G.16})$$

$$X_t = (1 - v_t)\theta D_{2,t}S_t \quad (\text{G.17})$$

The launch sub-module is composed by the following equations:

$$H_t = \eta L_t \quad (\text{G.18})$$

$$h_t = (1 - b_t)i_t^s = \frac{\eta}{\mu q_t} L_t \quad (\text{G.19})$$

Exogenous sources of growth are:

$$a_{t+1} = \exp(g_{a,t})a_t \quad (\text{G.20})$$

$$g_{a,t} = g_{a,0}\exp(-\delta_a t) \quad (\text{G.21})$$

$$q_{t+1} = \exp(g_{q,t})q_t \quad (\text{G.22})$$

$$g_{q,t} = g_{q,0}\exp(-\delta_q t) \quad (\text{G.23})$$

$$N_{t+1} = N_t \left(\frac{N^*}{N_t} \right)^\zeta \quad (\text{G.24})$$

Finally, the cost of launches is given by,

$$b_{t+1} = \exp(g_{b,t})b_t \quad (\text{G.25})$$

$$g_{b,t} = g_{b,0}\exp(-\delta_b t) \quad (\text{G.26})$$

G.1 Decentralized economy (*Laissez-faire*)

Although we do not simulate the model for a decentralized economy, it is nevertheless interesting to calculate the optimal investment decisions on Earth and space capital by households. In a decentralized economy, the negative externality of orbital debris is not internalized. Agents simply adapt to the space environment, treating the amount of orbital debris is considered exogenous. The household maximization problem, taking into account the accumulation process for both capital and satellites, is given by,

$$\mathcal{L} = E_0 \sum_{t=0}^{\infty} \beta^t U(\hat{c}_t) N_t$$

$$-\sum_{t=0}^{\infty} \lambda_t [c_t + k_{t+1} - (1 - \delta_k)k_t + \frac{1}{q_t(1 - b_t)} [s_{t+1} - (1 - \delta_s)s_t + (1 - v_t)\theta\bar{D}_{2,t}s_t] - r_t^k k_t - r_t^s s_t - \pi_t] \quad (\text{G.27})$$

where $\bar{D}_{2,t}$ is the exogenous amount of orbital debris.

First order conditions from $t = 0, 1, \dots, \infty$, are:

$$\frac{\partial \mathcal{L}}{\partial c_t} = \beta^t U'(\hat{c}_t) N_t - \lambda_t = 0 \quad (\text{G.28})$$

$$\frac{\partial \mathcal{L}}{\partial k_{t+1}} = -\lambda_t + \lambda_{t+1}(1 - \delta_k + r_{t+1}^k) \quad (\text{G.29})$$

$$\frac{\partial \mathcal{L}}{\partial s_{t+1}} = \frac{\lambda_t}{q_t(1 - b_t)} - \frac{\lambda_{t+1}}{q_{t+1}(1 - b_{t+1})} [1 - \delta_s - (1 - v_t)\theta\bar{D}_{2,t+1}] + \lambda_{t+1}r_{t+1}^s = 0 \quad (\text{G.30})$$

From the maximization problem, solving for the Lagrangian's multiplier, equilibrium conditions are given by,

$$U'(c_t)N_t = \beta E_t U'(c_{t+1})N_{t+1}[1 - \delta_k + r_{t+1}^k] \quad (\text{G.31})$$

$$U'(c_t)N_t = q_t(1 - b_t)\beta E_t U'(c_{t+1})N_{t+1} \left[\frac{1 - \delta_s - (1 - v_t)\theta\bar{D}_{2,t+1}}{q_{t+1}(1 - b_{t+1})} + r_{t+1}^s \right] \quad (\text{G.32})$$

Expression (G.31) is the standard Euler equation for optimal investment decisions in capital excluding satellites. Expression (G.32) is also an Euler equation, but it pertains to the investment decision in satellites, where the cost of destruction by collision is incorporated. The term $\theta\bar{D}_{2,t+1}$ accounts for the sudden, full depreciation of satellites stock due to collisions. As the quantity of orbital debris increases, the rental price of satellite to capital also increases.

The representative firm maximizes profits by choosing the appropriate levels of capital and satellites. Profits are defined as,

$$\pi_t = y_t - r_t^k k_t - r_t^s s_t \quad (\text{G.33})$$

From the profit maximization problem we have:

$$r_t^k = a_t f'_k(k_t, s_t) \quad (\text{G.34})$$

$$r_t^s = a_t f'_s(k_t, s_t) \quad (\text{G.35})$$

Equilibrium conditions are obtained by substituting (G.34) and (G.35) into (G.31) and (G.32),

$$U'(c_t)N_t = \beta E_t U'(c_{t+1})N_{t+1}[1 - \delta_k + a_{t+1}f'_k(k_{t+1}, s_{t+1})] \quad (\text{G.36})$$

$$U'(c_t)N_t = q_t \beta E_t U'(c_{t+1})N_{t+1} \left[\frac{1 - \delta_s - (1 - v_t)\theta \bar{D}_{2,t+1}}{q_{t+1}} + a_{t+1}f'_s(k_{t+1}, s_{t+1}) \right] \quad (\text{G.37})$$

Equating both expressions we find that the arbitrage condition for investing in both Earth and space capital is,

$$[1 - \delta_k + a_{t+1}f'_k(k_{t+1}, s_{t+1})] = q_t(1 - b_t) \left[\frac{1 - \delta_s - (1 - v_t)\theta \bar{D}_{2,t+1}}{q_{t+1}(1 - b_{t+1})} + a_{t+1}f'_s(k_{t+1}, s_{t+1}) \right] \quad (\text{G.38})$$

G.2 Centralized economy

This section presents the planning problem in which a central planner maximizes social welfare. The central planner chooses consumption, investment in Earth capital, and investment in satellites, to maximize social welfare. This is a first best, where the negative externality is fully internalized. The maximization problem solved by the central planner is given by,

$$\max_{c_t, i_t^k, i_t^s, D_t} E_0 \sum_{t=0}^{\infty} \beta^t U(\hat{c}_t) N_t \quad (\text{G.39})$$

subject to

$$c_t + i_t^k + i_t^s = y_t \quad (\text{G.40})$$

$$y_t = a_t f(k_t, s_t, N_t) \quad (\text{G.41})$$

$$k_{t+1} = (1 - \delta_k)k_t + i_t^k \quad (\text{G.42})$$

$$i_t^s = h_t + l_t \quad (\text{G.43})$$

$$l_t = b_t i_t^s \quad (\text{G.44})$$

$$s_{t+1} = (1 - \delta_s)s_t + q_t(1 - b_t)i_t^s - x_t \quad (\text{G.45})$$

$$x_t = (1 - v_t)\theta D_{2,t}s_t \quad (\text{G.46})$$

$$D_{i,t} = W_t + Z_t + F_{i,t} \quad i = 1, 2, 3 \quad (\text{G.47})$$

$$W_{t+1} = (1 - \delta_w - \varepsilon_w)W_t - \theta(D_{2,t} + (1 - v_t)S_t)W_t + \chi \delta_s S_t \quad (\text{G.48})$$

$$Z_{t+1} = (1 - \delta_z - \varepsilon_z)Z_t - \theta(D_{2,t} + (1 - v_t)S_t)Z_t + \varphi L_t \quad (\text{G.49})$$

$$F_{1,t+1} = (1 - \delta_f)F_{1,t} + \omega L_t + \phi_w \varepsilon_w W_t + \phi_z \varepsilon_z Z_t + \gamma_s X_t + \gamma_w D_{2,t} W_t + \gamma_z D_{2,t} Z_t \quad (G.50)$$

$$L_t = \frac{\mu}{\eta} q_t h_t \quad (G.51)$$

$$X_t = \mu x_t \quad (G.52)$$

$$F_{2,t} = (1 + \Gamma)F_{1,t} \quad (G.53)$$

Additionally, the mapping from the "economic" model to the "physical" model is given by the following expressions:

$$X_t = (1 - v_t)\theta D_{2,t} S_t \quad (G.54)$$

$$S_t = \mu s_t \quad (G.55)$$

$$H_t = \eta L_t \quad (G.56)$$

The maximization problem can be defined as:

$$\begin{aligned} \mathcal{L} = E_t \sum_{t=0}^{\infty} \beta^t U(\hat{c}_t) N_t & \\ - \sum_{t=0}^{\infty} \lambda_{1,t} \left[c_t + k_{t+1} - (1 - \delta_k)k_t + \frac{\eta}{\mu q_t (1 - b_t)} L_t - a_t f(k_t, s_t) \right] & \\ - \sum_{t=0}^{\infty} \lambda_{2,t} [x_t - (1 - v_t)\theta D_{2,t} S_t] & \\ - \sum_{t=0}^{\infty} \lambda_{3,t} \left[s_{t+1} - (1 - \delta_s)s_t - \frac{\eta}{\mu} L_t + x_t \right] & \\ - \sum_{t=0}^{\infty} \lambda_{4,t} [D_{2,t} - W_t - Z_t - (1 + \Gamma)F_{1,t}] & \\ - \sum_{t=0}^{\infty} \lambda_{5,t} [W_{t+1} - (1 - \delta_w - \varepsilon_w)W_t + \theta(D_{2,t} + (1 - v_t)S_t)W_t - \chi \delta_s S_t] & \\ - \sum_{t=0}^{\infty} \lambda_{6,t} [Z_{t+1} - (1 - \delta_z - \varepsilon_z)Z_t + \theta(D_{2,t} + (1 - v_t)S_t)Z_t - \phi L_t] & \\ - \sum_{t=0}^{\infty} \lambda_{7,t} [F_{1,t+1} - (1 - \delta_f)F_{1,t} - \omega L_t - \phi_w \varepsilon_w W_t - \phi_z \varepsilon_z Z_t & \\ - \gamma_s X_t - \gamma_w \theta D_{2,t} W_t - \gamma_z \theta D_{2,t} Z_t] & \quad (G.57) \end{aligned}$$

The Lagrangian multipliers for each constraint in period t are $\lambda_{1,t}$, $\lambda_{2,t}$, $\lambda_{3,t}$, $\lambda_{4,t}$, $\lambda_{5,t}$, $\lambda_{6,t}$, and $\lambda_{7,t}$. $\lambda_{1,t}$ is the standard shadow price of consumption. $\lambda_{2,t}$ is the cost of the probability

of collision. $\lambda_{3,t}$ is the price of satellite assets. $\lambda_{4,t}$ is the cost of the stock of orbital debris, and $\lambda_{5,t}$, $\lambda_{6,t}$, and $\lambda_{7,t}$ represents the shadow cost of derelict satellites, rocket bodies, and fragments, respectively.

First order conditions from the maximization problem, for $t = 0, 1, \dots, \infty$ are,

$$\frac{\partial \mathcal{L}}{\partial c_t} = \beta^t U'(c_t) - \lambda_{1,t} = 0 \quad (\text{G.58})$$

$$\frac{\partial \mathcal{L}}{\partial k_{t+1}} = -\lambda_{1,t} + \lambda_{1,t+1} [1 - \delta_k + a_{t+1} f'_k(k_{t+1}, s_{t+1})] = 0 \quad (\text{G.59})$$

$$\begin{aligned} \frac{\partial \mathcal{L}}{\partial s_{t+1}} = & \lambda_{1,t+1} a_{t+1} f'_s(k_{t+1}, s_{t+1}) + \lambda_{2,t} (1 - v_t) \theta D_{2,t+1} - \lambda_{3,t} + \lambda_{3,t+1} (1 - \delta_s - (1 - v_t) \theta D_{2,t+1}) \\ & - \lambda_{5,t+1} \chi \delta_s \mu + \lambda_{7,t} (1 - v_t) \theta \mu [\gamma_s D_{2,t} + \gamma_w W_t + \gamma_z Z_t] = 0 \end{aligned} \quad (\text{G.60})$$

$$\frac{\partial \mathcal{L}}{\partial L_t} = -\lambda_{1,t} \frac{\eta}{\mu q_t (1 - b_t)} + \lambda_{3,t} \frac{\eta}{\mu} + \lambda_{6,t} \varphi + \lambda_{7,t} \omega = 0 \quad (\text{G.61})$$

$$\frac{\partial \mathcal{L}}{\partial x_t} = -\lambda_{2,t} - \lambda_{3,t} + \lambda_{7,t} \gamma_s \mu = 0 \quad (\text{G.62})$$

$$\frac{\partial \mathcal{L}}{\partial D_{2,t}} = \lambda_{2,t} \theta s_t - \lambda_{4,t} + \lambda_{7,t} [\gamma_w \theta W_t + \gamma_z \theta Z_t] = 0 \quad (\text{G.63})$$

$$\frac{\partial \mathcal{L}}{\partial W_{t+1}} = \lambda_{4,t} - \lambda_{5,t} + \lambda_{5,t+1} (1 - \delta_w - \varepsilon_w) + \lambda_{7,t+1} [\phi_w \varepsilon_w + \gamma_w \theta D_{2,t}] = 0 \quad (\text{G.64})$$

$$\frac{\partial \mathcal{L}}{\partial Z_{t+1}} = \lambda_{4,t} - \lambda_{6,t} + \lambda_{6,t+1} (1 - \delta_z - \varepsilon_z) + \lambda_{7,t+1} [\phi_z \varepsilon_z + \gamma_z \theta D_{2,t}] = 0 \quad (\text{G.65})$$

$$\frac{\partial \mathcal{L}}{\partial F_{1,t+1}} = \lambda_{4,t} (1 + \Gamma) - \lambda_{7,t} + \lambda_{7,t+1} (1 - \delta_f) = 0 \quad (\text{G.66})$$

APPENDIX H: TERMINAL CONDITIONS

The neoclassical growth model assumes that the economy is populated by forward-looking, rational expectations agents who take their economic decisions in an infinite-horizon. However, numerical solutions can only be obtained over a finite number of periods. In practice, we numerically solve a nonlinear infinite-horizon economic growth model by approximating over a finite-horizon. This requires a transformation of the original infinite-horizon optimal control problem into an equivalent finite-horizon optimal control problem. The key issue in approximating an infinite-horizon equilibrium in a neoclassical growth model is determining the appropriate level of the capital stock in the terminal period of the finite-horizon solution.

As pointed out by Mercenier and Michel (1994), the numerical solution of nonlinear continuous-time optimization problems using mathematical programming techniques requires reformulating the problem into a discrete, finite-horizon approximation. This reformulation requires three key decisions. The first is the choice of the length of the finite planning horizon. The second concerns the treatment of post-terminal behavior. The third is related to the selection of the specific sequence of time intervals in the discretization process. Problems with the optimal trajectory can be addressed either by increasing the length of the decision horizon, at the cost of higher computational cost, or by reducing the frequency of the time intervals. The central issue is that the solution of the model over the period of interest should not be affected by the selection of the planning horizon or the terminal condition.

The general problem can be defined as an utility maximization problem, which can be divided in two parts,

$$\max_{c_t} W = \sum_{t=0}^T \left(\frac{1}{1+\rho} \right)^t U(\hat{c}_t) N_t + \sum_{t=T+1}^{\infty} \left(\frac{1}{1+\rho} \right)^t U(\hat{c}_t) N_t \quad (\text{H.1})$$

where the first part is the finite-horizon solution already computed from $t = 0$ to T and the second part represents the behavior of the economy from period $T + 1$ to infinity, and where the two sub-problems are linked through the capital stock at period $T + 1$.

The literature has addressed this issue proposing alternative terminal conditions to be incorporated into the model to determine investment in the last computational period (T), while also applying adjustments to approximate choices over the period $T + 1$ to infinity. Blake and Westaway (1995) argue that any distortionary effects of a terminal condition can be minimized by setting a terminal condition consistent with the steady state of the

model and sufficiently such that it does not affect model properties over the horizon of interest. In this way, a change either in the horizon period or in the terminal condition does not alter the solution over the relevant time frame. The simplest approach is to assume that the world ends at period T . This can be a valid method when the value of T is large and the discount rate is high, thus minimizing the effects of the terminal values on the optimal path. Because $\beta^t \rightarrow 0$ as $t \rightarrow \infty$, we can truncate the infinite horizon at a large finite period T . Other approaches assume that the economy reaches its steady state at time T . An alternative frequently used in climate-change economics is to adopt a fixed saving rate for the final periods of the simulation, combined with large time intervals. This is the strategy followed, for instance, by Nordhaus (1992, 1993) in solving the DICE model. For example, in DICE2016 (Nordhaus, 2017), a constant saving rate equal to the long-run saving rate is applied for the last 10 periods (50 years). In DICE2023 (Nordhaus, 2024), a saving rate of 0.28 is used for periods beyond 37 (the last 185 years).

This issue has been extensively studied in the planning literature, where alternative strategies for dealing with the terminal condition have been proposed. Frisch (1955) proposed the use of geometric growth terminal conditions for numerical planning problems. Chakravarty (1962) considered that terminal capital stock is given as a proportion of the initial capital stock, which implies that capital stock grows at some exogenous rate. Stoleru (1965) introduced the terminal condition that capital stock growth rate after T equals the exogenous rate of labor force (i.e., population). Manne (1970) formulated sufficient conditions under which any planning problem yields a solution that is not only optimal for a horizon T , but is also optimal for all finite horizon greater than T .

Barr and Manne (1967) assumed that at the terminal period T , the economy is at the steady state, where the growth rate is g_y . Under these assumptions, expression (H.1) can be written as,

$$\max_{c_t} W = \sum_{t=0}^{T-1} \left(\frac{1}{1+\rho} \right)^t U(c_t) + \sum_{t=T}^{\infty} \left(\frac{1}{1+\rho} \right)^t U(c_t(1+g_y^{t-T})) \quad (\text{H.2})$$

where the second term is a constant. Abstracting from the constant term, the maximization problem can be written as,

$$\max_{c_t} W = \sum_{t=0}^{T-1} \left(\frac{1}{1+\rho} \right)^t U(c_t) + \frac{1+\rho}{\rho(1+\rho)^T} U(c_T) \quad (\text{H.3})$$

$$\max_{c_t} W = \sum_{t=0}^T \hat{\beta}^t U(c_t) \quad (\text{H.4})$$

where the discount factor would be,

$$\hat{\beta}^t = \begin{cases} \left(\frac{1}{1+\rho}\right)^t & \text{for } t < T \\ \frac{(1+\rho)^{1-T}}{\rho} & \text{for } T \end{cases} \quad (\text{H.5})$$

At the terminal period, gross investment is determined by the size of capital stock in the terminal period, the exogenous growth rate (since all quantities grow at the same rate in the steady state), and the capital depreciation rate. The investment constraint would be,

$$i_T = (g_y + \delta)k_T \quad (\text{H.6})$$

A second approach assumes that the economy reaches the steady state at T . In this case, consumption from time T onward remains constant at c_T . Therefore, the discounted utility maximization problem can be expressed as,

$$\max_{c_t} W = \sum_{t=0}^{T-1} \left(\frac{1}{1+\rho}\right)^t U(c_t) + \frac{\beta^T}{1-\beta} U(c_T) \quad (\text{H.7})$$

The problem is that the economy is forced into a steady state at time T . **If T is large enough,**

Rutherford (1995) and Lau, Pahlke and Rutherford (2002) propose the use of a terminal condition for investment to ensure steady-state growth in the post-terminal period. This method avoids the need to specify an ex-ante growth rate at the final period T . Instead, it assumes that the growth rate of investment matches the growth rate of output (or consumption). Formally,

$$\frac{i_T}{i_{T-1}} = \frac{y_T}{y_{T-1}} \quad (\text{H.8})$$

where i_t is investment and y_t is output.

Lau, Pahlke and Rutherford (2002) review alternative methods of approximating the infinite-horizon problem and propose a new approach applicable to the complementarity format of the model.

Nordhaus (2008) assumes that investment at the terminal time must be at least 2% of the capital stock at that time. Cai et al. (2012) use Chebyshev function to represent the terminal value, accounting for an additional 800 years.

Böhringer, Löschel and Rutherford (2007) demonstrate that the turnpike properties of the growth model can be exploited to precisely represent post-terminal trajectories and

reduce the economic horizon needed to accurately approximate transition paths. This condition is combined with a constraint for the final period that requires a minimum level of investment, such as,

$$i_T \geq (g_n + \delta_k)k_T \quad (\text{H.9})$$

and

$$h_T \geq \frac{(g_n + \delta_s)s_T}{q_T} \quad (\text{H.10})$$

APPENDIX I: ADDITIONAL RESULTS

In this appendix, we present additional figures showing the trajectories of further variables of the model. In particular, we illustrate the relative contributions of each type of debris emissions source. The significance of these debris emissions sources depends on the specific debris mitigation policy implemented.

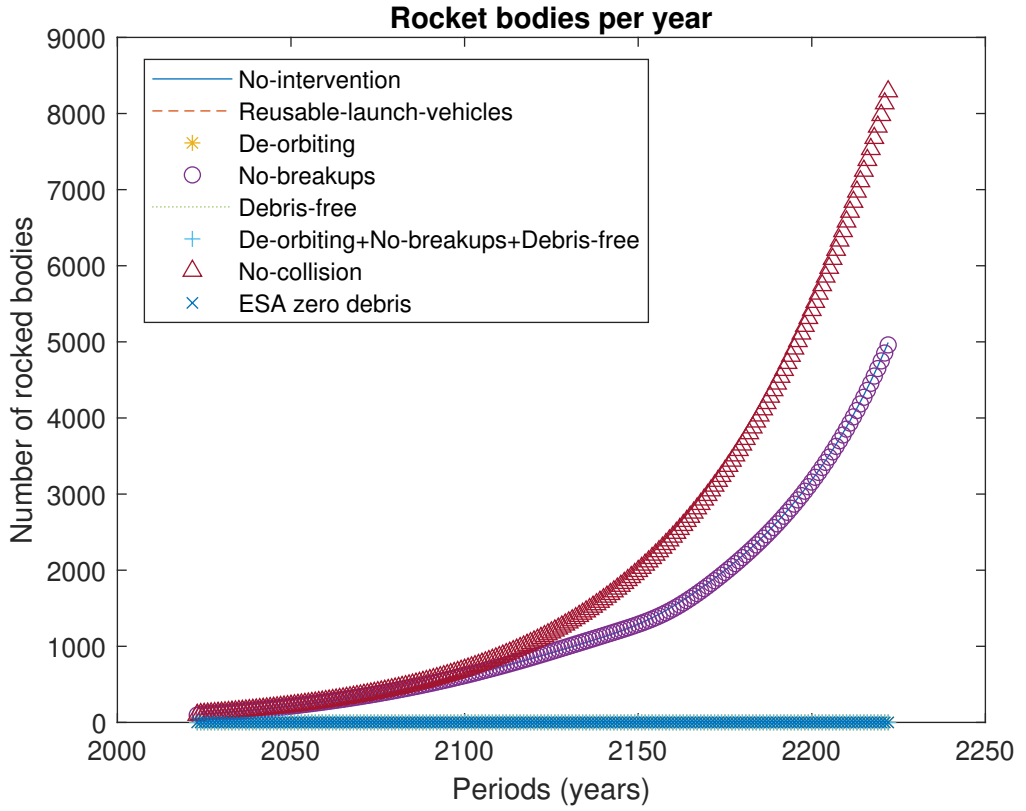


FIGURE I.1. Number of rocket bodies per year

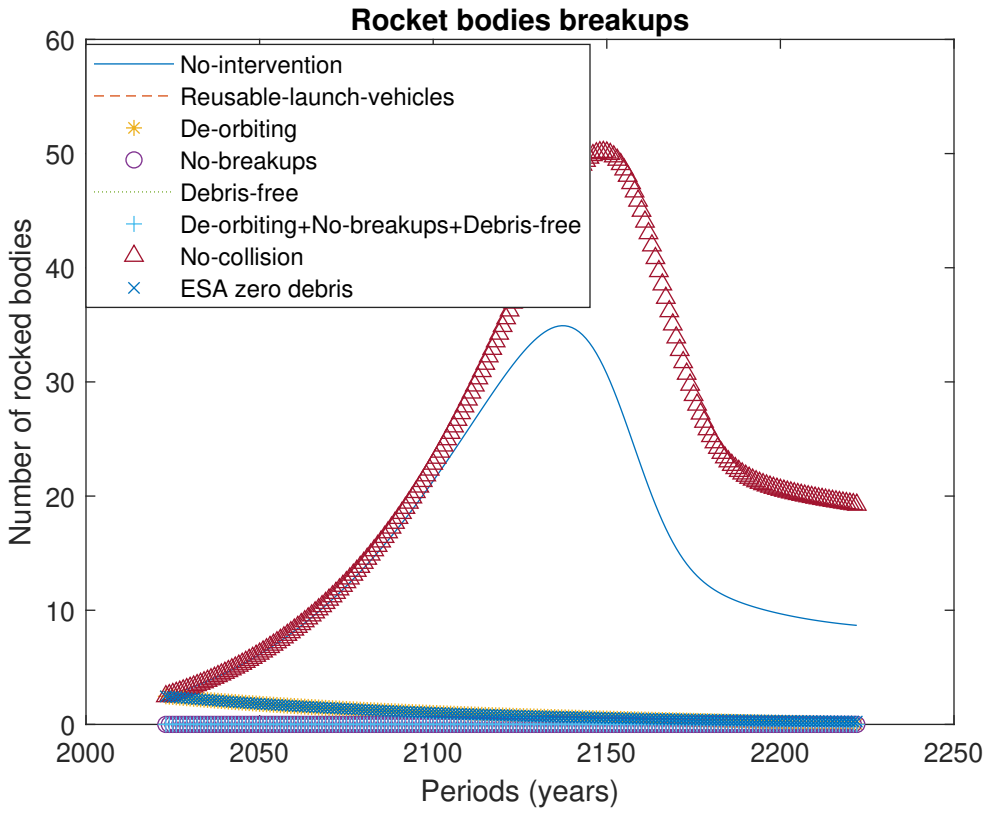


FIGURE I.2. Number of breakups of rocket bodies per year

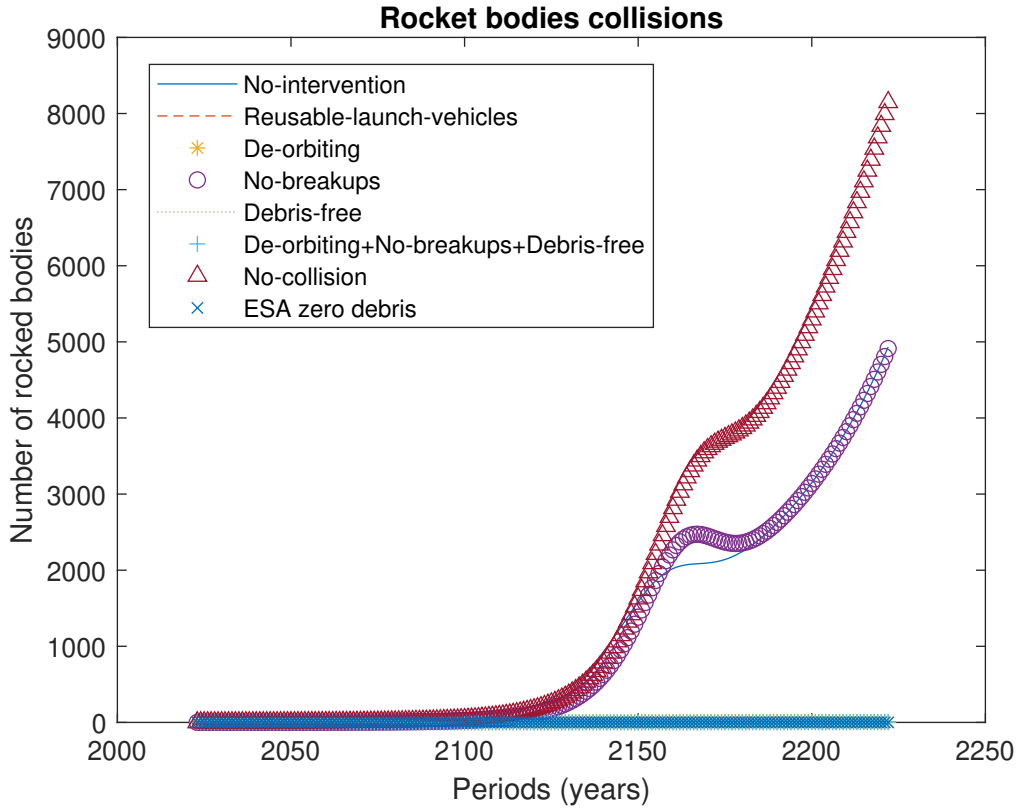


FIGURE I.3. Number of collisions of rocket bodies per year

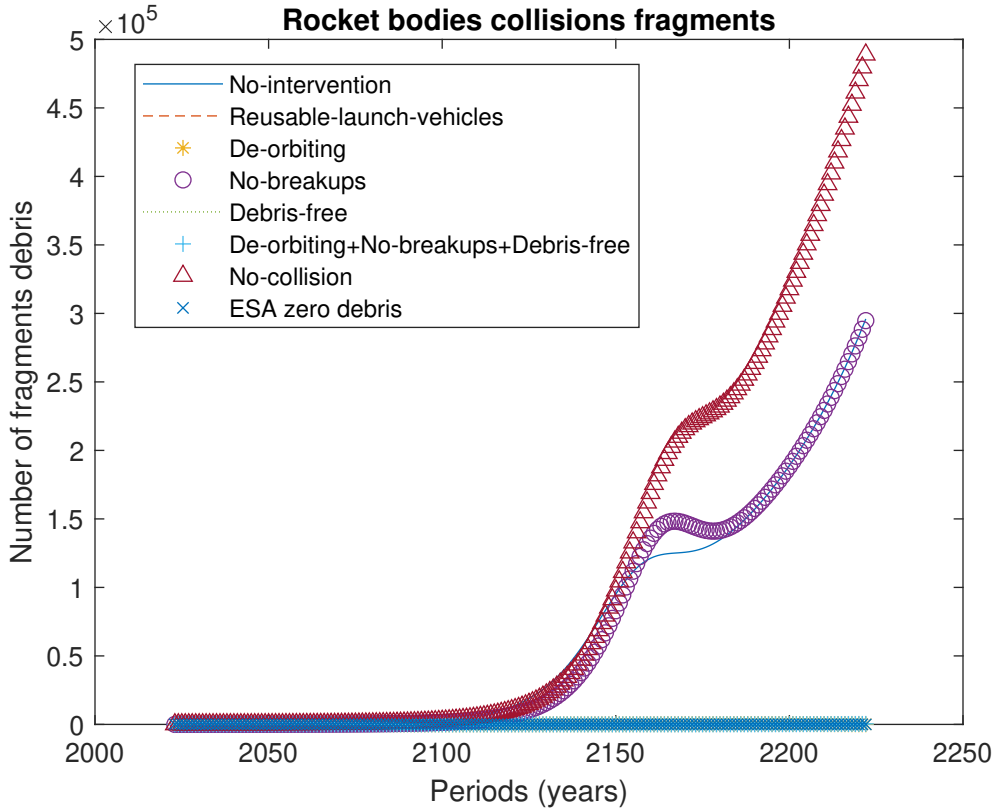


FIGURE I.4. Number of fragments debris larger than 10 cm produced by the collision of rocket bodies per year

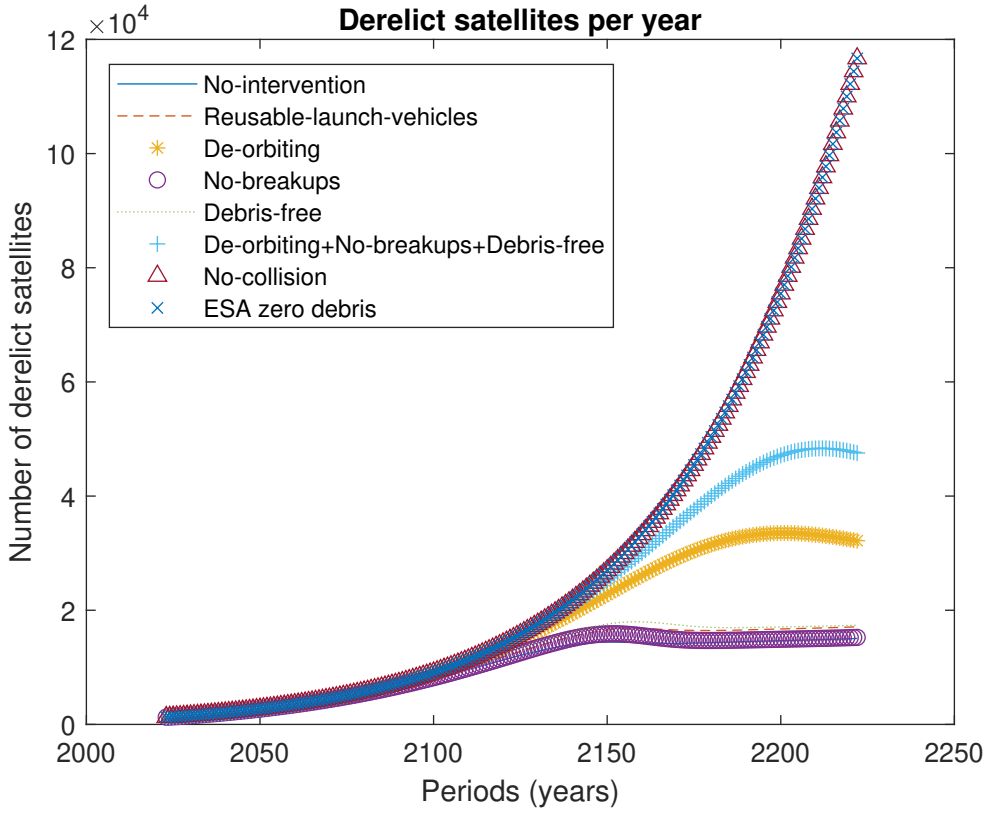


FIGURE I.5. Number of derelict satellites per year

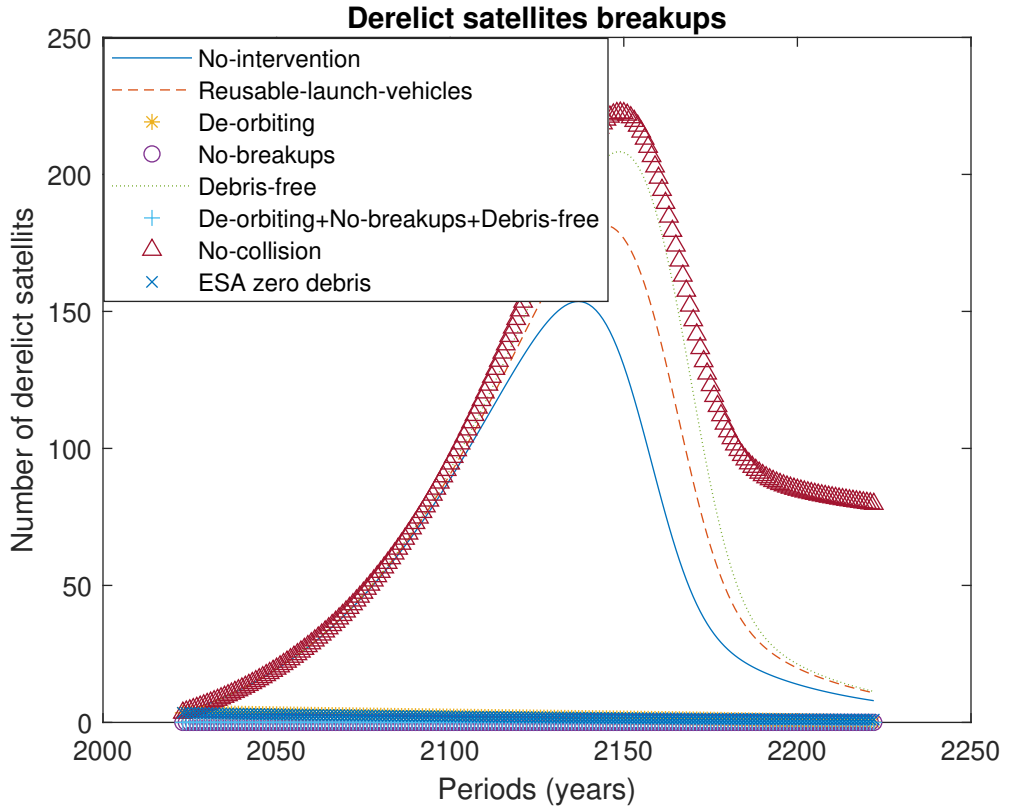


FIGURE I.6. Number of breakups of derelict satellites per year

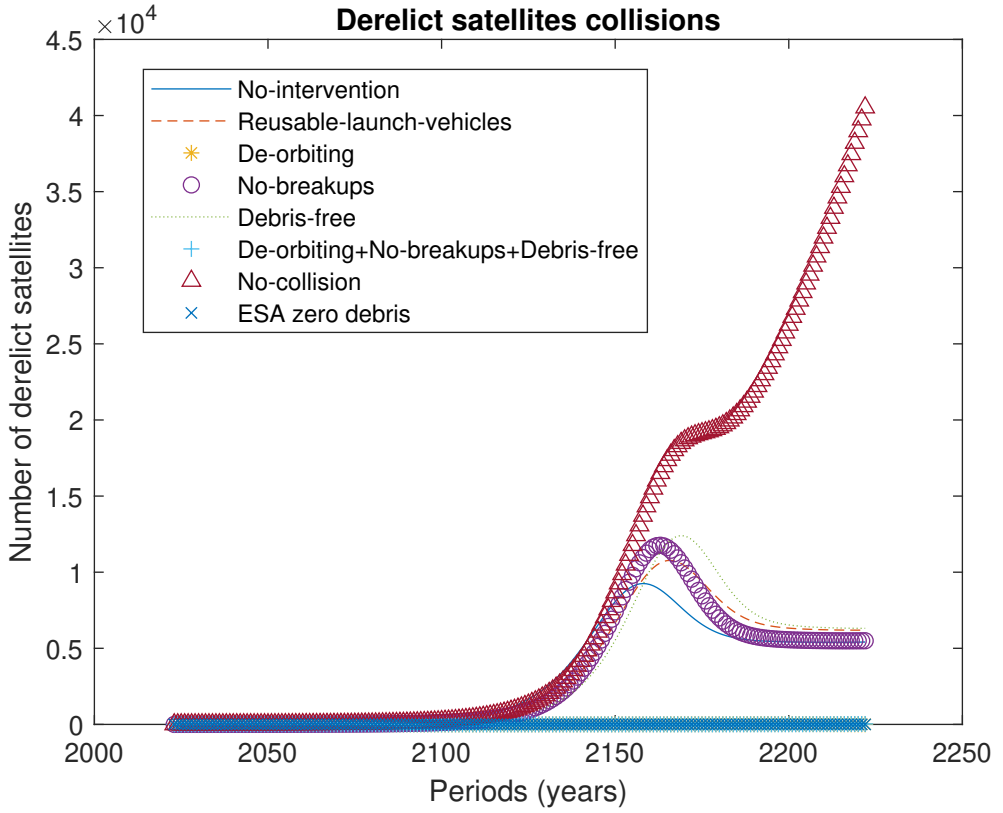


FIGURE I.7. Number of collisions of derelict satellites per year

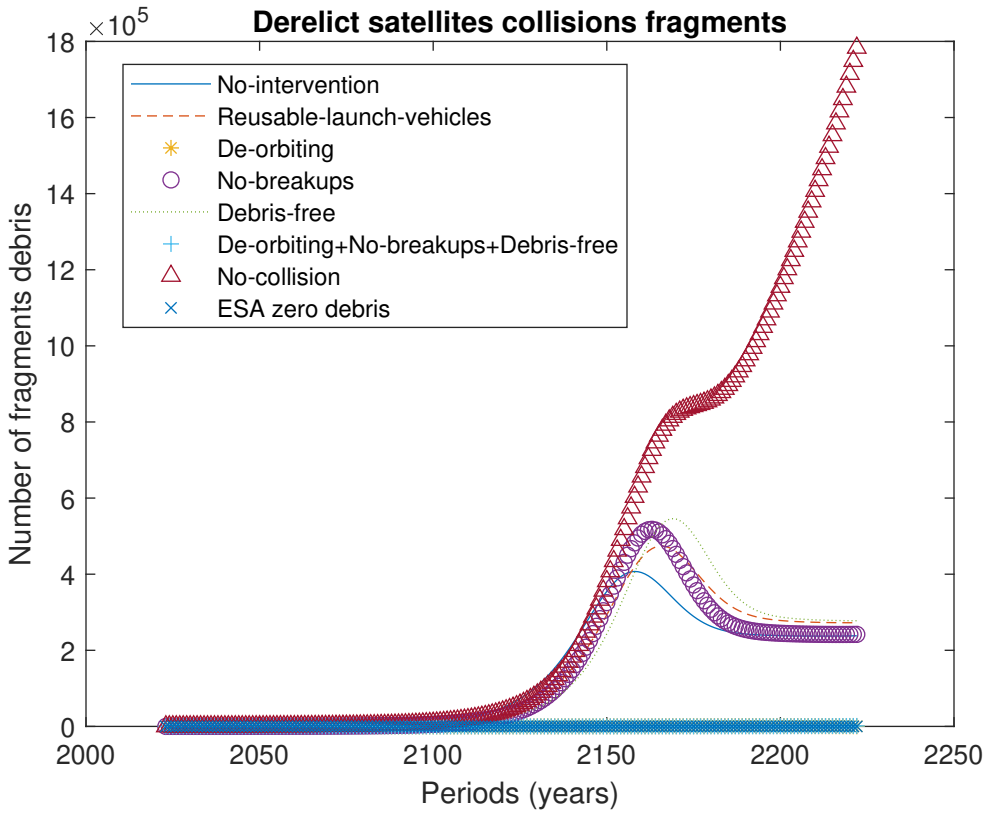


FIGURE I.8. Number of fragments debris larger than 10 cm produced by the collision of derelict satellites per year

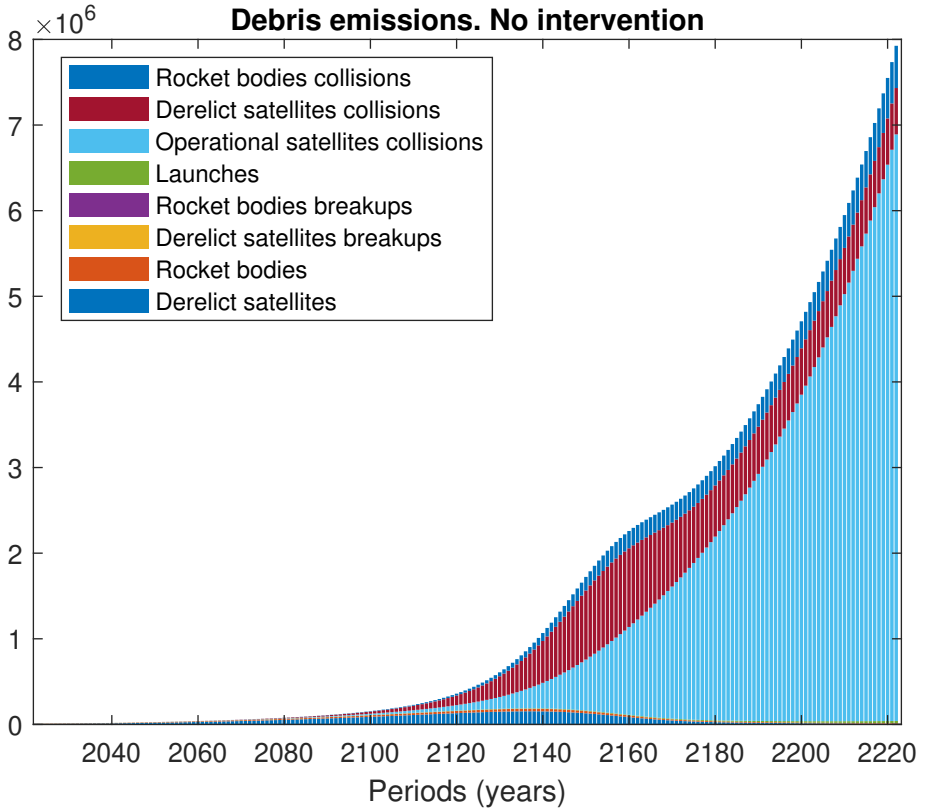


FIGURE I.9. Source of debris emissions (debris > 10 cm). No intervention scenario

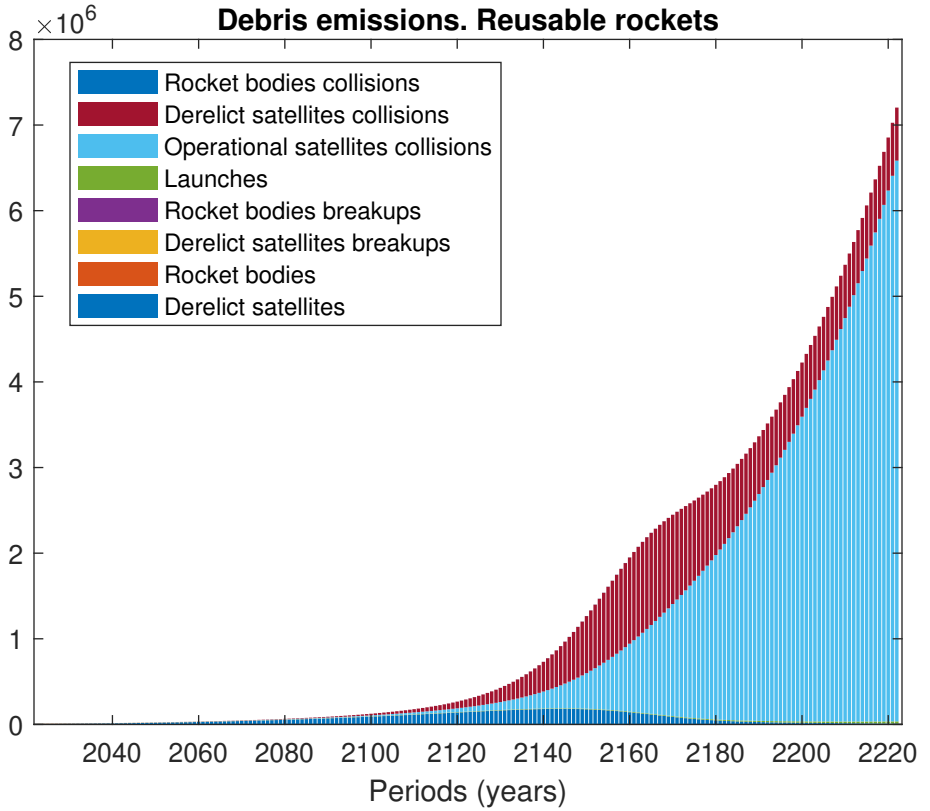


FIGURE I.10. Source of debris emissions (debris > 10 cm). Reusable rockets scenario

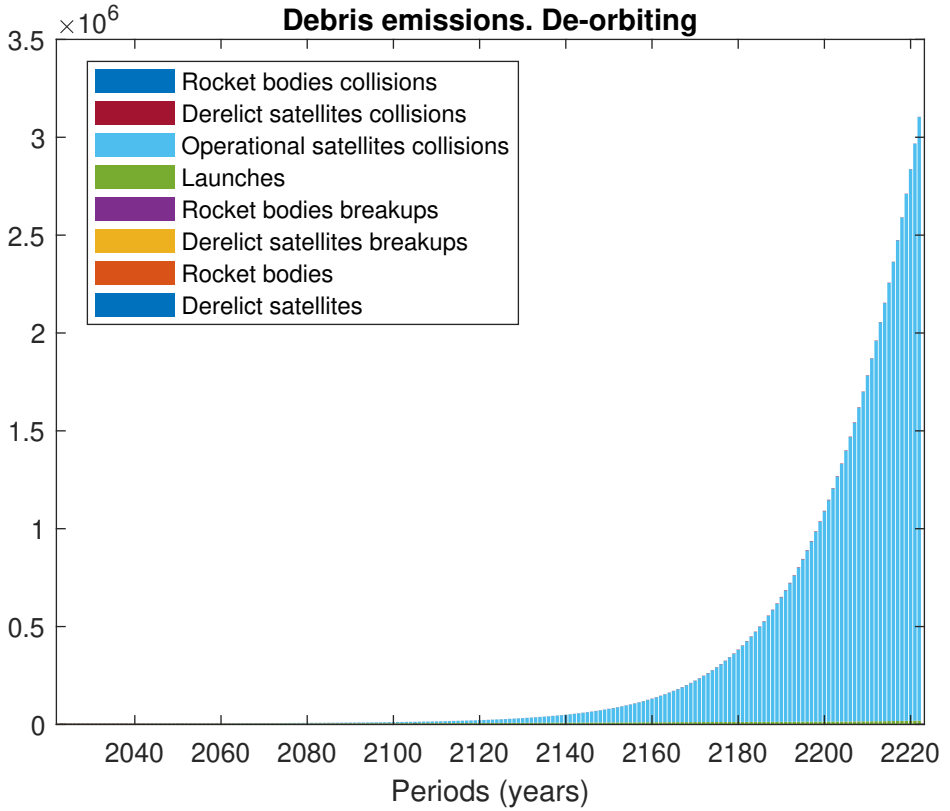


FIGURE I.11. Source of debris emissions (debris > 10 cm). De-orbiting scenario

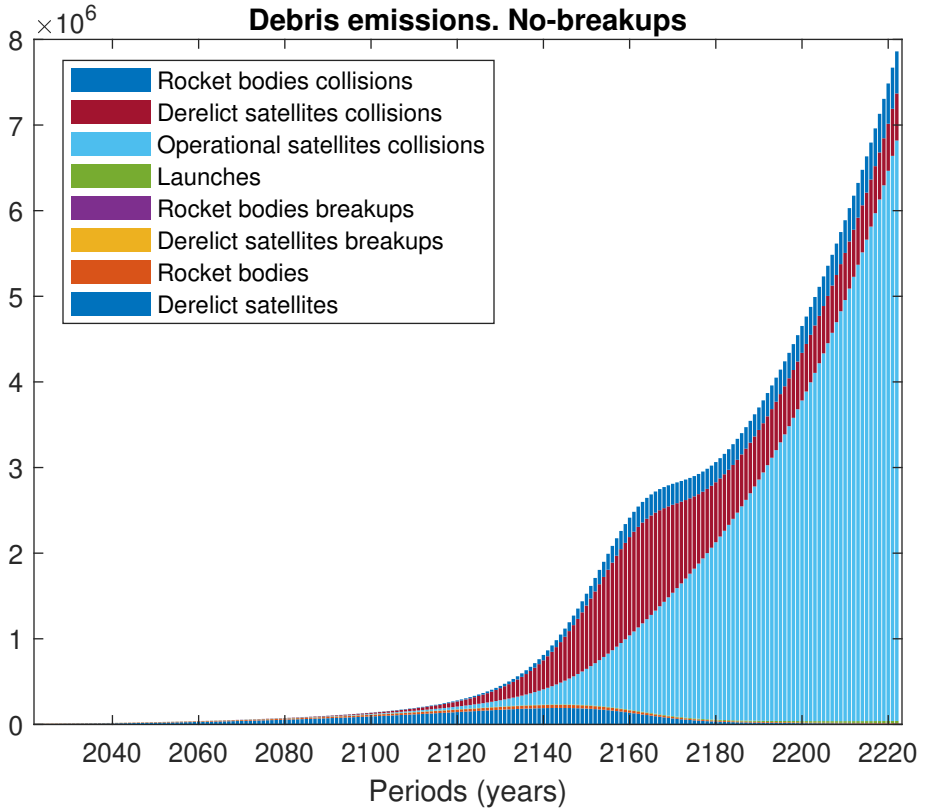


FIGURE I.12. Source of debris emissions (debris > 10 cm). No-breakups scenario

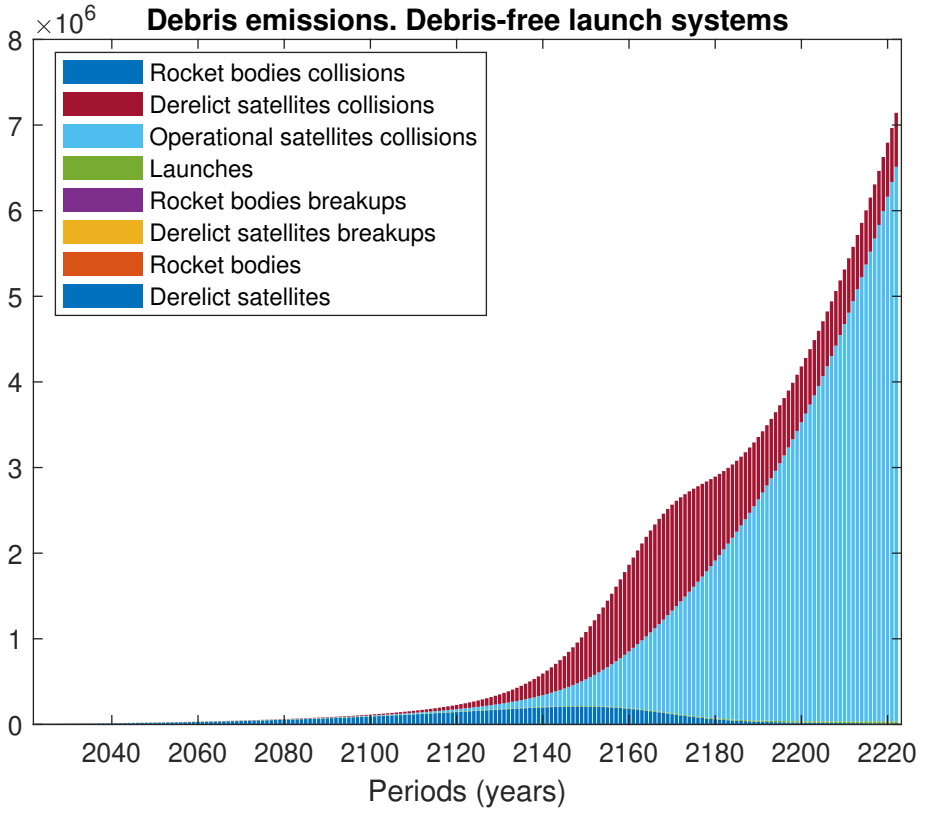


FIGURE I.13. Source of debris emissions (debris > 10 cm). Debris-free launch systems scenario

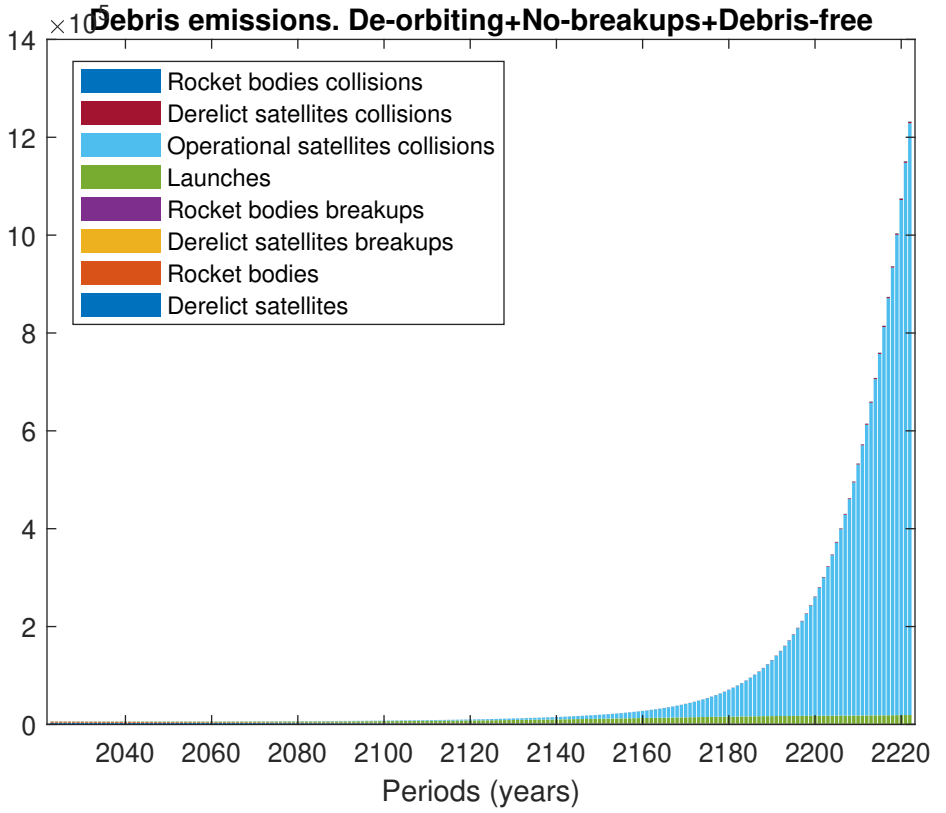


FIGURE I.14. Source of debris emissions (debris > 10 cm). De-orbiting+No-breakups+Debris-free launch systems scenario

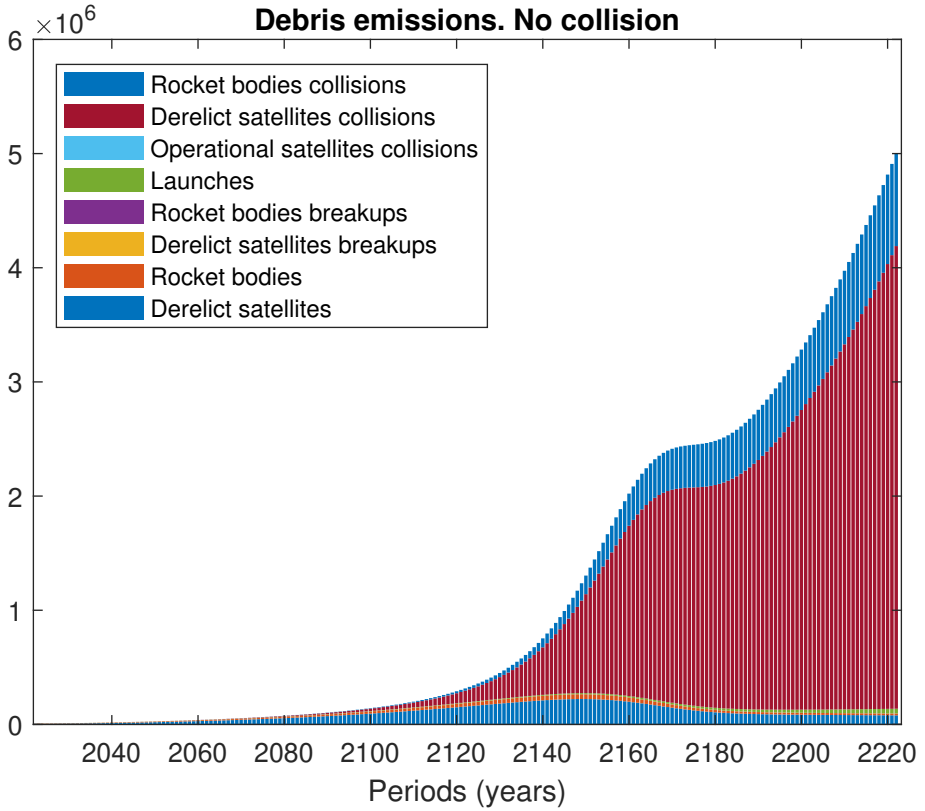


FIGURE I.15. Source of debris emissions (debris > 10 cm). No collision scenario

APPENDIX J: COMPUTER CODE

To perform the numerical simulations, the model is reformulated as a non-linear programming (NLP) problem. Specifically, the simulations cover the period from 2023 to 2272, providing a 250 year planning horizon, with results generated at an annual frequency. The last 50 years are discarded, and only the horizon 2023 to 2222 is considered, in order to eliminate distortions arising from the finite-horizon terminal condition. The model is implemented and solved using GAMS with the CONOPT4 algorithm. As highlighted by Cai (2019), GAMS offers greater flexibility compared to MATLAB, and CONOPT4 is recognized as a more robust and efficient solver for non-linear programming problems than MATLAB's *fmincon* algorithm.

To ensure robustness, the model is also solved in MATLAB using the CasADi framework (Andersson et al., 2019), following the implementation approach developed by Kellett et al. (2018). For context, the DICE (Dynamic Integrated Climate-Economy) model, originally developed by Nordhaus (1992, 1993), remains the most influential integrated assessment model (IAM) in the literature. Nordhaus's DICE model was initially designed and implemented in GAMS, but alternative implementations have emerged over time. For instance, Kellett et al. (2018) developed MATLAB code to solve DICE2013R and DICE2016R using CasADi, while Lemoine (2020) introduced a solution method for DICE2016R using the KNITRO solver.

The GAMS file is named *DISE_2024_01.gms*. Results are saved in Excel files. Figures in the manuscript are produced in MATLAB, using the script *Figures.m*, which is executed after *DISE_2024_01.gms* have been run in GAMS and the results stored in Excel files.

There is also a version of DISE-2024 in MATLAB. The files are *dise2024.m* as the main script, *Space1999.m* containing the initial values and the calibration, and the function file *dynamics.m* for the computational algorithm. To run this MATLAB version, it is necessary to have CasADi (Andersson et al., 2019) installed.

Finally, there is a companion app for a full sensitivity analysis of DISE-2024. This is a GAMS MIRO app, which allows users to solve the model using the GAMS engine and perform a comprehensive sensitivity analysis on the model's key parameters. This app can be found at https://miro.gams.com/gallery/app_direct/dise2024.

REFERENCES

- [1] Adilov, N., Alexander, P., Cunningham B. and Albertson, N. (2022). An analysis of launch cost reductions for low Earth orbit satellites. *Economics Bulletin*, 42(3): 1561-1574.
- [2] Ackerman, F., Stanton, E. A. and Bueno, R. (2013). Epstein-Zin utility in DICE: Is risk aversion irrelevant to climate policy? *Environmental and Resource Economics*, 56: 73-84.
- [3] Andersson, J. A. E., Gillis, J., Horn, G., Rawlings, J. B. and Diehl, M. (2019). CasADi – A software framework for nonlinear optimization and optimal control. *Mathematical Programming Computation*, 11(1): 1-36.
- [4] Anz-Meador, H., Opiela, H. and Liou, J. C. (2022). History of On-orbit Satellite Fragmentations, 16th Edition Orbital Debris Program Office, NASA.
- [5] Australian Space Weather Agency. 1999. *Satellite orbital decay calculations*. Sidney: Australia.
- [6] Barr, J. R. and Manne, A. S. (1967). Numerical experiments with finite horizon planning models. *Indian Economic Review*, 2(1): 1-29.
- [7] Blake, A. P. and Westaway, P. F. (1995). An analysis of the impact of finite horizons on macroeconomic control. *Oxford Economic Papers*, 47(1): 98-116.
- [8] Bongers, A. and Torres, J. L. (2023). Orbital debris and the market for satellites. *Ecological Economics*, 209: 107831.
- [9] Bongers, A. and Torres, J. L. (2024). Star Wars: Anti-satellite weapons and orbital debris. *Defence and Peace Economics*, 35(7): 826-845.
- [10] Bongers, A., Ortiz, C. and Torres, J. L. (2025). DISE: A dynamic integrated space-economy model for the evaluation of debris mitigation policies. *Environmental and Resource Economics*, forthcoming.
- [11] Bureau of Economic Analysis (2023). *Space Economy Data, 2012-2021*.
- [12] Byers, M. and Boley, A. (2023). *Who Owns Outer Space? International Law, Astrophysics and the Sustainable Development of Space*. Cambridge University Press.
- [13] Cai, Y. (2019). Computational methods in environmental and resource economics. *Annual Review of Resource Economics*, 11: 59-82.

- [14] Chetty, R. (2006). A new method of estimating risk aversion. *American Economic Review*, 96(5): 1821–1834.
- [15] Corrado, L., Grassi, S., Paolillo, A. and Silgado, E. (2023). The macroeconomic spillovers from space activity. *PNAS*, 120(43), e2221342120.
- [16] Evans, D. J. (2005). The elasticity of marginal utility of consumption: Estimates for 20 OECD countries. *Fiscal Studies*, 26(2): 197–224.
- [17] Epstein, L. G. and Zin, S. E. (1989). Substitution, risk aversion, and the temporal behavior of consumption and asset returns: A theoretical framework. *Econometrica*, 57(4): 937-969.
- [18] Farinella, P. and Cordelli, A. (1991). The proliferation of orbiting fragments: a simple mathematical model. *Science and Global Security*, 2: 365-378.
- [19] Frisch, R. (1955). The mathematical structure of a decision model: The Oslo sub-model. *Metroeconomica*, 7(3): 111-136.
- [20] Gallois, P. (1987). Life expectancy of communication satellites, *Electronics and Power* 33 (9): 547-550.
- [21] Greenwood, J., Hercowitz, Z. and Krusell, P. (1997). Long-Run Implications of Investment-Specific Technological Change. *American Economic Review*, 87(3): 342–362.
- [22] Guyot, J. and Rouillon, S. (2023). Sustainable management of space activity in low Earth orbit. *Journal of Environmental Economics and Policy*, 13(2): 188-212.
- [23] Hassell, M. P. (1975). Density-dependence in single-species populations. *British Ecological Society*, 44(1): 283-295.
- [24] Kawamoto, S., N. Nagaoka, T. Sato, and T. Hanada. 2019. "Impact on Collision Probability by Post Mission Disposal and Active Debris Removal." First International Orbital Debris Conference.
- [25] Kendrick, D. and Taylor, L. (1970). Numerical solution of nonlinear planning models. *Econometrica*, 38(3): 453-467.
- [26] Kessler, D. J. and B. G. Cour-Palais. 1978. "Collision frequency of artificial satellites: The creation of a debris belt." *Journal of Geophysical Research* 83 (A6): 2637-2646.
- [27] Krag, H., M. Serrano, V. Braun, P. Kuchynka, M. Catania, J. Simiski, M. Schimmerohn, X. Marc, D. Kujiper, I. Shurmer, A. O'Connell, M. Otten, I. Muñoz, J. Morales, M.

- Wermuth and D. McKissock. 2017. A 1 cm space debris impact onto the Sentinel-1A solar array. *Acta Astronautica* 137: 434-443.
- [28] Krisko, P.H. (2007). The predicted growth of the low-Earth orbit space debris environment - An assessment of future risk for spacecraft. *Journal of Aerospace Engineering*, 221(6): 975-985.
- [29] Krisko, P.H., Johnson, N.L. and Opiela, J.N. (2001). EVOLVE 4.0 orbital debris mitigation studies. *Advances in Space Research*, 28(9): 1385-1390.
- [30] Lafleur, J.L. (2011). Extension of a simple mathematical model for orbital debris proliferation and mitigation. *American Astronautical Society*, 11-173.
- [31] Lau, M. I., Pahlke, A. and Rutherford, T. F. (2002). Approximating infinity-horizon models in a complementarity format: A primer in dynamic general equilibrium analysis. *Journal of Economic Dynamics and Control*, 26(4): 577-609.
- [32] Letizia, F., C. Colombo, H. G. Lewis, and H. Krag. 2017. Extending the ECOB space debris index with fragmentation risk estimation. Proc. 7th European Conference on Space Debris, Darmstadt, Germany, 18–21 April 2017, published by the ESA Space Debris Office.
- [33] Lewis, H.G. (2020). Understanding long-term orbital debris population dynamics. *Journal of Space Safety Engineering*, 7: 164-170.
- [34] Lewis, H.G., Swinerd, G.G., Newland, R.J. and Saunders, A. (2009). The fast debris evolution model. *Advances in Space Research*, 44: 568-578.
- [35] Liou, J.C., Hall, D.T., Krisko, P.H. and Opiela, J.N. (2004). LEGEND - a three-dimensional LEO-to-GEO debris evolutionary model. *Advances in Space Research*, 34: 981-986.
- [36] Locke, J., Colvin, T. J., Ratliff, L., Abdul-Hamid, A. and Samples, C. (2024). *Cost and benefit analysis of mitigating, tracking, and remediating orbital debris*. Office of Technology, Policy, and Strategy. NASA.
- [37] Mains, D. L. and Sorge, M. E. (2022). The IMPACT satellite fragmentation model. *Acta Astronautica*, 195: 547-555.
- [38] Mains, D. L., Peterson, G. E., McVey, J. P., Maldonado, J. C. and Sorge, M. E. (2024). Forensic analysis of recent debris-generating events. *Journal of Space Safety Engineering*, 11: 388-394.

- [39] Manne, A. S. (1970). Sufficient conditions for optimality in an infinite horizon development plan. *Econometrica*, 38(1): 18-38.
- [40] Metha, P. M., Smriti, N. P., Crip, N. H., Sheridan, P. L., Siemes, C., Marchet, G. and Bruinsma, S. (2022). Satellite drag coefficient modeling for Thermosphere science and mission operations. *Advances in Space Research*, 72(12): 5443-5459.
- [41] McDowell, J. (2019). *Space Activities 2018*. Jonathan's Space Report.
- [42] McDowell, J. (2020). *Space Activities 2019*. Jonathan's Space Report.
- [43] McDowell, J. (2021). *Space Activities 2020*. Jonathan's Space Report.
- [44] McDowell, J. (2022). *Space Activities 2021*. Jonathan's Space Report.
- [45] McDowell, J. (2023). *Space Activities 2022*. Jonathan's Space Report.
- [46] McDowell, J. (2024). *Space Activities 2023*. Jonathan's Space Report.
- [47] McKnight, D., Witner, R., Letizia, F., Lemmens, S., Anselmo, L., Pardini, C., Rossi, A., Kunstadter, C., Kawamoto, S., Aslanov, V., Dolado-Pérez, J. C., Ruch, V., Lewis, H., Nicolls, M., Jing, L., Dan, S., Dongfang, W., Baranov, A. and Grishko, D. (2021). Identifying the 50 statistically-most-concerning derelict objects in LEO. *Acta Astronautica*, 181: 282-291.
- [48] Mercenier, J. and Michel, P. (1994). Discrete-time finite horizon approximation of infinite horizon optimization problems. *Econometrica*, 62(3): 635-656.
- [49] NASA (2007). Detection of debris from Chinese ASAT test increases; One minor fragmentation event in second quarter of 2007. *Orbital Debris Quarterly Review* 11(3): 1-2.
- [50] NASA (2011). Fiftieth anniversary of first on-orbit satellite fragmentation. *Orbital Debris Quarterly News*, 15(3): 3-5.
- [51] NASA (2020). The tracked objects in Low Earth Orbit: 2000–2020. *Orbital Debris Quarterly Review* 24(4): 11.
- [52] OECD 2020. Space sustainability: The economics of space debris in perspective. OECD Science, Technology and Industry Policy Papers n. 87.
- [53] Pardini, C. and L. Anselmo. 2014. Review of past on-orbit collisions among cataloged objects and examination of the catastrophic fragmentation concept. *Acta Astronautica*, 100: 30-39.

- [54] Percy, T. (2015). *Simplified population growth modelling for low earth orbit*. Dissertations, 76. University of Alabama.
- [55] Prieto, D. M., Graziano, B. P. and Robers, P. C. E. (2014). Space drag modelling. *Progress in Aerospace Sciences*, 64(1): 56-65.
- [56] Ramsey, F. P. (1928). A mathematical theory of saving. *Economic Journal*, 38(152): 543-559.
- [57] Rutherford, T. F. (1995). Extension of GAMS for complementarity problems arising in applied economic analysis. *Journal of Economic Dynamics and Control*, 19: 1299-1324.
- [58] Sen, A. K. (1967). Terminal capital and optimal savings, in G. H. Feinstein (ed.), *Socialism, Capitalism, and Economic Growth: Essays Presented to Maurice Dobb*, Cambridge University Press.
- [59] Space Foundation (2023). *The Space Report 2023 Q2*.
- [60] Squire, M. D., Cooke, W. J., Williamsen, J., Kessler, D., Vesely, W. E., Hull, S. H., Schonberg, W., Peterson, G. E., Jenkin, A. B. and Cornford, S. L. (2015). Joint Polar Satellite System (JPSS) micrometeoroid and orbital debris (MMOD) assessment. NASA.
- [61] Stoleru, L. G. (1965). An optimal policy for economic growth. *Econometrica*, 33(2): 321-348.
- [62] Szpiro, G. (1986). Measuring risk aversion: An alternative approach. *Review of Economics and Statistics*, 68(1): 156-159.
- [63] United Nations (2024). *World Population Prospects 2024*. Population Division, Department of Economics and Social Affairs, United Nations.
- [64] Wang, X. W. and Liu, J. (2019). An introduction to a new space debris evolution model: SOLEM. *Advances in Astronomy*, 2019: 2738276. []